The Dissertation Committee for Benjamin Kyle Scholl Certifies that this is the approved version of the following dissertation:

A Comparative Study of Cortical Computations in the Mammalian Visual cortex

Committee:

_____
Nicholas J. Priebe, Supervisor

_____
Wilson S. Geisler

_____
Richard W. Aldrich

_____
Jonathan W. Pillow

_____
Judith A. Hirsch

A Comparative Study of Cortical Computations in the Mammalian Visual cortex

by

Benjamin Kyle Scholl, B.S.

Dissertation

Presented to the Faculty of the Graduate School of

The University of Texas at Austin

in Partial Fulfillment

of the Requirements

for the Degree of

Doctor of Philosophy

The University of Texas at Austin

May 2015

Acknowledgements

This dissertation and the many projects I was privileged to work on would never have been possible without the guidance and support of my wonderful adviser Nicholas. He encouraged me to pursue multiple avenues of research throughout graduate school. His teachings ranged from technical advice on electrophysiology to synthesizing a scientific question out of the rubble of a deconstructed journal article. Of course his humor should not be left unspoken of, as his interesting jokes and our banter was ever helpful during long experiments, and particularly during night shifts. For the support he has provided and the knowledge I have obtained during my time in his lab, I am forever grateful.

Thank you to the neuroscience community at the University of Texas in Austin, particularly the Center for Perceptual Systems and Institute of Neuroscience. These institutes have provided a wonderful and fostering environment to thrive. Further, they provided the resources for me to enjoy a number of scientific opportunities. A great thanks to the members of my dissertation committee: Bill Geisler, Rick Aldrich, Jonathan Pillow, and Judith Hirsch for helping to shape this dissertation into the document it is today and guidance throughout the course of my graduate career. I also thank Wesley Thompson, whose office was down the hall from our old lab and whose door was always open for me to burst into with questions or conversation.

A tremendous thanks to my undergraduate advisor Mike Wehr, for providing the spark that was my passion in neuroscience and encouraging me towards further academic exploration. Without those wonderful years in his lab and his guidance, I would have never had pursued a doctorate in neuroscience.

I've had the fortune of working beside many wonderful scientists who I consider colleges and friends: Andrew Tan, a longtime collaborator and friend, has always been there for me in any capacity, both academic and otherwise; Sari Andoni, a lab member who would always take time to help me code; Jagruti Pattadkal, who was a impressive graduate student to work alongside; and Johannes Burge, a friend and collaborator, who taught me about striking a balance between life and stereopsis.

A very special thanks to my wonderful friends and fellow classmates: Jake, Leor, Kenneth, Akram, and Steve. Without them, I would never have made it this far. They provided a much needed recreational outlet (e.g. living room karaoke, beer, random debates), as well as cohort of scientific peers to fallback onto when times were tough in the lab.

Finally, I would like to thank my family for their decades of support and encouragement. From a young age they challenged me in every way possible and always pushed me to reach my full potential, despite my best reluctance at times. They provided the catalyst from which I could grow, and for that, I am indebted to them.

A Comparative Study of Cortical Computations in the Mammalian Visual cortex

Benjamin Kyle Scholl, Ph.D.

The University of Texas at Austin, 2015

Supervisor: Nicholas J. Priebe

A common feature of all mammals is the cerebral cortex, which is essential for higher−order functions and processing information to generate motor actions. While cortical circuits exhibit a striking uniformity in anatomical organization, it is unknown whether these circuits preform similar computations across mammalian species. In this dissertation I compare the emergence of two computations in the primary visual cortex (V1) of carnivores and rodents. A cortical computation is a transformation in neural representation, such that the spiking output of a cortical neuron exhibits a selectivity not present in the inputs from upstream neurons. Here I explore two computations: orientation selectivity, the preference of neurons for oriented edges in the visual world, and binocularity, the integration of signals from the two eyes.

In the first section, I compare the emergence of orientation selectivity in the early visual pathway of mouse and cat. Recordings from thalamic relay cells and V1 neurons in both species reveal orientation selectivity in mouse V1 is not emergent, and could be inherited subcortically. In a second set of experiments, I measure orientation selectivity and the organization of V1 orientation preference in a grasshopper mouse with predatory behavior, compared to the scavenger lab mouse. Here I find the same functional properties.

In the second section, I focus on the integration of ocular inputs in V1 of mouse and cat. I first compare disparity selectivity in cats, where convergence of ocular inputs has long been established, with mice, where ocular integration had not previously been investigated. Similar to cats, mouse V1 neurons were sensitive to binocular disparity, albeit to a lesser degree, and could be described by a linear feed−forward model. I next explore the disruption of binocular disparity tuning in both animals. In cats, strabismus induced during development causes increased monocularity in V1 and a loss of disparity selectivity. In mice, monocular deprivation causes increased ocular input, which also manifests as decreased disparity selectivity. Finally, I explore how excitatory and inhibitory neurons in mouse V1 integrate binocular signals. Paravalbumin−expressing inhibitory interneurons are more binocular but less disparity tuned than surrounding cortical neurons, providing a canonical mechanism explaining loss of disparity selectivity in both carnivores and rodents.

Table of Contents

List of Figures

Chapter 1: General introduction

A hallmark of mammalian evolution is the development of the cerebral cortex. The neocortex is evident in every mammal studied and possesses a distinct layered structure with repeating cellular motifs; a structure which is quite similar across cortical areas and across species (Kaas, 1980; Gilbert, 1983; Douglas and Martin 2004; Hirsch and Martinez, 2006). The rules by which axonal afferents and efferents organize within cortical circuitry seems to be universal (Douglas and Martin, 2004). Similar cortical cell types (excitatory and inhibitory) and their relative proportions appear universal (Markram et al., 2004). Further, sensory modalities (e.g. visual, auditory, somatosensory representations) are organized across the cortical surface in relatively the same locations (Kaas, 1980; Kaas, 1989). From the abundance of conserved features in the mammalian neocortex, a simple hypothesis surfaces: the uniformity of cortical circuits gives rise to a common set of cortical computations.

Here I define a cortical computation as a transformation in neural representation, such that the spiking output of a cortical neuron exhibits a selectivity not present in the inputs from upstream neurons. In essence, a cortical computation is the transformation of inputs to form a novel output. A receptive field is defined as the basic area in sensory stimulus space for which an individual neuron is selective. For example, in the visual cortex receptive fields are first defined by retinotopic space, and in the auditory cortex receptive fields are first defined by tonotopic space. These basic receptive field properties, however, would not wholly be considered cortical computations. These sensory maps are generally inherited from the organization of neurons transforming physical information into electrical signals. Instead, a computation would be the emergence of specific receptive properties that are absent in upstream neurons providing inputs.

In this dissertation I explore whether there exists common cortical computations using a comparative approach, focusing on the primary visual cortex (V1) of carnivores and rodents. V1 is highly conserved in mammalian evolution, as it has been identified in all mammalian species (Krubitzer and Kaas, 2005). Mammalian V1 possesses conserved anatomical features: it is located in the occipital portion of the neocortex,

receives a major axonal projection from the thalamus or lateral geniculate nucleus, and is the first site in the early visual system where signals from the two eyes converge (Kaas, 1980; Pettigrew, 1986; Krubitzer and Kaas, 2005; Van Hooser, 2007). Many functional properties of individual cells, such as the preference for oriented edges in visual space (orientation selectivity), are highly conserved across mammals. Likewise, in every species for which ocular integration has been sought, the sensitivity for depth in individual neurons has been demonstrated, albeit for far fewer mammalian species. The work presented in this dissertation uses V1 as a model system to study generalized cortical computations, specifically focusing on the formation of orientation selectivity and the integration of ocular signals.

Would orientation selectivity and binocular integration in different mammals emerge through common computations? On one hand, given the uniformity of cortical circuits, we might expect the same set of computations explains these emergent properties. However, even if cortical circuits are broadly similar in laminar structure and cell type, perhaps more intricate elements differ. Then, we might discover that neocortical circuits have evolved to use more than one strategy to solve similar computational problems (Hirsch and Martinez, 2006). This could parallel analog circuits, where the same core devices can be wired together in a different ways to generate a variety of input/output relationships.

This dissertation is divided into two sections. The first explores the emergence and presence of orientation selectivity in the early visual pathway of rodents and carnivores. I address whether the same computational model of cortical orientation selectivity can account for its emergence in the lab mouse and cat. In this section I also examine the properties of V1 neurons in a carnivorous mouse and compare with the lab mouse. In the second section of this dissertation I focus on the integration of ocular inputs in mouse and cat V1. I first compare disparity selectivity in cats, where convergence of ocular inputs has long been established, with mice, where ocular integration had not previously been investigated. Following this functional comparison, I next explore the disruption of binocular integration in both animals. In cats, an ocular misalignment (strabismus) is induced to disrupt disparity selectivity. In mice, monocular deprivation of the contralateral eye is used to cause a disruption in binocular circuitry.

Finally, using genetic tools available for mice, I explore how excitatory and inhibitory neurons in mouse V1 integrate binocular signals.

SECTION 1: *ON THE FORMATION OF ORIENTATION SELECTIVITY*

Chapter 2: Introduction

Section Overview

In this section, I compare the emergence of orientation selectivity in the early visual pathway of cats and rodents. For decades, this receptive field property has been rigorously measured in carnivores and primates. There is a rich history of developing and testing of models of orientation selectivity in cat, since their discovery by Hubel and Wiesel in 1962. More recently, similar measurements are conducted in rodents, as rodents provide a powerful model system for dissecting neural circuits with genetic tools. Given the emerging emphasis in studying rodents, it is important to understand the similarities and differences with other more well−studied animal models. Specifically, the enormous devotion to studying mouse primary visual cortex (V1) requires a comparison and quantification of V1 computations with more classical model systems. For example, the presence of orientation preference among neurons in mouse V1 dose not necessarily mean their overall selectivity rivals that of cat V1 neurons or that the emergence of their receptive field properties follows canonical models. The same argument also applies to comparisons between other mammalian species as well, as comparative physiology beyond mapping modalities has rarely been undertaken in the field neuroscience, except for a handful of species outside the cat (Chisum et al., 2003; Heimel et al., 2005; Zaltsman et al., 2015).

In the first chapter of this section, I explore the transformation of receptive properties from the thalamus to cortical neurons in the cat and mouse. Here I show a modest degree of orientation selectivity already exists in subcortical neurons in the mouse, which is distinct from the cat. These data suggest a different model describes the emergence of orientation selectivity in mouse V1, compared to the cat. Potential

models discussed include: inheritance of orientation selectivity from the thalamus or a complete re−computation and loss of subcortical information.

In the second chapter of this section, I preform a within−order comparison of orientation selectivity between rodents with carnivorous and scavenger behaviors. The rationale behind this study was two−fold: (1) orientation selectivity in V1 had never been established in a carnivorous rodent and (2) across all mammals studied, organization of orientation preferences is almost exclusively found in carnivores and primates. Thus, I first sought to establish whether neurons in V1 of the carnivorous grasshopper mouse were orientation selectivity and if there existed a systematic map of neuron selectivities like that in other carnivores. Here I find both rodents (the lab mouse and grasshopper mouse) share V1 orientation selectivity and a lack of organization of orientation preferences across individual neurons. These data suggest that both rodents evolved with a similar early visual system, despite striking differences in behavior. Further, if the presence of an orientation map and emergence of orientation selectivity in V1 are inherently linked, these data suggest that possessing carnivorous behavior is not a constraint on the formation of such circuitry.

The early visual system and a feed−forward model of orientation selectivity

In the visual system, sensory information is initially transduced from photons to electrical potentials by retinal photoreceptors. From the photoreceptors, incoming visual information undergoes a number of transformations within the laminar series of neurons in retina, ultimately progressing to retinal ganglion cells, which constitute the output from the peripheral to central nervous system. Retinal ganglion cells have circularly−symmetric receptive fields with an antagonistic center/surround organization, meaning they are unselective for the orientation of objects in visual space

(Kuffler, 1953). In mammals, retinal ganglion cells project to the lateral geniculate nucleus (LGN) of the thalamus, where relay cells in turn send visual information to the first cortical station: the primary visual cortex (V1). While the receptive field profiles of both retinal ganglion cells and their target LGN relay cells are circularly symmetric, V1 neurons are sensitive to several complex visual stimulus attributes, including stimulus orientation, direction and binocular disparity (Hubel & Wiesel, 1962; Pettigrew et al., 1968; Ohzawa and Freeman 1986). In many cases this selectivity is exquisite: V1 neurons may not respond to visual stimulation at all unless the stimulus features specifically match the neuron's preference. A prime example of this selectivity is the orientation selectivity of V1 neurons: a bar of light oriented along one spatial axis might evoke a robust spiking response in a visual cortical neuron, but the same bar oriented along the orthogonal spatial axis would evoke no response.

When Hubel and Wiesel first described cortical orientation selectivity (1962), they proposed a simple and elegant model to explain its emergence; a model which continues to be a reference point for computational models of cortical processing. In their model, neurons in layer IV of the cortex, which receive the bulk of the direct input from the thalamus relay cells (Hubel and Wiesel, 1962; Gilbert, 1977; Bullier and Henry, 1979), become orientation selective through the convergence of multiple LGN relay cells (Fig. 2.1). Thalamic relay cells are themselves generally unselective for orientation since they have circularly–symmetric receptive fields. Hubel and Wiesel hypothesized that multiple LGN relay cells with spatially–offset receptive fields along a single axis in visual space could converge onto a target cortical cell (Fig. 2.1). In this way, a visual stimulus oriented along the axis of the spatial offset activates the afferent LGN relay cells simultaneously and produces a large synaptic input onto the recipient simple cell (Fig. 2.1).

This simple model for cortical orientation selectivity predicts that the relative timing of LGN relay cells is an essential component for the generation of orientation selectivity. Because LGN neurons have circular receptive fields, they respond equally well to all orientations, but their relative timing will vary with stimulus orientation: the spiking responses of LGN relay cells will be nearly simultaneous when an oriented stimulus is presented at the target V1 neuron's preferred orientation but will be spread out in time, or asynchronous, for the orthogonal orientation (Fig. 2.1).

The elegance of this model lies in the feed–forward nature of the systematic transformation of visual information from LGN relay cells to V1: the only requirement being spatial organization of converging excitatory thalamocortical afferents. There is substantial evidence supporting this simple feed–forward model in carnivores. In the cat, layer 4 of primary visual cortex is composed of neurons which receive direct thalamocortical input (Hubel and Wiesel, 1962; Gilbert, 1977; Bullier and Henry, 1979; Hirsch and Martinez, 2006; Martinez et al, 2005; Ferster et al., 1996; Ferster and Lindström, 1983). These neurons, called simple cells, have receptive fields composed of oriented and segregated subregions, each giving exclusively ON or OFF responses (response to light onset/dark offset or light offset/dark onset). The LGN relay cells that provide direct input to target simple cells have receptive fields that overlap in spatial position and polarity (Reid and Alonso, 1995; Tanaka, 1983). Further, inactivation of the cerebral cortex does not disrupt orientation tuning of synaptic input onto simple cells (Ferster et al., 1996; Chung and Ferster, 1998; Jagadeesh et al., 1997). These results support, at least in part, the original proposal by Hubel and Wiesel for the generation of cortical orientation selectivity, at least in carnivores.

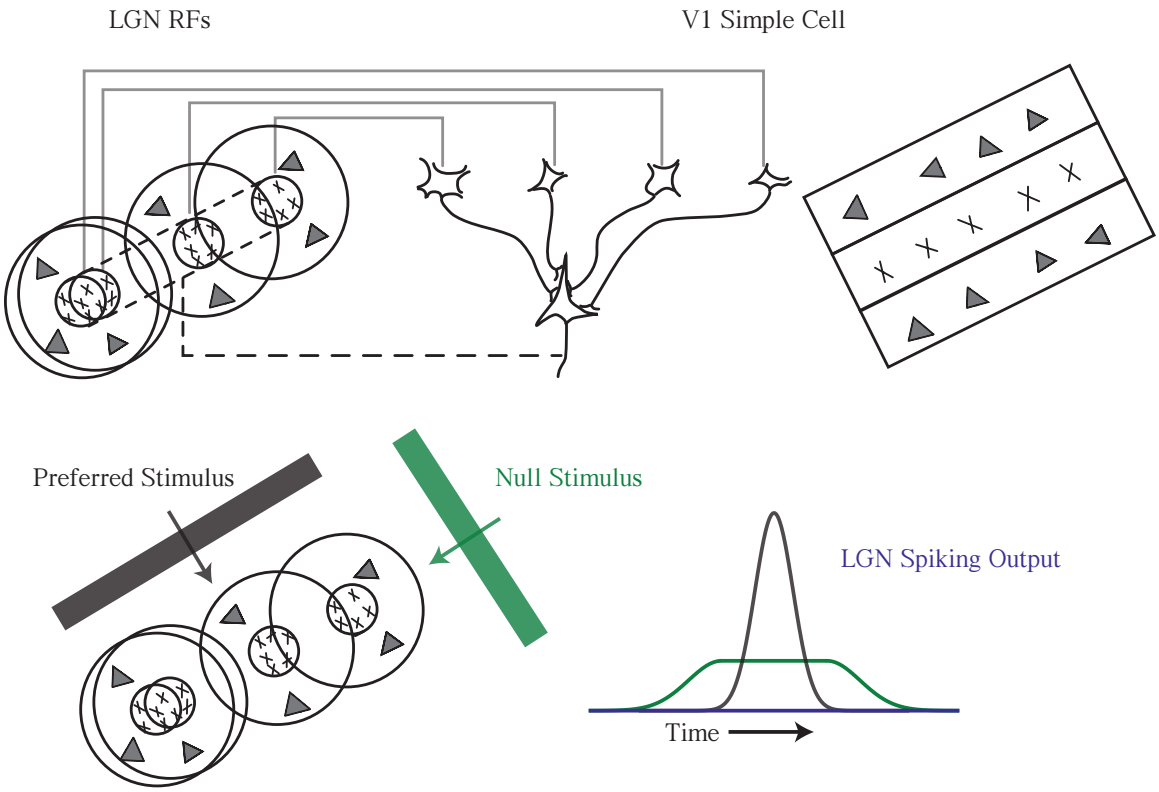

Figure 2.1: Hubel and Wiesel feed–forward model of orientation selectivity
LGN relay cell receptive fields spatially aligned along one axis form the basis of the receptive field of a single V1 simple cell (adapted from Hubel and Wiesel, 1962). A stimulus oriented along this axis activates all LGN cells simultaneously, generating a large synchronous spiking response. The orthogonal stimulus activates the LGN cells asynchronous, producing a temporally uncorrelated spiking response.

Chapter 3: Emergence of orientation selectivity in the mammalian visual pathway[1]

ABSTRACT

Orientation selectivity is a property of mammalian primary visual cortex (V1) neurons, yet its emergence along the visual pathway varies across species. In carnivores and primates, elongated receptive fields first appear in V1, while in lagomorphs such receptive fields emerge earlier, in the retina. Here we examine the mouse visual pathway and reveal the existence of orientation selectivity in lateral geniculate nucleus (LGN) relay cells. Cortical inactivation does not reduce this orientation selectivity, indicating that cortical feedback is not its source. Orientation selectivity is similar for LGN relay cells spiking and subthreshold input to V1 neurons, suggesting that cortical orientation selectivity is inherited from the LGN in mouse. In contrast, orientation selectivity of cat LGN relay cells is small relative to subthreshold inputs onto V1 simple cells. Taken together, these differences show that while orientation selectivity exists in visual neurons of both rodents and carnivores, its emergence along the visual pathway, and thus its underlying neuronal circuitry, are fundamentally different.

INTRODUCTION

In every mammal for which the neuronal response selectivity of primary visual cortex (V1) has been examined, orientation selectivity has been observed. In cat V1, where orientation selectivity was first described, thalamic LGN relay cells are

[1]Published article: Scholl B., Tan A.Y.Y., Corey J., and Priebe N.J. (2013). Emergence of orientation selectivity in the visual pathway. *Journal of Neuroscience* 33(26): 10616–10624.

characterized by circularly symmetric receptive fields, whereas their postsynaptic cortical targets display elongated receptive fields, endowing V1 neurons with a selectivity for stimulus orientation not present in the LGN (Chapter 2; Hubel and Wiesel, 1959; 1962). It was this dramatic change in receptive field properties that led Hubel and Wiesel to propose a simple feedforward model in which multiple spatially–offset LGN relay cells with circularly–symmetric receptive fields converge onto a single V1 neuron to generate elongated receptive fields (Hubel and Wiesel, 1962) (Fig. 2.1). The ubiquity of orientation selectivity across mammals has also led to it being considered a canonical cortical computation (Douglas et al., 1989; Douglas and Martin, 2004). While the recent advent of rodent models allows for dissection of neural circuitry using genetic techniques, it remains unknown whether these species demonstrate this canonical transformation between the LGN and V1.

Orientation selectivity is present in mouse V1, albeit to a weaker degree than that found in the cat (Dräger, 1975; Wagor et al., 1980; Métin et al., 1988; Sohya et al., 2007; Niell and Stryker, 2008; Kerlin et al., 2010; Runyan et al., 2010; Tan et al., 2011; Li et al., 2012). It is unclear, however, the degree to which cortical orientation selectivity in rodents reflects processing occurring within V1 (Fig. 3.1A), or the inheritance of response selectivity from subcortical structures (Fig. 3.1B). Evidence for subcortical orientation selectivity has been observed in lagomorphs, where strong retinal orientation and direction selectivity are observed (Barlow et al., 1964; Levick, 1967), and in carnivores, where orientation biases have been associated with systematic asymmetries of retinal ganglion cell arbors (Boycott and Wässle, 1974; Cleland and Levick, 1974; Hammond, 1974; Levick and Thibos, 1980; Leventhal and Schall, 1983; Shou et al., 1995). Orientation selectivity has also been observed in the LGN of rodents (Marshel et al., 2012; Piscopo et al., 2013) and marmosets (Cheong et al., 2013), although the relationship between this selectivity and that found in V1 is

unknown. Subcortical orientation biases could therefore play a role in the generation of cortical orientation selectivity and work in conjunction with the Hubel and Wiesel framework (Fig. 3.1C).

To uncover the origin of orientation selectivity observed in rodent V1 we compared orientation selectivity of single neurons in mouse LGN and V1. In mouse, we find a similar degree of orientation selectivity among LGN relay cells as the subthreshold input to V1 neurons. Inactivating cortex did not eliminate orientation selectivity in LGN relay cells. In contrast to the mouse, our measurements of orientation selectivity in cat increases between the LGN and V1. Our data demonstrate that orientation selectivity is dramatically enhanced between the LGN and cortex in the cat but not the mouse. It is evident that the organization of visual processing, and thus the underlying circuitry, differs between these two mammals.

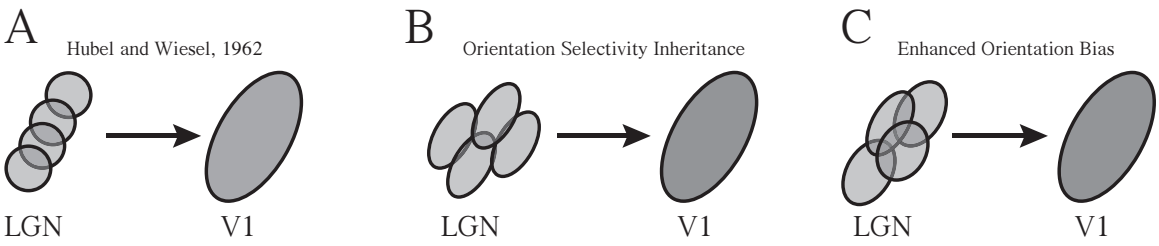

Figure 3.1: Hubel and Wiesel feed–forward model of orientation selectivity
(A) Spatially–offset LGN relay cells are combined to generate orientation selectivity in a Hubel and Wiesel framework (Hubel and Wiesel, 1962). (B) Cortical orientation selectivity could be inherited from subcortical structures. (C) Orientation bias of relay cells could generate orientation selectivity in combination with a Hubel and Wiesel framework.

RESULTS

Orientation selectivity in mouse LGN

We measured orientation selectivity in relay cells of mouse LGN using extracellular single–unit recordings in anesthetized animals. We first verified our location within the LGN (Appendix A) and then isolated the activity of individual neurons by separating each neuron's waveform from the surrounding multi–unit activity. We measured the neuron's orientation selectivity using drifting gratings presented to the contralateral eye of 72 LGN relay cells, of which for 18 cells we also presented dark and light spots to measure the spatial receptive field.

We observed a range of orientation selectivity across relay cells of mouse LGN. Responses of some neurons were modulated substantially by different stimulus orientations, evident both in the mean cycle–averaged spiking responses (Fig. 3.2A, *top*) and the peak (F1 + F0, Appendix B) responses (Fig. 3.2A, *bottom*). To quantify the degree of orientation selectivity for each recorded neuron, we computed the orientation selectivity index (OSI) from the peak response to 12 orientations (Ringach et al., 2002; Tan et al., 2011; Appendix B)

For the example LGN relay cell shown in Fig. 3.2A, modest orientation selectivity in the peak response was reflected by the OSI measurement (OSI = 0.26). Other relay cells were modulated little by oriented gratings, evident both in their mean cycle–averaged responses and the OSI (Fig. 3.2B, OSI = 0.02). While some relay cells had high firing rates and little spontaneous activity (Fig. 3.2A–B), we also recorded from cells with lower firing rates that were selective for orientation (Fig. 3.2C) or largely unmodulated by oriented gratings (Fig. 3.2D). A few relay cells also showed

high background firing rates, such that response modulations evoked by gratings protruded from high spontaneous activity (Fig. 3.2D).

Across the population we discovered that a modest amount of orientation selectivity was common (mean OSI = 0.19 ± 0.14 s.d., median OSI = 0.15, n = 53). We include, in our sample population, relay cells for which sine and square wave gratings were used to measure orientation selectivity (sine: n = 48, square: n = 24). To be sure that using square and sine wave gratings to measure orientation selectivity does not alter our results, however, we employed two additional analyses. First, we compared the median OSI between these sample populations and found no significant difference in selectivity ($p = 0.31$). Second, for a subset of relay cells, orientation selectivity was measured with both sine and square wave gratings. There was no statistical difference between OSI based on sine and square wave gratings ($n = 11$, $p = 0.51$). For tuned LGN neurons (OSI > 0.20, n = 22), we also examined orientation preference to determine if all orientations are represented equally. Despite finding a broad range of orientation preferences, there was an overrepresentation along the horizontal axis, similar to previous reports (Marshel et al., 2012; Piscopo et al., 2013). In these tuned geniculate cells, the mean tuning width from Gaussian fits (Appendix B) were modest (mean sigma = 39 ± 22 deg s.d.).

Of neurons that were orientation selective (OSI > 0.20), many were biased for a particular direction. Direction selectivity was measured by comparing the preferred and opposite (null) direction responses at the same orientation to generate the direction selectivity index (DSI) (Appendix B). A DSI value of 0 indicates no direction selectivity, whereas a DSI value of 1 indicates complete selectivity. For example the relay cell shown in Fig. 3.2C has a DSI of 0.89 ($p < 0.05$, bootstrap analysis, Sokal and Rohlf, 1995), while the relay cell shown in Fig. 3.2A has a DSI of 0.03. From

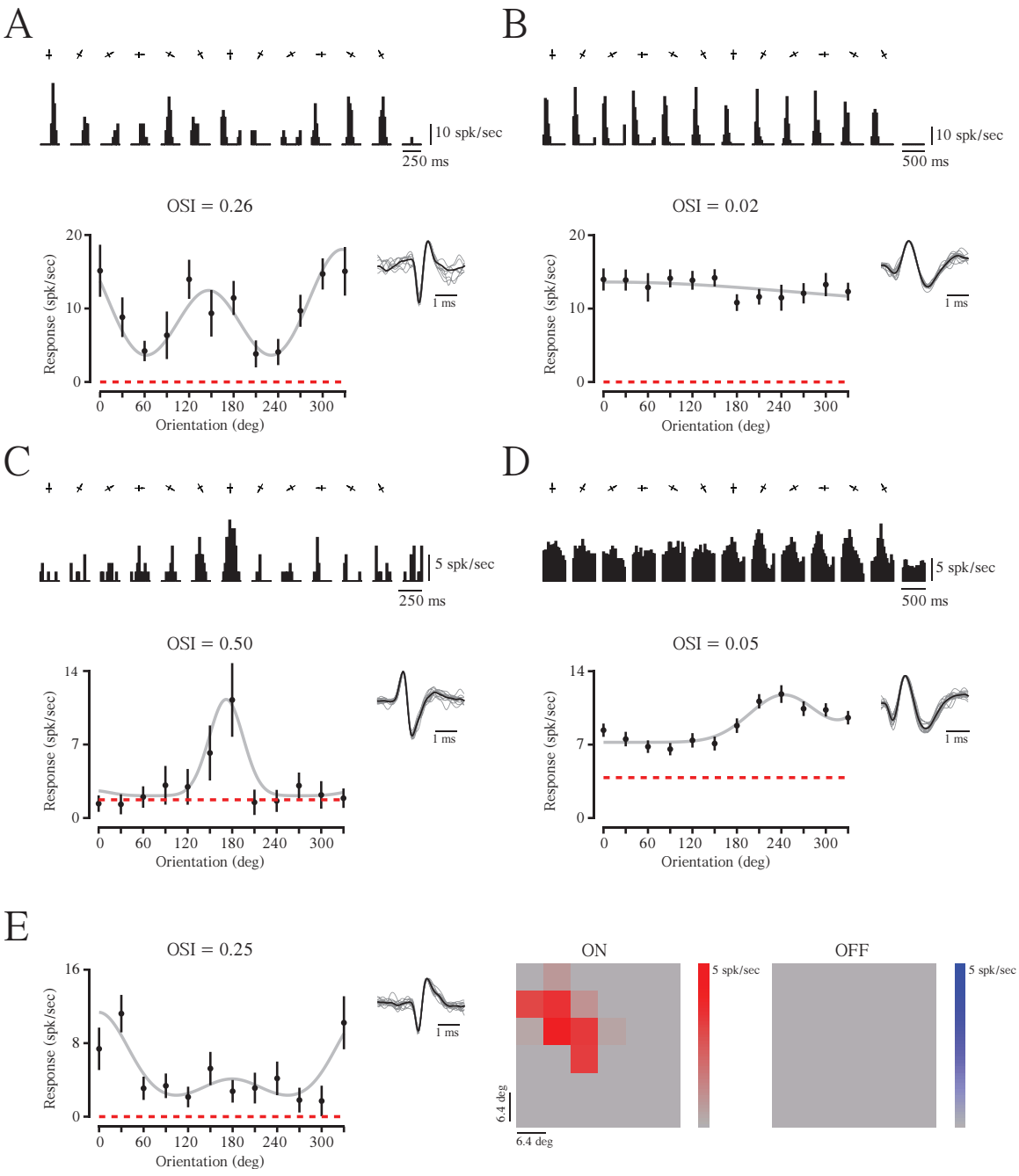
A
10 spk/sec
250 ms
OSI = 0.26
Response (spk/sec)
Orientation (deg)
1 ms
B
10 spk/sec
500 ms
OSI = 0.02
Response (spk/sec)
Orientation (deg)
1 ms
C
5 spk/sec
250 ms
OSI = 0.50
Response (spk/sec)
Orientation (deg)
1 ms
D
5 spk/sec
500 ms
OSI = 0.05
Response (spk/sec)
Orientation (deg)
1 ms
E
OSI = 0.25
Response (spk/sec)
Orientation (deg)
1 ms
ON
OFF
5 spk/sec
5 spk/sec
6.4 deg
6.4 deg

Figure 3.2: Orientation selectivity in neurons of the mouse LGN

(A) Example of an orientation− selective relay cell in mouse LGN. Mean cycled−averaged spiking responses to drifting gratings of each orientation (0 to 330 deg) are shown next to spontaneous activity during blank (mean−luminance) periods. The orientation selectivity index (OSI) was measured from peak responses (F1+F0), plotted for all orientations (black) with the mean spontaneous activity (red dashed line) and a Gaussian fit (gray). Sample waveforms for this isolated neuron are also shown. (B) Example of an non−selective cell. (C) Another example of a selective neuron which is direction selective, has high spontaneous firing rate, and lower spike rate for peak responses. (D) Example of an orientation−biased cell with large spontaneous activity. (E) Example of a neuron with oriented receptive field subregions matching the selectivity measured with drifting gratings. Orientation tuning and sample isolated waveforms (*left)* shown alongside the mean responses to white (ON) and black (OFF) patches of 2−dimensional sparse noise stimulus (*right*).

the 30 neurons that we assayed in mouse LGN, the average DSI was 0.46 ± 0.25 s.d., where 83% of all neurons exhibited DSI values significantly different from 0 ($p < 0.05$, bootstrap analysis, Sokal and Rohlf, 1995).

For a subset of mouse LGN relay cells (n = 18) we also measured receptive field locations that responded to dark or light stimuli by presenting a slow sparse noise stimulus (Gardner et al., 1999). The receptive field properties revealed a match between the orientation selectivity measured using drifting gratings. Neurons that showed modest orientation selectivity were found to have elongated spatial configurations that matched the orientation preference (Fig. 3.2E). For orientation selective neurons (OSI > 0.20, n = 7), the orientation preferences (Appendix A) derived from drifting gratings and that derived from the 2−dimensional Fourier transform of the receptive field map, were similar ($\Delta\Theta$ = 23 ± 32 degrees, mean ± s.d.). Therefore the orientation preference of individual mouse LGN neurons is related to the underlying spatial structure of their receptive fields. The large variability in the correspondence between orientation preference based on gratings and flashed spots, may be related to the nonlinear nature of receptive fields observed in several neurons.

Contribution of cortical feedback to mouse LGN orientation selectivity

The orientation selectivity we observed in mouse LGN could be due to feedforward input from the retina or feedback projections from excitatory V1 neurons in layer 5/6 (Sillito et al., 1994). We isolated the contribution of retinal feedforward connections to LGN response selectivity by inactivating V1 with muscimol, a $GABA_A$ receptor agonist (Appendix A). While muscimol was present on the cortex, we recorded multiunit activity in layers 5/6 of V1. Shortly after muscimol application (20 minutes), spontaneous cortical activity was reduced; 40 minutes following muscimol application,

spontaneous cortical activity ceased (Fig. 3.3A). Additionally, a flashing LED light was used to stimulate the contralateral eye and no visual activity could be evoked in cortex either.

Even in this absence of cortical activity, we continued to observe LGN relay cells with orientation selectivity, evident in peak responses to oriented gratings and sparse noise maps of receptive field on and off subregions (Fig. 3.3B). We also observed LGN relay cells with little orientation tuning (Fig. 3.3C), demonstrating great similarity to the population of neurons we recorded from mouse LGN without cortical application of muscimol ($n = 19$, mean OSI = 0.22 ± 0.17 s.d., median = 0.14). There was no statistical difference in mean OSI between LGN relay cells recorded with or without cortical inactivation ($p = 0.57$). There was no statistical difference in mean OSI between LGN relay cells recorded with or without cortical inactivation ($p = 0.57$). These data demonstrate that the orientation selectivity evident in relay cells of the mouse LGN can occur in the absence of any contribution from visually−evoked or spontaneous cortical activity, suggesting that thalamic orientation selectivity is either inherited from retinal inputs or the result of processing within the LGN itself.

Comparison of orientation selectivity across visual processing stages

While orientation selectivity is clearly evident in responses of mouse LGN relay cells, there may be additional processing in mouse visual cortex to generate the observed cortical orientation selectivity. To answer this question, we compared OSI values measured in neurons of mouse LGN with those measured in neurons of mouse V1 using intracellular recordings. Intracellular records provide a measure of the selectivity

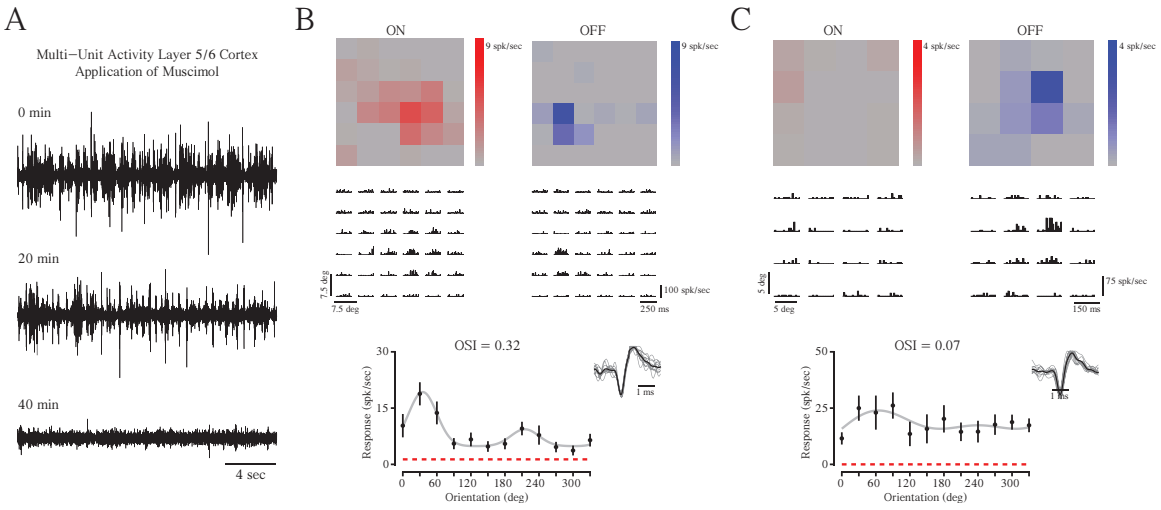

Figure 3.3: Orientation selectivity of mouse LGN relay cells is unaffected by cortical inactivation

(A) Inactivation of layer 5/6 in visual cortex by application of muscimol, a $GABA_A$ receptor agonist. Multi−unit activity is reduced 20 minutes after application and completely abolished after 40 minutes. Visually−evoked activity in visual cortex was abolished after 40 minutes of application. (B) Example of an orientation−selective neuron and corresponding receptive field subregions recorded after cortical inactivation. ON and OFF subregions shown alongside recorded spiking activity to sparse noise stimuli. (C) Example an nonselective cell with a circular receptive field.

of synaptic input, based on subthreshold responses, as well as the selectivity of the suprathreshold activity, based on action potentials. The range of orientation selectivity found across our mouse LGN relay cell records was similar to the range of orientation selectivity found at the level of subthreshold membrane potential responses in V1 neurons (n=32, Fig. 3.4A *top*), although median OSI of subthreshold input to V1 neurons was less ($V1_{Vm}$ = 0.09, LGN = 0.15, $p < 0.001$). No difference in subthreshold selectivity was observed between simple (median = 0.09, n = 12) and complex (median = 0.08, n = 20) cells ($p = 0.29$). A comparison of LGN records to the subthreshold membrane potential responses of V1 simple cells alone yielded no differences in OSI (LGN median OSI = 0.15, V1 Vm median OSI = 0.09, $p = 0.11$). While the degree of selectivity evident in subthreshold responses is low, our measured distribution closely matches values reported by other groups (Li et al., 2012).

In these same intracellular records, the degree of spike rate orientation selectivity was measured and found to be significantly higher than that found both in LGN relay cells (mean OSI = 0.38 ± 0.24 s.d., median = 0.37, n = 21; $p < 0.001$) and in V1 subthreshold input ($p < 0.001$) (Fig. 3.4A *top*). No differences in selectivity were evident between simple (mean = 0.31 ± 0.14 s.d., median = 0.37, n = 5) and complex (mean = 0.29 ± 0.18 s.d., median = 0.29, n = 16) cells ($p = 0.71$). These spike rate OSI values are consistent with those previously reported (Sohya et al., 2007; Kerlin et al., 2010). Across a larger population of extracellularly recorded V1 neurons that included both simple (n = 37) and complex (n = 8) inhibitory and excitatory neurons, modest orientation selectivity was evident (mean OSI = 0.33 ± 0.14 s.d., median = 0.33). This degree of orientation selectivity was also significantly greater than both the LGN and V1 subthreshold input ($p < 0.001$ and $p < 0.001$, respectively). No significant differences in OSI were found between simple (mean = 0.33 ± 0.16 s.d., median =

0.33, n = 37) and complex (mean = 0.23 ± 0.09 s.d., median = 0.24, n = 8) cells (p = 0.09), although there was a general trend for simple cells to show greater selectivity.

In both intracellular and extracellular spiking records, we found no significant difference in OSI between simple and complex cells, although there was a general trend for simple cells to show greater selectivity. Simple cells were found throughout cortical layers 2/3 and 4 (Neill and Stryker, 2008) and there was no relationship between recording depth and cell type (slope = −0.001 ± 0.001 s.e., n = 25, bootstrapped PCA, Sokal and Rohlf, 1995). There was also no relationship between spike rate OSI and recording depth (slope = 0.0002 ± 0.0003 s.e., n = 23, bootstrapped PCA, Sokal and Rohlf, 1995), although our sample does not contain records from deeper layers where orientation selectivity differs (Neill and Stryker, 2008). Both LGN and V1 responses in mice are generally low (LGN median peak spike rate: 14.7 spk/sec, V1 median peak spike rate: 14.9 spk/sec), and such low firing rates could potentially interfere with estimates of orientation selectivity. However, we found no significant relationship between the degree of orientation selectivity and the peak firing rate (spk/sec) of neurons (LGN slope = 0 ± 0.002 s.d., V1 slope = 0 ± 0.004 s.d., bootstrapped PCA, Sokal and Rohlf, 1995). To further determine whether low selectivity is related to noisy responses, we computed 95% confidence intervals of OSI (Appendix A). If low selectivity were related to noisy estimates of OSI, the 95% confidence intervals should be higher for neurons with low selectivity, and yet we find more selective neurons to have larger confidence intervals (LGN slope = 8.7 6.8 s.d., V1 slope = 5.4 3.4 s.d., bootstrapped PCA, Sokal and Rohlf, 1995).

Our records from different sites along the mouse visual pathway show that the degree of orientation selectivity found in the input to cortical neurons already exists at the level of the LGN relay cells, indicating that V1 orientation selectivity may

therefore be inherited from the LGN rather than the result of an additional transformation (Fig. 3.1B). Even when restricting comparisons to V1 simple cells and relay cells, there was a clear absence of any selectivity enhancement. This lack of response transformation between the LGN and V1 was also evident in normalized orientation tuning curves from neurons across all three visual stages (Fig. 3.4B, *top*). We did find a difference between the degree of orientation selectivity in the level of membrane potential and spike rate that results from the biophysical spike threshold rectification (Anderson et al., 2000; Carandini and Ferster, 2000; Priebe and Ferster, 2008; Jia et al., 2010; Tan et al., 2011).

The similarity in orientation selectivity between LGN relay cells and V1 neurons in mouse led us to consider whether such similarity also exists in cat, where orientation selectivity was first described (Hubel and Wiesel, 1962). We measured the responses of cat LGN relay cells extracellularly (n = 35), as well as the subthreshold membrane potential and suprathreshold spiking responses of cat V1 simple cells (n = 41), which are predominately found in layer 4 and receive direct thalamocortical excitatory input (Alonso et al., 2001; Chung and Ferster, 1998; Ferster et al., 1996; Levay and Gilbert, 1976; Reid and Alonso, 1995; Usrey et al., 1999). Cat LGN relay cells are known to show subtle orientation selectivity (Shou and Leventhal, 1989; Soodak et al., 1987; Thompson et al., 1994; Vidyasagar and Heide, 1984), attributed to an orientation bias in retinal ganglion cells (Boycott and Wässle, 1974; Cleland and Levick, 1974; Hammond, 1974; Levick and Thibos, 1980; Leventhal and Schall, 1983; Shou et al., 1995), and this was evident in our extracellular records (mean OSI = 0.09 ± 0.08, median = 0.07) (Fig. 3.4A *bottom*). Identified X−cells (n = 16) and Y−cells (n = 11) exhibited no differences in OSI (p = 0.54). The degree of orientation selectivity in these relay cells was less than that measured in mouse (cat LGN median OSI = 0.07, n = 35, mouse LGN median OSI = 0.15, n = 72, p = 0.003). Specifically, 42% of all

mouse geniculate cells were considered orientation tuned (OSI > 0.20), while only 10% of cat geniculate cells showed the same degree of tuning. These subpopulations did not differ in median selectivity ($p = 0.96$).

In contrast to mouse V1 neurons, subthreshold responses in cat V1 simple cells exhibited a greater degree of orientation selectivity (mean OSI = 0.29 ± 0.20, median = 0.27) than cat LGN relay cells ($p < 0.001$) and mouse subthreshold input ($p < 0.001$). As in mouse V1 neurons, a further enhancement of orientation selectivity was observed in the spiking responses of cat V1 neurons (mean OSI = 0.74 ± 0.22, median = 0.82, Fig. 3.4A, *bottom*). In cat, response transformation from the LGN to V1 was also evident in normalized orientation tuning curves across all three visual stages (Fig. 3.4B, *bottom*). The systematic increase in orientation selectivity in the cat, from LGN relay cell responses, to subthreshold membrane potential responses, to V1 neuron spiking responses indicates a dramatic transformation across the visual pathway (Fig. 3.4A–B, *bottom*). In contrast, in the mouse visual pathway, a progression of increasing selectivity does not occur between the LGN and subthreshold V1 responses (Fig. 3.4A–B, *top*). Absence of a selectivity increase in mouse, compared to that observed in cat, suggests a fundamental difference in the processing of visual information between these two species.

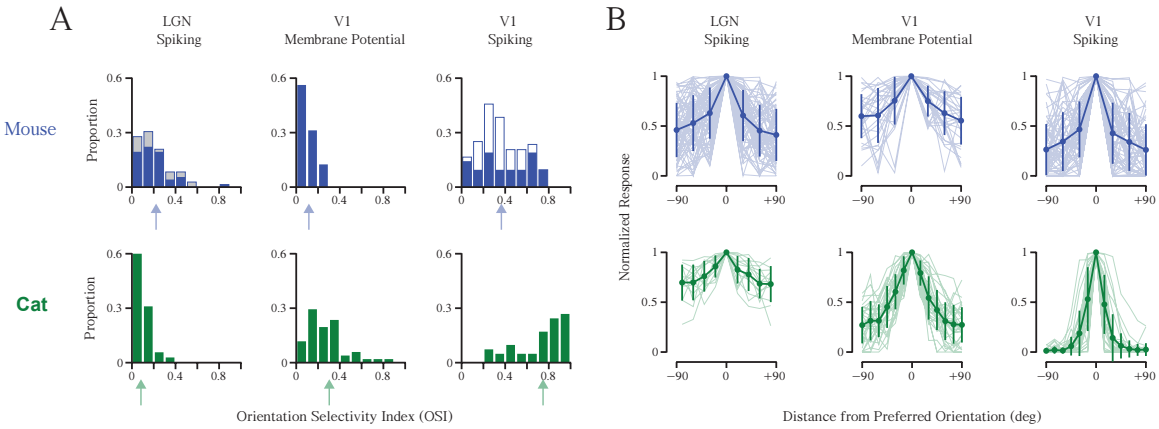

Figure 3.4: Comparison of orientation selectivity in mouse and cat

Distributions of OSI in mouse (blue) and cat (green) LGN spiking responses, V1 subthreshold membrane potential responses, and V1 spiking responses. Arrows indicate mean value for each distribution. V1 spiking OSI is based on the suprathreshold responses from intracellular records. Measurements made during cortical inactivation shown for mouse (gray). In the mouse, some of the spiking OSI measurements were based on extracellular single−unit records (open blue). OSI distributions in mouse LGN and V1 subthreshold input are similar, while those in the cat show an enhancement of selectivity. In V1 of both mouse and cat, there is an enhancement of selectivity from subthreshold to spiking responses. (B) Orientation tuning curves centered around preferred orientation (± 90 deg) are shown across the visual pathway in mouse (blue) and cat (green). Each tuning curve was normalized by the peak response at the preferred orientation. Mean and standard deviation are plotted over each population (light shading). Note that tuning curves shown for the cat LGN are from a subset of neurons (n = 13/35) for which we measured responses with small angle increments.

DISCUSSION

Our current understanding of neural processing in the mammalian brain has been strongly shaped by the characterization and subsequent analysis of neuronal response selectivities for specific stimulus features along the visual pathway, primarily relying on the visual systems of lagomorphs, carnivores, and primates. Today, the rodent visual system has become the focus of much investigation, given its compatibility with sophisticated genetic and imaging techniques, despite less transparency into its visual processing mechanics. How similar is the rodent model to the historical models, and how readily can we overlay our current state of knowledge onto the new rodent model? Here we have examined and compared the emergence of orientation selectivity along the visual pathway of mouse and cat. In the mouse, we find a similar degree of orientation selectivity in the LGN relay cells as in the subthreshold membrane potential responses of V1 neurons (Fig. 3.4A, *top*). LGN relay cell orientation selectivity persisted even after cortical inactivation, indicating that cortical feedback connections are not the source of the selectivity (Fig. 3.3). Our results provide no evidence for a dramatic transformation in orientation selectivity between the LGN and V1 of the mouse (Fig. 3.4A–B, *top*). In striking contrast, in the cat, there is a dramatic transformation in orientation selectivity between the LGN relay cells and their cortical targets (Fig. 3.4A–B, *bottom*). Cat LGN cells display weak orientation selectivity, while subthreshold membrane potential responses in V1 show greater selectivity. In both the mouse and cat, cortical neuron subthreshold orientation selectivity was enhanced by spike threshold to generate greater spiking selectivity. In summary, while orientation selectivity exists in V1 of both rodents and carnivores, our results demonstrate that its generation, and thus the underlying neuronal circuitry, are distinct.

Not only is there a difference in the emergence of orientation selectivity between mouse and cat, but the functional cortical organization in each species is distinct (Fig. 3.5). In cat V1, orientation selectivity is organized in a columnar fashion (Hubel and Wiesel, 1963), whereas in mouse V1 no such organization is evident (Ohki et al., 2005; see Chapter 4). Even in the gray squirrel, a highly visual rodent with strong cortical orientation selectivity, no clear functional organization for orientation selectivity exists in V1 (Heimel et al., 2005). Lagomorphs, like rodents, lack an orientation map in visual cortex, although a clustering of orientation preferences in neurons has been reported (Chow et al., 1971; Murphy and Berman, 1979) (Fig. 3.5). Primates, like carnivores and in contrast to rodents and lagomorphs, exhibit both strong cortical orientation selectivity and a clear orientation selectivity map (Hubel and Wiesel, 1968; Essen and Zeki, 1978; T'so et al., 1990; Bosking et al., 1997), although the emergence of orientation selectivity within cortex differs between primate species (Fitzpatrick, 1996) (Fig. 3.5). Additionally, like carnivores, some species of primates have subpopulations of LGN relay cells that exhibit orientation selectivity (Cheong et al. 2013, Smith et al., 1990; Xu et al., 2002) (Fig. 3.5). The presence of orientation selectivity in primate koniocellular neurons suggests that a specific subcortical pathway transmits orientation selective signals as we find in many mouse LGN cells, although the relationship between primate koniocellular neurons and rodent or cat LGN cells is unclear.

While the Hubel and Wiesel feedforward model has elegantly described the emergence of cat cortical orientation selectivity, the mechanisms underlying subcortical orientation selectivity are less clear. It is possible that subcortical orientation selectivity in the mouse could stem either from processing within the retina (Weng et al., 2005; Elstrott et al., 2008), or from interactions within the LGN (Levick et al., 1969). In the rabbit, for example, a subset of retinal ganglion cells (RGCs) are

known to be sensitive to horizontally and vertically oriented stimuli (Barlow et al., 1964; Levick, 1967; Stewart et al., 1971), and the emergence of this property depends on an interplay between synaptic excitation and inhibition (Taylor et al., 2000; Venkataramani and Taylor, 2010). While these RGCs prefer only horizontal or vertical orientations, selectivities for all orientations are present in rabbit V1 (Chow et al., 1971), though a bias for horizontal and vertical persists (Murphy and Berman, 1979). As in lagomorphs, retinal orientation selectivity has been observed in rodents (Weng et al., 2005; Elstrott et al., 2008; Girman, 2010), but it is unclear exactly how excitation and inhibition combine to generate the selectivity, although recent work has suggested that a developmentally driven asymmetric synaptic wiring between starburst amacrine cells and RGCs drive direction tuning (Wei et al., 2011). An additional factor contributing to retinal orientation selectivity across mammals is the radial bias in dendritic structure of RGCs (Boycott and Wässle, 1974; Cleland and Levick, 1974; Hammond, 1974; Levick and Thibos, 1980; Leventhal and Schall, 1983; Shou et al., 1995; Weng et al., 2005). During development the retina grows outward and stretches RGC dendrites in a radial fashion, creating systematic orientation preferences in RGC responses. This radial bias, coupled with synaptic mechanisms for horizontal and vertical orientation selectivity, could provide signals driving orientation selective responses that we observed in mouse LGN relay cells (Fig. 3.1B–C). In addition, within the thalamus multiple RGCs may converge onto a single target relay cell (Levick et al., 1969). Any spatial offset of convergent RGC inputs would create a bias in orientation selectivity in the fashion suggested by Hubel and Wiesel (1962) (Fig. 3.1A).

In contrast to the mouse, orientation selectivity in the cat increases dramatically in V1 relative to LGN relay cells, but the weak orientation selectivity and orientation biases evident in relay cells may nonetheless provide essential signals for the generation or modulation of cortical orientation selectivity. Those biases may underlie

a known overrepresentation of horizontal and vertical preferences and the organization of orientation selectivity within V1 (Kaschube et al., 2010; Schall, 2011). Further, while the orientation selectivity of synaptic inputs is not altered by cortical inactivation (Ferster et al., 1996; Chung and Ferster, 1998), that oriented input could arise both from summation of spatially offset LGN relay cell receptive fields as well as the orientation biases of the relay cells themselves (Fig. 3.1C). Consistent with this hypothesis, the spatial polarity of LGN relay cells matches that of target cortical cells (Alonso et al., 2001; Reid and Alonso, 1995), but recent evidence indicates that the spatial offsets of relay cells are not sufficient to account fully for cortical orientation selectivity (Kuhlmann and Vidyasagar, 2011; Viswanathan et al., 2011; Stanley et al., 2012). Therefore, the spatial offset of LGN relay cell receptive fields and their orientation biases could combine synergistically to generate cortical orientation selectivity.

There are many possible combinations of receptive fields that could generate orientation selectivity, including randomly distributed inputs (Hansel and Van Vreeswijk, 2012) or oriented receptive fields spatially aligned to generate a distinct orientation. The presence of subcortical orientation selectivity strongly suggests feedforward inheritance in generating cortical selectivity, but it is possible for this selectivity to be discarded and regenerated within V1. Simultaneous recordings from connected LGN−V1 pairs, as done in the cat (Alonso et al., 2001; Reid and Alonso, 1995), would be able to distinguish between these possibilities. While it is remains unknown which mechanism explains the observed cortical orientation selectivity, we have demonstrated its emergence along the visual pathway is distinct between mice and cats.

The emergence of orientation selectivity in V1 is considered the classic example of a computation performed by the cerebral cortex. In carnivores, cortical orientation

selectivity clearly emerges from less selective LGN relay cell inputs, even when the LGN relay cell inputs are forced to innervate auditory cortex instead of visual cortex (Von Melchner et al., 2000; Sharma et al., 2000). The presence of orientation selectivity in V1 of every mammal in which it has been measured has supported the idea that its emergence reflects a fundamental function of neocortex. Here we demonstrate that despite consistency across mammalian visual systems, the underlying mechanisms for emergence of response selectivity are not the same from species to species. Like the differences we have shown here between mouse and cat, it is also known that orientation selectivity emerges at different stages in cat and monkey (Fig. 3.5). In the cat, orientation selectivity is apparent in the thalamorecipient layer 4 neurons (Hubel and Wiesel, 1962), whereas in the monkey and tree shrew it emerges in layer 2/3 (Hubel and Wiesel, 1968; Essen and Zeki, 1978; Blasdel and Fitzpatrick, 1984; Schall et al., 1986; Smith et al., 1990; T'so et al., 1990; Chisum et al., 2003; Gur et al., 2005) (Fig. 3.5).

The differences in the emergence of orientation selectivity cannot be simply ascribed to the evolutionary ancestral relationship between mammals, particularly since rodents are more closely related to primates than carnivores. Many additional factors may play a role in determining at which stage orientation selectivity first emerges. Notably, cats and macaques are predators, while mice are herbivores. The lateralization of the eyes, the presence or absence of a fovea, the degree to which animals are nocturnal or diurnal, and the reliance on vision may play important roles in determining the emergence and organization of orientation selectivity. We suggest that despite the ubiquity of cortical orientation selectivity, a diversity of mechanisms exists for its generation.

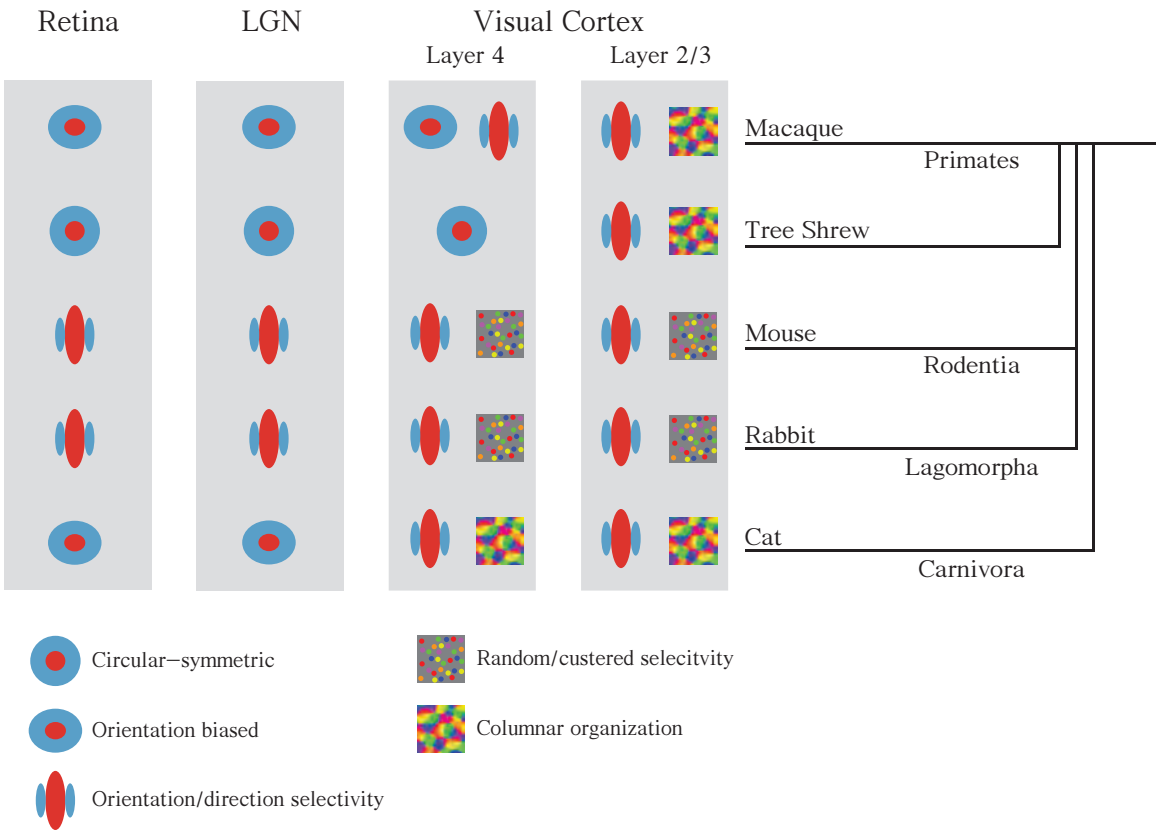

Figure 3.5: Comparison of orientation selectivity emergence across mammalian species

Orientation selectivity emerges in the retina of lagomorphs and rodents and is inherited by V1 neurons. In species of carnivores and primates, the transformation driving orientation selectivity occurs in visual cortex, although some selectivity in cat and primate is observed in the retina and LGN. Recordings along the visual pathway from macaque (Hubel and Wiesel, 1968; Essen and Zeki, 1978; Schall et al., 1986; Smith et al., 1990; T'so et al., 1990; Gur et al., 2005), tree shrew (Fitzpatrick, 1996; Bosking et al., 1997; Chisum et al., 2003), mouse (Dräger, 1975; Métin et al., 1988; Ohki et al., 2005; Weng et al., 2005; Ohki and Reid, 2007; Elstrott et al., 2008; Marshel, 2012; Piscopo et al., 2013), rabbit (Barlow et al., 1964; Levick, 1967; Levick et al., 1969; Stewart et al., 1971; Murphy and Berman, 1979; Taylor et al., 2000; Venkataramani and Taylor, 2010), and cat (Hubel and Wiesel, 1959; 1961; 1962; 1963; Boycott and Wässle, 1974; Cleland and Levick, 1974; Hammond, 1974; Levay and Gilbert, 1976; Levick and Thibos, 1980; Leventhal and Schall, 1983; Vidyasagar and Heide, 1984;

Soodak et al., 1987; Shou and Leventhal, 1989; Thompson et al., 1994; Reid and Alonso, 1995; Shou et al., 1995; Ferster et al., 1996; Chung and Ferster, 1998; Usrey et al., 1999; Alonso et al., 2001; Kuhlmann and Vidyasagar, 2011; Viswanathan et al., 2011; Stanley et al., 2012). Note that the first emergence of orientation selectivity in the primate may depend on whether the thalamic inputs derive from the magno− or parvocellular pathway (Gur et al., 2005), and could either be located in layer 4Ca or layer 4Cb (Blasdel and Fitzpatrick, 1984; Ringach et al., 2002). Also note that although tree shrews are more closely related to primates than lagomorphs or rodents, they are not considered primates and the phylogenetic relationships remain unresolved (Cronin and Sarich, 1980; Luckett, 1980; MacPhee, 1993).

Chapter 4: Similar cortical micro–organization in rodents with predatory and scavenger behavior

ABSTRACT

Mammalian neocortical circuits are spatially organized according to neural response selectivity. Although all species possess topographically ordered cortical sensory representations, for example the respective retinotopic and tonotopic maps of the visual and auditory systems, this does necessarily generalize to computations preformed by cortical neurons. Orientation selectivity in carnivores and primates is spatially organized in the visual cortex, while in rodents and lagomorphs there is a random, 'salt–and–pepper' map. The hypothesis that animals with orientation maps are predators rather than scavengers or prey is consistent with previous data. Here we dispel this distinction by revealing that a carnivorous rodent with predatory behavior, the grasshopper mouse (*Onychomys Arenicola*), has a 'salt–and– pepper' organization of orientation preference, similar to other rodents. Through a combination of two–photon microscopy and extracellular electrophysiology, we determine that the microstructure of visual cortical neurons in the grasshopper mouse is the same as the inbred C57/BL6 laboratory mouse.

INTRODUCTION

The functional organization hypothesis of cortical circuits has become a cornerstone of systems neuroscience since it was first postulated (de Nó 1949; Mountcastle, 1957). As first defined, cortical neurons sharing particular response

properties and overlapping sensory receptive field locations are spatially organized. Spatial organization of orientation selectivity, an emergent response selectivity in the primary visual cortex (V1), is evident in cats (Hubel and Wiesel 1962; 1963; Bonhoeffer and Grinvald 1991), ferrets (Chapman et al. 1996; Nauhaus et al. 2012), etruscan tree shrews (Weliky et al. 1996; Bosking et al. 1997), new world primates (O'Keefe et al. 1998; Xu et al. 2004; McLoughlin and Schiessl 2006), and old world primates (Hubel and Wiesel 1968; Essen and Zeki 1978; Ts'o et al. 1990). Rodents, however, do not possess a map of orientation selectivity and have a random or "salt–and–pepper" organization (Ohki et al. 2005; Ohki 2007). This is true even for highly visual rodents like the squirrel (Van Hooser et al. 2005).

Factors impacting the presence or absence of an orientation map have not been identified. While body and brain size are weakly correlated with the emergence of an orientation map (Van Hooser et al. 2005; Keil et al. 2012), there are a number of outliers such as small animals possessing spatial organization (pigmy marmosets) and larger ones which do not (lagomorphs). Peripheral acuity might play a role since mammals with a cone–based visual system are weakly linked to orientation maps (Van Hooser et al. 2005; Keil et al. 2012), but again, outliers such as the nocturnal owl monkey and prosimian bush baby with little or no retinal foveal cone–specialization (Ogden 1975; Wikler and Rakic 1990) possess a orientation map in V1 (O'Keefe et al. 1998; Xu et al. 2004; 2005). Another potential factor is the relationship between species behavior and a columnar architecture. Mammals with predatory behavior (carnivores and primates) often posses orientation columns while scavengers and potential prey for larger creatures (rodents and lagomorphs) lack functional organization (Van Hooser et al. 2005; Keil et al. 2012). A natural question then, is whether predatory behavior in a rodent would provide the necessary constraints to impose a columnar organization of orientation selectivity in V1.

Here we address whether a carnivorous rodent with predatory behaviors, the grasshopper mouse (*Onychomys Arenicola*), has a columnar organization of orientation selectivity in V1. Using extracellular single unit recordings and *in vivo* two−photon calcium imaging we find that the grasshopper mouse cortical organization is identical to that of the C57/BL6 laboratory mouse. Two−photon calcium imaging of hundreds of cells revealed a random 'salt−and−pepper' map of orientation preference in both rodent species. Across populations, tuning strength and orientation preferences were also similar between animals. Extracellular records from tangential penetrations in V1 yielded neurons with a variety of orientation preferences, further confirming a lack of organization. Our recordings suggest that a functional columnar organization in V1 does not dependent on mammals exhibiting predatory versus scavenger behaviors, and the emergence of this architecture is dependent on other factors yet to be established.

RESULTS

We compared the functional architecture of layer 2/3 in primary visual cortex (V1) of the C57/BL6 lab mouse with that of the carnivorous grasshopper mouse (*Onychomys Arenicola*) (Figure 4.1A). Southern grasshopper mice are predominately found in Texas, the Southern United States and Mexico (The mammals of Texas). Unlike other rodents, grasshopper mice are highly carnivorous (Horner et al. 1964; Landry 1970), preying insects, scorpions, and even other mammals (Horner et al. 1964; Ruffer 1968; Timberlake and Washburne 1989). Grasshopper mice are comparatively aggressive hunters and tenacious predators, resistant to many aversive tactics by their prey (Timberlake and Washburne 1989; Langley 1994). Grasshopper mice have even developed a resistance to the toxins from some prey, such as the Arizona bark scorpion venom (Rowe and Rowe 2008; Rowe et al. 2013). While most animals might learn to

avoid noxious prey, grasshopper mice persistently attack even insects with formidable defenses, enabling them to exploit prey avoided by other species (Sarko et al. 2011; Rowe et al. 2013). Because of these reasons, the grasshopper mouse serves as an ideal model to investigate differences in the functional architecture of V1 within the rodent order.

Anatomical measurements have charted the location and relative size of V1 in grasshopper mice (Sarko et al. 2011), although direct recordings from these neurons had yet to be undertaken. We first identified the location of V1 (Figure 4.1B) and made extracellular single unit records to establish the basic retinotopic organization and determine whether orientation selectivity was a property of these neurons. Spiking responses to orientation drifting gratings ($0 - 315$ deg) of individual neurons were measured using single unit extracellular recording. In both rodent species, we observed neurons selective for orientated drifting gratings (Figure 4.1C, *top*) and those which were visually responsive, but unselective (Figure 4.1C, *bottom*). Each cell's selectivity or lack thereof was characterized by a vector strength index or OSI (Orientation Selectivity Index) (Appendix B) (Ringach et al. 2002; Tan et al. 2011). A comparison between populations showed that the extent of selectivity in V1 was comparable (Figure 4.1D), but neurons recorded in the grasshopper mice were slightly less selective for oriented gratings (*Onychomys Arenicola*: median OSI = 0.20, mean OSI = 0.24 ± 0.18 s.d.; C57/BL6: median OSI = 0.25, mean OSI = 0.31 ± 0.21 s.d.; p = 0.001 Mann−Whitney Test). From these data we also computed a direction selectivity index (DSI, Appendix B) and found slightly higher DSI for grasshopper mice (*Onychomys Arenicola*: median DSI = 0.31, mean DSI = 0.39 ± 0.29 s.d.; C57/BL6: median DSI = 0.29, mean DSI = 0.35 ± 0.26 s.d.; p = 0.01 Mann−Whitney Test).

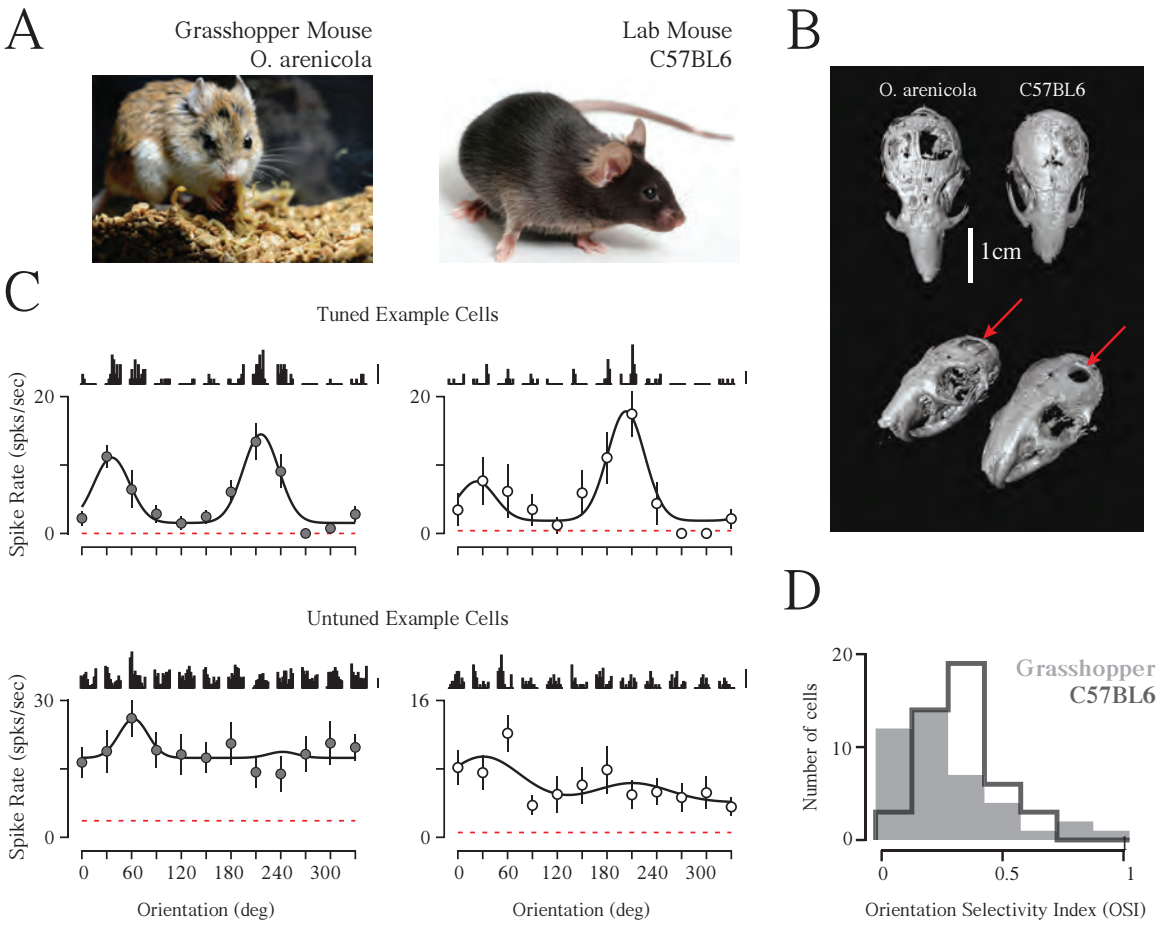

Figure 4.1: Orientation selectivity in primary visual cortex of predatory grasshopper and lab mice

(A) Carnivorous grasshopper mouse (*Onychomys Arenicola*) (*left*) (picture courtesy of AH Rowe) and C57/BL6 lab mouse (*right*). (B) CT scans of rodent skulls with craniotomy over primary visual cortex (V1, red arrows). (C) Example orientation tuning curves of spiking responses from neurons in V1. (D) Distributions of orientation selectivity index (OSI) in both rodents.

Electrophysiological recordings from individual V1 neurons revealed similar orientation and direction selectivity between grasshopper mice and inbred laboratory mice. Given this evidence, we next examined whether there is a functional columnar organization orientation preference in grasshopper mice. To quantify the degree of organization at the cellular level we performed *in vivo* two−photon calcium imaging using bulk loading (Appendix A) (Stosiek et al. 2003; Kerr and Greenberg 2005; Garaschuk et al. 2006; Golshani and Portera−Cailliau 2008). After identifying a portion of V1 by mapping receptive field locations with extracellular multi−unit recordings, hundreds of neurons were loaded with a calcium indicator in a 200−300 μm area (Figure 4.2A−B, *left*). To measure responses from labeled neurons we pseudo−randomly presented oriented drifting gratings (0 – 315 deg) while recordings changes in calcium fluorescence ($\Delta F/F$) at multiple depths 20−25 μm apart to image all layer 2/3 neurons labeled. Time courses of activity were generated for each cell by averaging pixels within each cell's mask across all imaging frames (Figure 4.2A−B, *left*) (Appendix A). Our visual response criterion required cells to have a significant response to at least one grating, relative to the blank or period matched to average grating luminance (ANOVA, $p<0.05$). Across all C57/BL6 lab mice (n = 5, aged 1 – 2 months) we identified a total of 1814 neurons, of which 1117 were visually responsive (62%). Across all grasshopper mice (n = 11, aged 8 – 24 months) we identified 2820 neurons, of which 1500 were visually responsive (53%).

In grasshopper mice, clear changes in calcium florescence were evident during presentation of orientation gratings (Figure 4.2A). Individual cell calcium responses could show upwards of a 20−40% change in florescence, visibly standing out from the lack of activity during blank periods, and also distinct from neuropil activity. In an example record shown in Figure 4.2A (cell 1), calcium responses during individual

trials and trial−average revealed a cell highly selective for a single oriented grating (180 degrees). Trial−averaged mean responses were also used to construct a tuning curve and fit with a double Gaussian (Appendix B) (Figure 4.2A, *right*). The selectivity of this particular neuron was evident in both a high OSI (0.54) and high degree of directional tuning (DSI = 1.0). Other neurons were equally selective but showed little direction tuning (Figure 4.2A, *cell 2*). Finally, a number of neurons exhibited little tuning preference altogether, despite being activated by the visuals stimulus (Figure 4.2A, *cell 3*). In general, individual neurons were distinct from the weakly active and untuned background neuropil change in florescence (Figure 2A, *neuropil*). All the same features of individual V1 neurons were also uncovered in C57/BL6 mice, as depicted by a few examples (Figure 4.2B).

Immediately, we noticed that neighboring cells could be tuned for a wide range of orientations (Figure 4.2A−B, *left*). As shown in an example imaging plane from a grasshopper mouse, nearby cellular orientation preferences could differ by >45 degrees, suggesting that rodents with predatory behavior lack a functional columnar architecture. In the lab mouse, previously characterized as having an random 'salt−and−pepper' organization of orientation preferences (Ohki 2007), we also observed that even a few neighboring cells could have vastly different orientation and direction preferences.

Large scale maps of grating direction (0 − 360 deg) and orientation (0 − 180 deg) preferences in individual neurons confirmed that both the predatory grasshopper mouse and C57/BL6 lab mouse lack a functional organization in layer 2/3 of V1 (Figure 4.3). In an example imaging session from a grasshopper mouse (Figure 4.3A), cellular masks were color−coded based on their preference for a particular direction (*top*) or orientation (*bottom*) and the intensity of the color were modulated according to the cell's OSI. For this illustration cellular locations were also collapsed across

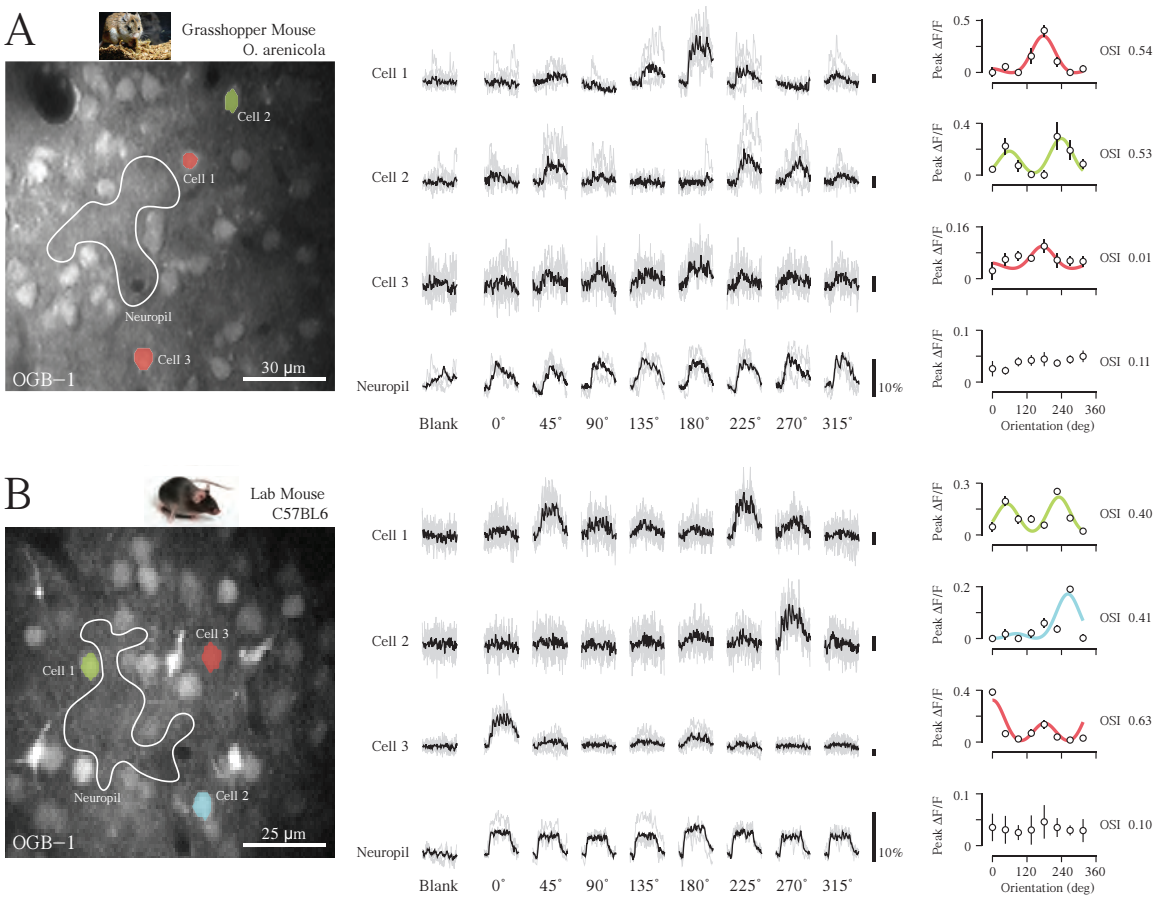

Figure 4.2: Two−photon calcium imaging of predatory grasshopper and lab mouse

(A) Example structural image of OGB−1 fluorescence collected from a grasshopper mouse (*left*). Three example V1 cell masks overlaid and color−coded based on preferences. Example neuropil mask also shown (white outline). Scale bar is 30 microns. Individual trial and mean changes in fluorescence (ΔF/F) to each visual stimulus and blank (mean luminance) periods shown for each example cell and neuropil (*middle*). Time course of responses is 2 sec and scale bars are 10 % ΔF/F. Mean ΔF/F across stimuli plotted for each cell (*right*). Data fit with double Gaussian and color−coded based for orientation preference. (B) Same as in (a) for example imaging session in a lab mouse.

multiple focal planes (from 190−270 microns). Both the map of directional preferences and orientation preference showed a dramatic lack of organization in the grasshopper mouse (Figure 4.3A), a hallmark of the random 'salt−and−pepper' map observed in the C57/BL6 lab mouse (Figure 4.3B). To quantify the similarity micro−organization in both animals we computed a circular−linear correlation coefficient (Batschelet 1981), comparing distance and the absolute value of the difference in orientation preference between pairs of cells (Figure 4.3C−D). Using only orientation selective cells (OSI > 0.1) within single imaging planes, we found no spatially dependent relationship between in predatory or inbred rodents (*Onychomys Arenicola*: r = 0.01, p = 0.70; C57/ BL6: r= 0.01, p =0.72; circular−linear correlation coefficient, Batschelet 1981). We also compared distributions of OSI between animals and found neurons from grasshopper mice were slightly less tuned but both exhibited the same extent of selectivity (Figure 4.3E−F), consistent with extracellularly−recorded data.

As further confirmation of homologous orientation maps in these rodents, we referred to our extracellular recordings of single units to compare stimulus preference and the distance between neuronal pairs. From tangential penetrations in grasshopper mice, we made recorded from several single units, evident from distinct isolated waveforms (Figure 4.4A) (Appendix A). After passing through the cortical tissue, we injected lesioning current (2 nA, 1−2 sec) to create a histological mark. In some animals (n = 4), we preformed a Nissl stain and were successful in recovering the lesion and electrode tract (Figure 4.4A, *left inset*), from which we were able to reconstruct our tangential penetration (Hubel and Wiesel 1963). Even within a single penetration, we observed a wide range of orientation preferences, depicted in this example by elongated bars and the computed preference from Gaussian fits of spiking responses (Figure 4.4A). Within each tangential penetration with at least 2 selective cells (OSI > 0.10), we computed the distance between cells and the absolute value of

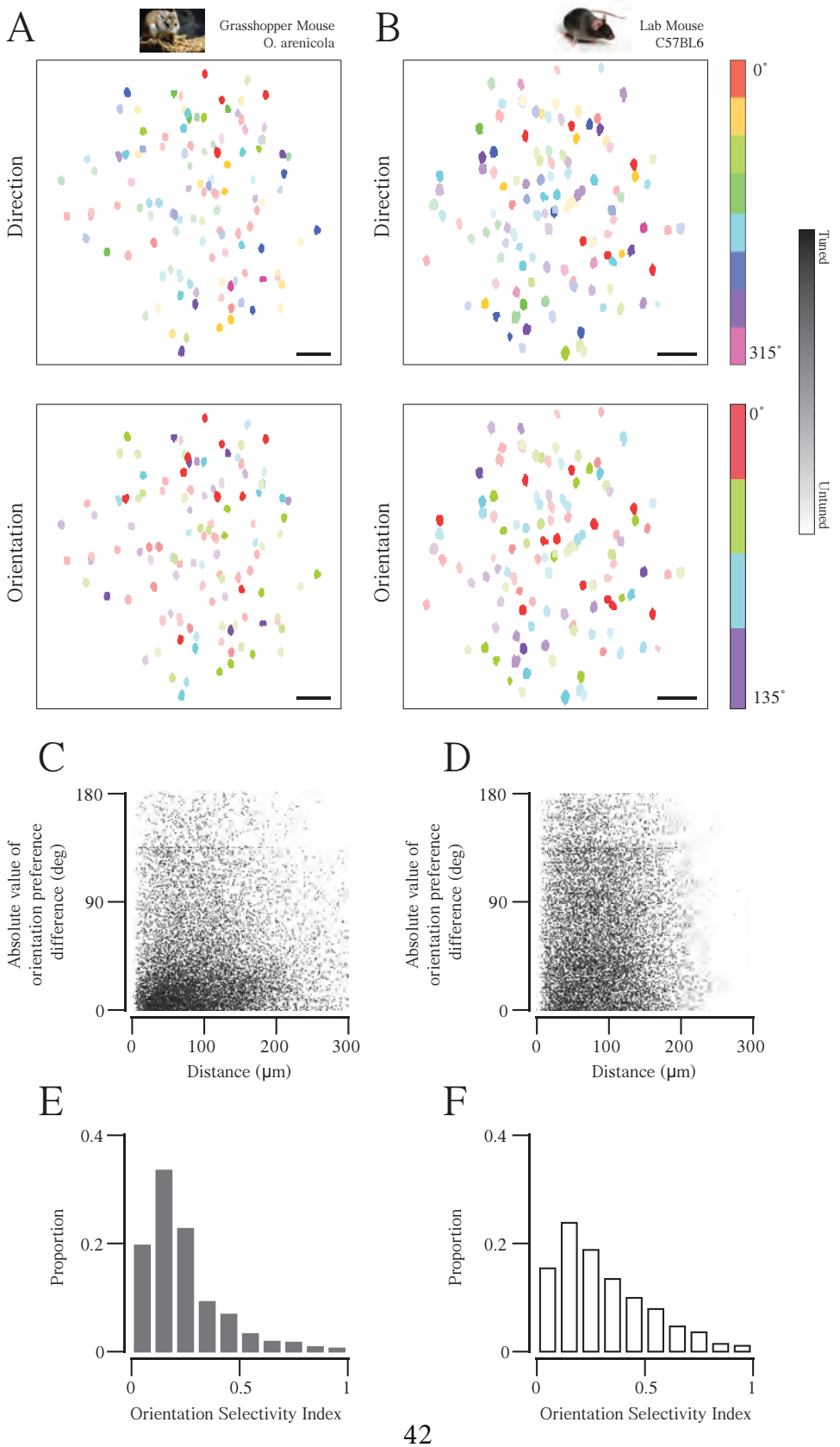
A
Grasshopper Mouse
O. arenicola
B
Lab Mouse
C57BL6
Direction
Orientation
0˚
315˚
135˚
Tuned
Untuned
C
D
Absolute value of orientation preference difference (deg)
180
90
0
0
100
200
300
Distance (μm)
E
F
Proportion
0.4
0.2
0
0.5
1
Orientation Selectivity Index

Figure 4.3: Random 'salt−and−pepper' micro−organization of direction and orientation preference in grasshopper and lab mice

(A) Example map of direction (*top*) and orientation (*bottom*) preferences in V1 neurons of a grasshopper mouse. Color intensity indicates individual cell orientation selectivity index (OSI). Map generated by collapsing across depth (190 − 270 microns). Scale bar is 50 microns. (B) Same as in (a) for imaging session in a normal mouse (depths 275 − 340 microns). (C−D) Relationship of distance between cells and absolute value of orientation preference difference for grasshopper and lab mice (respectively). Spatial distances computed within single focal planes. (E−F) Distributions of orientation selectivity index (OSI) from calcium responses for grasshopper and lab mice (respectively).

their orientation preference difference (Figure 4.4B). In agreement with individual examples and our two−photon measurements, we found no significant relationship between cell distance and preference dissimilarity from extracellular recordings in the *Onychomys Arenicola* grasshopper mouse ($r = 0.15$, $p = 0.67$, circular−linear correlation coefficient, Batschelet 1981). Here our electrophysiological measurements and two−photon microscopy have revealed a similar micro−organization of orientation preferences in the predatory carnivorous grasshopper mouse and C57/BL6 inbred lab mouse, that is, a random 'salt−and−pepper' map.

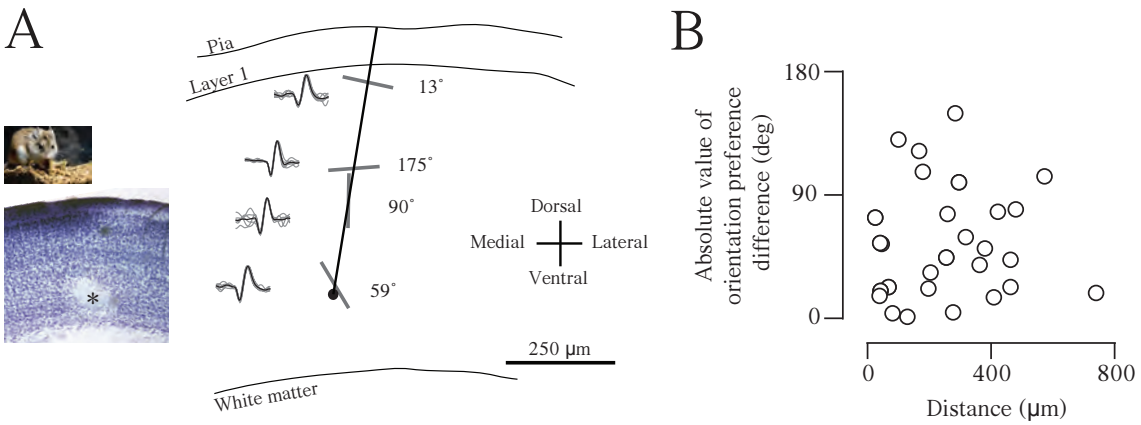

Figure 4.4: Relationship of orientation preference along tangential electrode recording tract in grasshopper mice

(A) Example extracellular recordings along reconstructed along tangential recording tract. Nissl stain of fixed brain slice with microelectrode current lesion (Asterix) shown in inset. Separate single unit recordings shown along tract with example action potential waveforms and oriented bars depicting orientation preferences. (B) Relationship of absolute value of orientation preference difference and distance between recordings within single penetrations.

DISCUSSION

All mammalian species posses a representation of the sensory periphery across the cortex, although this does not necessary generalize to centrally–computed properties of cortical neurons. Here we address whether a carnivorous rodent with predatory behaviors, the grasshopper mouse (*Onychomys Arenicola*), has a columnar organization of orientation selectivity in V1 using extracellular single unit recordings and two–photon calcium imaging. After establishing that neurons in primary visual cortex of grasshopper mice are orientation selective, we used two–photon imaging to reveal a random 'salt–and–pepper' map of orientation preference, similar to that of the C57/BL6 lab mouse. Across populations of both extracellular recordings and calcium responses, neurons exhibited similar tuning strength and orientation preference in both rodents, although those in the grasshopper tend to be slightly less selective. We confirmed a lack of columnar organization in V1 of the grasshopper mouse by reconstructing tangential extracellular electrode penetrations of single cells. This within species comparison definitely shows that the presence of a functional columnar organization in V1 is independent of an animal's behavior, specifically those exhibiting predatory versus scavenger behaviors.

There are a number of factors which could be responsible for the presence or absence of orientation columns in visual cortex. For example, there might be link between the locus of the emergence of orientation selectivity and the formation of a cortical map. In the mouse early visual system, orientation selectivity is evident in the cortical input (thalamic relay cells) (Scholl et al., 2013c) and this information is potentially inherited from retinal ganglion cells (Zhao et al.,2013). In comparison, the cat early visual system shows a strong emergence of orientation selectivity in the input to V1 simple cells. Unfortunately, the combination of intracellular subthreshold

measurements in V1 and extracellular measurements of thalamic spiking activity have only been reported for these two animal models. In the case of the grasshopper mouse, as for other non−primate mammals, it is unknown whether LGN cells already possess information about stimulus orientation. Receptive fields of LGN relay cells in primates are generally circular−symmetric, although a recent report revealed a subpopulation of koniocellular neurons in the marmoset LGN are selective for orientation (Cheong et al., 2013). A reason for the absence of these receptive properties in cat and primate ganglion cells could potentially be retinal specialization. In these animals, unlike rodents and lagomorphs, there exists a fovea or area−centralis: a high density region of ganglion cells which can provide fine spatial resolution in that retinotopic location. Perhaps then, as mammals evolved and gained a fovea, the presence of receptive field properties like orientation and direction selectivity were lost or migrated to the visual periphery. This would, of course, require concurrent reorganization of thalamocortical inputs in V1 to build the necessary circuit for transforming circular−symmetric receptive fields into orientated receptive fields.

The presence or absence of orientation columns may also be dependent on cortical evolution. It is not clear whether the emergence of orientation selectivity and the formation of a map result from convergent or divergent evolution. More specifically, V1 properties in cats and primates either results from convergent evolution or inheritance from a common ancestor. If a common ancestor possessed orientation selectivity and an orientation map, then the loss of these properties in rodents and lagomorphs should result from divergent evolution. To date, however, orientation selectivity has never been established in mammals from mammalian orders older than Rodentia or Lagomorpha. Perhaps measurements from animals such as the armadillo (Superorder: Xenarthra, Order: Cingulata) or northern shrew tenrec (Order: Afrosoricida) could help distinguish between these different hypotheses.

SECTION 2: *Integration of signals from the two eyes*

Chapter 5: Introduction

Section Overview

In this section, I focus on the integration of ocular inputs in the primary visual cortex (V1) of cats and mice. In both animals, signals from the two eyes are first combined in V1. For many mammals, binocular integration is an important first step in the development of stereopsis, the perception of depth from disparity or local spatial offsets between retinal images (Joshua, 1970; DeAngelis et al., 1995). Individual neurons in carnivores are shown to be sensitive to disparity in their spiking activity: some binocular stimuli elicit large spiking responses, while others reduce responses, relative to monocular stimulation alone (Hubel and Wiesel, 1962; Pettigrew et al., 1968; Ohzawa and Freeman, 1986).

Thus far, disparity selectivity has been only reported in primates and carnivores. Prior to the studies presented in this dissertation, binocularity in rodents had only been measured by ocular dominance: comparing the relative strength between responses evoked by visual stimulation of either eye (Hubel and Wiesel, 1962; Gordon and Stryker, 1996; Hanover et al., 1999; Tagawa et al., 2005; Hofer et al., 2006; Mrsic–Flogel et al., 2007). Given an emerging emphasis on mouse V1 and the advent genetic tools to dissect circuitry, the identification and characterization of binocular disparity selectivity in mice would provide a common cortical computation to study (Huberman and Niell, 2011). Further, it is important to compare similarities and differences of this receptive field property with more classical model systems, specifically cat V1.

In the first chapter of this section I use extracellular and intracellular electrophysiology to compare binocular disparity selectivity in cats, where ocular integration has long been established, and mice, where ocular integration had never

been investigated. Similar to cats, mouse V1 neurons are found to be sensitive to binocular disparity, albeit to a lesser degree, and can be described by a simple threshold−linear model based on monocular responses alone. Further, predictions from this simple model are confirmed by intracellular recordings from simple cells in mouse and cat V1. These measurements suggests that the integration of ocular signals in simple cells of visual cortex reflects a canonical computation shared between cat and mouse.

I next explore the disruption of binocular disparity tuning in both animals. In chapter 7, I induced strabismus (misalignment between the two eyes) during development in cats, which is known to cause increased monocularity in V1 (Hubel and Wiesel, 1965; Blakemore, 1976; Crewther et al., 1985; Chino et al., 1994; Roelfsema et al., 1994; Sengpiel and Blakemore, 1994; Sengpiel et al., 1994; Fries et al., 1997; Smith et al., 1997; Schmidt et al., 2004; Sengpiel et al., 2006; Ranson et al., 2012). Here I find a loss of disparity selectivity, particularly evident in simple cells, and a suppression of binocular responses potentially mediated by binocular inhibition. In chapter 8, I induced monocular deprivation in mice, which is known to cause an increase in the relative amount of synaptic input from each eye (Gordon and Stryker, 1996). Here, like for V1 neurons in strabismic cats, I find a loss of binocular disparity selectivity is the result of ocular dominance plasticity in mouse V1.

In the final chapter, I use available genetic tools in mice to explore how excitatory and inhibitory neurons in mouse V1 integrate binocular signals. Specially, I use a mouse model with paravalbumin−expressing (PV+) inhibitory interneurons expressing a red florescent protein in combination with two−photon imaging of a calcium reporter. Here I find that PV+ inhibitory neurons are more binocular but less disparity tuned than surrounding cortical neurons. Both the increased binocularity and weak disparity selectivity can be explained by inhibitory neurons integrating across the

functional properties of neighboring cortical neurons. Local integration by PV+ interneurons provides another canonical computation which could potentially explain the loss of disparity selectivity in strabismic cats and monocularly deprived mice.

Feed–forward model of binocular disparity selectivity

Building upon the original model of orientation selectivity proposed by Hubel and Wiesel (1962) (Fig. 2.1), the binocular receptive field properties of simple cells can be illustrated as shown in Figure 5.1. Sets of LGN relay cells from each eye, illustrated by spatially organized circular–symmetric receptive fields, synapse onto a single cortical neuron. In cat V1, this first stage of ocular integration is proposed to occur in simple cells of layer 4 (Ohzawa and Freeman 1986, Ohzawa, 1998), which receive direct excitatory thalamocortical input (Alonso et al., 2001; Chung and Ferster, 1998; Ferster et al., 1996; Levay and Gilbert, 1976; Reid and Alonso, 1995; Usrey et al., 1999). In carnivores and primates, V1 disparity selectivity fully emerges through the disparity–energy model, whereby tuning of complex cells in the superficial layers of cortex results from the summing and squaring of binocular simple cells (Ohzawa, 1998; Read et al., 2002). Simple cell disparity selectivity arises through the spatial arrangement of left and right eye receptive fields and a linear combination of ocular inputs. If receptive fields are completely overlapping, the resulting binocular disparity would be 0. However, if receptive fields were separated in visual space, this could drive a cortical cell's preference for a specific binocular disparity (Fig. 5.1). For example, two bars of the preferred orientation drifting across each receptive field at the preferred disparity would produce the largest synaptic input onto the cortical neuron. This preferred binocular input would be larger than the input from either eye alone or binocular stimulation at a non–preferred disparity (Fig. 5.1, *bottom*). In general, the

spatial configuration of stimuli in each eye, particularly the binocular disparity of the stimulus between the eyes, along with the specific receptive field configuration of each neuron may determine whether responses are enhanced during binocular stimulation (Ohzawa and Freeman, 1986).

Incorporating a simple biophysical mechanism can explain how V1 simple cell responses would be enhanced or suppressed by different binocular disparities. Passing the aggregate synaptic input through a threshold–nonlinearity (Priebe, 2008) could both obscure responses to non–preferred binocular disparities and greatly enhance responses to stimuli with the preferred spatial configuration, similar to the emergence of orientation selectivity (Finn et al., 2007) and direction selectivity (Priebe and Ferster, 2005). This mechanism is explored in detail within the framework of a linear model in Chapter 6 and the disruption of binocular disparity in Chapter 7.

Although the architecture of mouse V1 differs from that of cat, the presence of binocular simple cells presents the opportunity to study an emergent cortical computation, potentially arising through similar mechanisms as described by the disparity–energy model (Ohzawa, 1998). In particular, there is only a single cortical region receiving input from both eyes (e.g. absence of ocular dominance columns), simple and complex are heterogeneously organized across cortical layers (Niell and Stryker, 2008) and thalamocortical afferents innervate throughout cortical layers 1–4 (Antonini et al., 1999). Nonetheless, at least for simple cells, the same model of disparity selectivity could apply. Further, if such models describe disparity selectivity in mouse V1, it might serve as an early evolutionary model of binocularity observed in carnivores and primates.

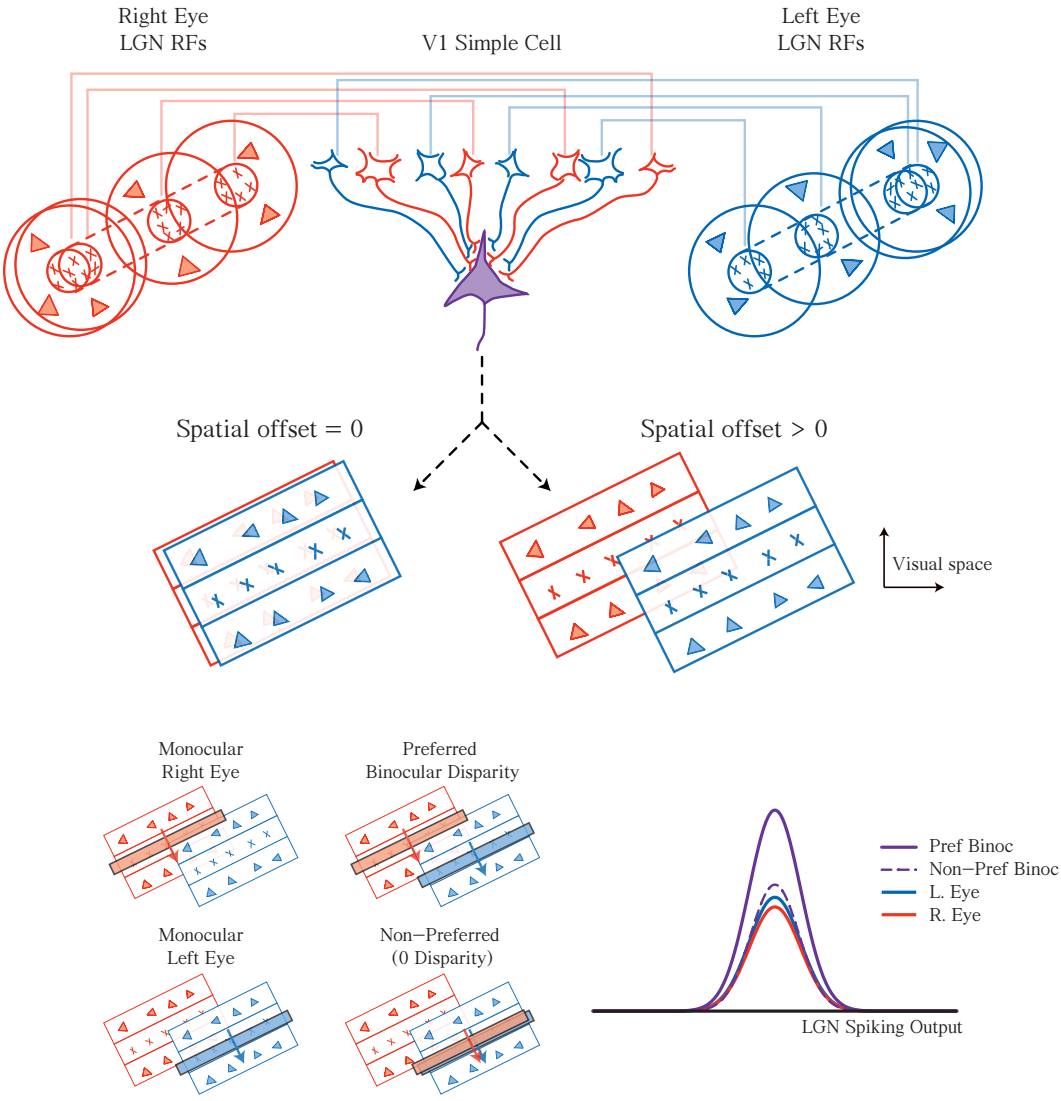

Figure 5.1: Feed−forward model of binocular disparity selectivity
LGN relay cells from each eye synapse onto the same cortical neuron. The aggregate input from each set of LGN cells generates a cortical receptive field in visual space. The spatial configuration between cortical receptive fields between each eye drive disparity preference. For example, a spatial offset of 0 between left and right receptive fields would result in a preference for 0 binocular disparity. Simultaneous activation of both sets of LGN relay cells in the preferred spatial configuration (*bottom*) can generate synaptic input onto the cortical neuron greater than stimulation of either eye alone or a non−preferred binocular disparity.

Chapter 6: Binocular integration and disparity selectivity in mouse and cat[1]

ABSTRACT

Signals from the two eyes are first integrated in primary visual cortex (V1). In many mammals, this binocular integration is an important first step in the development of stereopsis, the perception of depth from disparity. Neurons in the binocular zone of mouse V1 receive inputs from both eyes, but it is unclear how that binocular information is integrated and whether this integration has a function similar to that found in other mammals. Using extracellular and intracellular recordings, we demonstrate that mouse V1 neurons are tuned for binocular disparities, or spatial differences, between the inputs from each eye, thus extracting signals potentially useful for estimating depth. The disparities encoded by mouse V1 are significantly larger than those encoded by cat and primate. Interestingly, these larger disparities correspond to distances that are likely to be ecologically relevant in natural viewing, given the stereo−geometry of the mouse visual system. Across mammalian species, it appears that binocular integration is a common cortical computation used to extract information relevant for estimating depth. As such, it is a prime example of how the integration of multiple sensory signals is used to generate accurate estimates of properties in our environment.

INTRODUCTION

[1]Work includes unpublished data and work from a published article: Scholl B., Burge J., and Priebe N.J. (2013). Binocular integration in mouse primary visual cortex. *Journal of Neurophysiology* 109(12): 3013−3024.

To enable accurate estimates of behaviorally relevant properties of the environment, sensory systems integrate information from multiple sources. For example, in the visual system, signals from the left and right eyes are integrated to provide information about depth. In mammals, left and right eye signals first converge in V1. The different vantage points of the eyes create local spatial offsets in the retinal images, offsets known as binocular disparities. Binocular disparity changes with the depths of objects in the environment. Neurons that encode retinal image information relevant for estimating binocular disparity therefore provide information relevant for binocular depth perception (Barlow and Blakemore, 1967; Nikara and Bishop, 1968; Pettigrew et al., 1968; Blakemore, 1969; Joshua, 1970; Hubel and Wiesel, 1973). Binocular disparity selectivity can be observed in individual neurons; some binocular stimuli elicit large increases in responses, while others reduce responses, relative to monocular stimulation alone (Hubel and Wiesel, 1962; Pettigrew et al., 1968; Ohzawa and Freeman, 1986).

Disparity selective binocular neurons have been reported in many animals, including carnivores and primates. Such neurons have not, however, been reported in rodents. In recent years, mice have become an increasingly important model for the study of visual processing and cortical plasticity. Genetic techniques are now available to dissect underlying circuitry and its emergence during development. Here, we report evidence that mice have binocular neurons strikingly similar to those underlying depth perception in other mammals.

Mouse V1 is comprised of two zones: the monocular zone, where individual neurons respond only to the contralateral eye, and the binocular zone, where neurons respond to stimulation of either eye (Dräger, 1975; Wagor et al., 1980; Schuett et al., 2002; Kalatsky and Stryker, 2003). To date, binocularity in rodent V1 has been characterized by measuring ocular dominance: the difference in spiking response

strength elicited by stimulating each eye separately (Hubel and Wiesel, 1962; Gordon and Stryker, 1996; Hanover et al., 1999; Tagawa et al., 2005; Hofer et al., 2006; Mrsic−Flogel et al., 2007). Because ocular dominance is measured by independent stimulation of each eye it does not reveal the nature of binocular integration. It is therefore unknown whether mouse V1 neurons integrate binocular information that could provide a basis for stereoscopic depth perception (Huberman and Niell, 2011).

Mouse binocularity may be unrelated to binocular disparity selectivity and may reflect the use of independent signals from each eye to improve signal detection (Legge, 1984; Anderson and Movshon, 1989; Pardhan and Rose, 1999; Simpson et al., 2009). Our records, however, are inconsistent with the hypothesis that binocularity exists solely to improve signal detection. Rather, our records indicate that binocular neurons in mouse V1 are selective for binocular disparity. A detailed comparison of mouse and cat disparity selectivity reveals that mouse neurons are modulated less by binocular disparity. A simple threshold−linear model based on monocular responses alone accounts for much of the binocular responses in both mouse and cat V1 simple cells. Predictions of this simple model are confirmed in simple cells from both animals using intracellular recordings to reveal the subthreshold input. These recordings demonstrate that a common pattern of binocular integration occurs in V1 across mammalian species.

RESULTS

Neuronal responses to binocular stimulation in mouse V1

To explore binocular integration in mouse V1 and compare it to that found in cat V1, we made extracellular single−unit recordings in anesthetized animals. In mice, we first mapped V1 to find the binocular zone. We selected receptive field locations

within the central 30 degrees of the visual field, where there is clear overlap of left and right eye projections. In cats, recordings were made from the central 15 degrees of vision, where most neurons receive binocular inputs. Here we report extracellular records from 68 mouse V1 neurons and 69 cat V1 neurons. Drifting sine−wave gratings were presented in both monocular and binocular conditions. Gratings were presented binocularly by placing a mirror in front of one eye so that each eye could be stimulated by a visual stimulus presented on a separate monitor (Fig. 6.1A).

Mouse V1 neurons in the binocular zone are known to receive inputs from both eyes but it is unknown how these neurons respond to binocular stimulation. We first compared how neurons responded to drifting gratings during monocular and binocular stimulation, using the same drifting gratings since neuronal stimulus preferences for each eye are matching (Wang et al., 2010) (Appendix A). For some cortical neurons, binocular stimulation led to a dramatic response enhancement relative to the responses elicited by monocular stimulation (Fig. 6.1B *left*). For other neurons, binocular stimulation resulted in a profound response suppression, relative to the responses evoked monocularly (Fig. 6.1B *right*). Interestingly, similar patterns of responses were observed even for neurons that would be considered monocular from their responses to each eye alone (Fig. 6.1B *bottom*).

If binocularity in mouse V1 acted solely to increase signal detection sensitivity, binocular stimuli should be more detectable than monocular stimuli by a factor of $\sqrt{2}$ (Legge, 1984; Anderson and Movshon, 1989; Pardhan and Rose, 1999; Simpson et al., 2009). Because the error of n measurements decreases in proportion to $\sqrt{n}$, we expect sensitivity to increase by $\sqrt{2}$ using two eyes. We tested whether there was increased sensitivity for binocular stimulation compared to monocular (contralateral) stimulation across all mouse records by computing the changes in signal detection sensitivity (d')

for monocular (contralateral) and binocular stimulation (Appendix B). Binocular and monocular response detection sensitivity was similar on average across mouse V1 neurons ($d'_{binocular}$ = 1.12 ± 0.55 SD, d'_{contra} = 1.02 ± 0.61 SD, $p < 0.25$). The ratio of d' for monocular and binocular stimulus conditions for V1 neurons (geometric mean = 1.10 ± 0.22 SD) was less than expected ($\sqrt{2}$) under a signal detection improvement hypothesis and was highly variable across neurons (Fig. 6.1C). These results suggest that binocularity in mouse V1 neurons does not function solely to increase signal detection.

The observed diversity in d' values may be due to binocular receptive fields that compare between inputs from each eye and are selective for binocular disparity. For some neurons the particular binocular stimulus employed is matched to their binocular disparity preference and thus evoked response enhancement (62%). For other neurons, the binocular stimulus is mismatched to their binocular disparity preference and suppressed responses (34%). As in carnivores and primates, the spatial configuration of stimuli in each eye, particularly the binocular disparity of the stimulus between the eyes, along with the specific receptive field configuration of each neuron may determine whether responses are enhanced or suppressed during binocular stimulation (Ohzawa and Freeman, 1986).

Our analysis of d−prime is meant to mimic a natural detection task, in which the stimulus would activate some neurons more than others, depending on the depth of the object. If we find a binocular stimulus that best evokes a response for each neuron, the ratio of d' for monocular and chosen binocular conditions increases substantially (geometric mean = 1.8 ± 0.78 SD). On the other hand, if we select the binocular condition evoking the weakest response in each neuron, the d' ratio declines (geometric

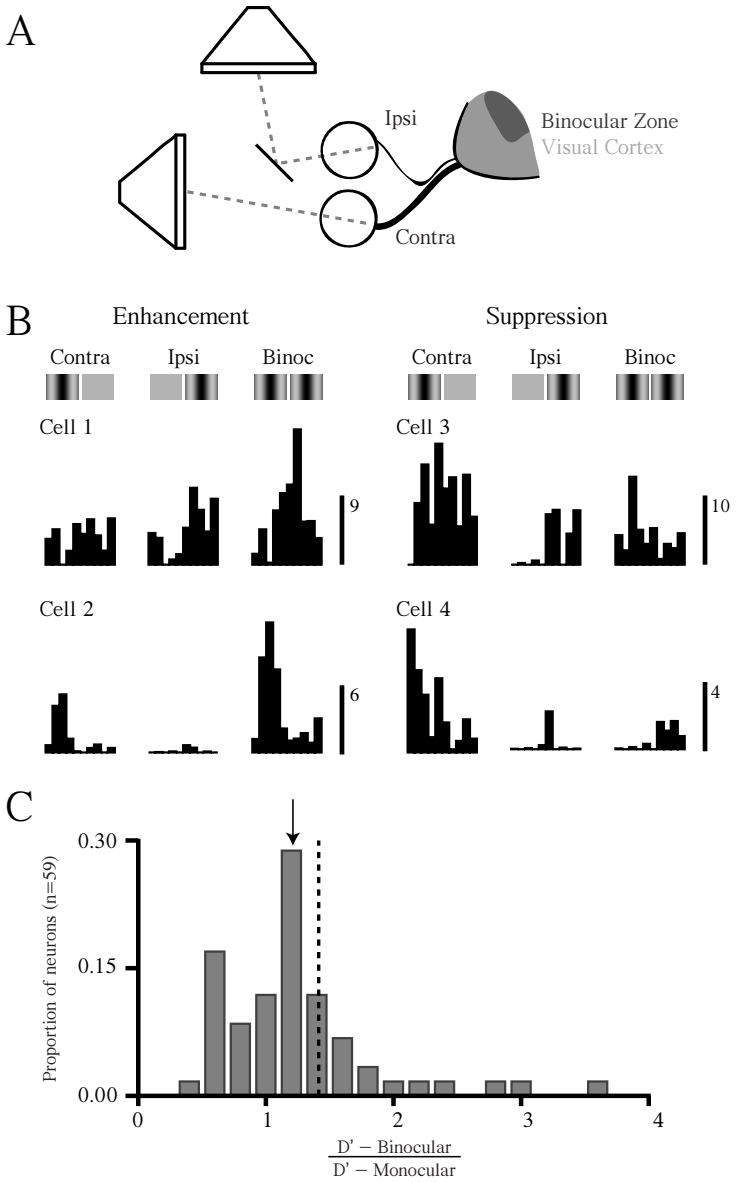

Figure 6.1: Dichoptic stimulation in mouse V1 neurons shows enhancement and suppression

(A) Schematic for dichoptic stimulation and organization of binocular zone in mouse primary visual cortex. (B) Mouse V1 neurons responding to contralateral and ipsilateral stimulation show enhanced (left) or suppressed (right) binocular responses. Scale bars indicate spike rate (spk/sec). (C) Distribution of ratios of response detection sensitivity of mouse V1 neurons under binocular and monocular stimulation. Arrow indicates geometric mean and dashed red line shows expectation for dichoptic detection sensitivity.

mean = 0.82 ±0.54 SD). Changes in d' ratios measured by tailoring the spatial configuration of binocular stimuli for each neuron, suggest that the neurons are selective for binocular disparity and indicate that it is important to measure how mouse binocular neurons respond to a range of binocular disparities.

Binocular cues for depth in mice

The response properties of binocular neurons in mouse V1 should be strongly influenced by signals that stimulate the visual system, and the tasks for which those signals are used in natural viewing (Burge & Geisler, 2014). Here, we consider how the response properties of binocular neurons might be shaped by natural signals, if binocular neurons in mouse V1 support binocular depth perception (i.e. stereopsis). Canonical V1 binocular neurons are selective for disparity but are not invariant; that is, their responses are strongly modulated both by disparity and spatial frequency content. Thus, the V1 population should encode the retinal image information relevant for estimating disparity. Subsequent decoding (i.e. disparity estimation) may result in neural populations that are both selective and invariant.

Here, we show how the stereo-geometry of the mouse visual system (Fig. 6.2A) can be used to predict the spatial frequency selectivity of mouse binocular neurons that also, surprisingly, corroborate previous neurophysiological measurements of these neurons (Fig. 6.2C) (Niell and Stryker, 2008; Vreysen et al., 2012). The stereo-geometry of the mouse visual system determines the range of binocular disparities that may stimulate the mouse visual system, and therefore, may be useful to encode.

Binocular disparities, the local differences between the retinal images, arise due to the different viewing positions of each eye. The binocular disparity (δ), in visual angle, of corresponding points in the left and right eyes is defined as:

$$\delta = \alpha_L - \alpha_R \qquad (1)$$

where α_L and α_R are the angles between the retinal projections of a target and the preferred binocular locus (defined below) in the left and right eyes. The functional relationship between binocular disparity and depth, under the small angle approximation, is given by:

$$\delta = \frac{-\Delta I}{\left(d_{pref} + \Delta\right) d_{pref}} = \frac{-I}{\left(\frac{d_{pref}}{\Delta} + 1\right) d_{pref}} \qquad (2)$$

where I is the inter−ocular distance, d_{pref} is the preferred binocular viewing distance, and Δ is the depth of an object. Depth is defined as the difference between the object and the preferred viewing distance (d_{pref}): $\Delta = d_{object} - d_{pref}$, where d_{pref} is the viewing distance at which a target will project onto the retinas at the preferred binocular locus, the corresponding retinal locations where disparity estimates are most precise. In primates and carnivores, that binocular locus is the fovea or area centralis, and the preferred binocular viewing distance is the current fixation distance. Mice do not have a well−defined fovea, so it is not straight−forward to determine the viewing distance at which disparity would be encoded with the greatest precision.

It is possible, however, to place constraints on the preferred binocular viewing distance by considering three facts about mouse vision. First, mice typically have +10.0 diopters of refractive error (la Cera et al., 2006), which means that targets positioned at 10 cm will be in best focus. Second, mice are largely unable to change the refractive

power of their eyes (Chalupa and Williams, 2008). Third, mice have limited eye movements (Chalupa and Williams, 2008). Together, these facts about the mouse visual system suggest that the preferred binocular viewing distance is fixed straight head at a distance of 10 cm (Fig. 6.2A,B). For the analysis that follows, we assume that this distance is the preferred operating range for mouse binocular vision. Note that because of the difficulty refracting small eyes, there may be an effective refractive error somewhat different than 10 diopters. Modest changes in this value do not qualitatively affect our conclusions.

To determine the widest range of disparities that could potentially stimulate the mouse visual system, we first consider the largest uncrossed disparity that could be formed in the mouse visual system. The largest uncrossed disparity is created by an object at infinity. With a mouse inter−ocular separation of 1 cm and a preferred binocular viewing distance of 10 cm, the largest possible uncrossed disparity is −5.7 deg (eq. 2). Uncrossed disparities with magnitudes larger than −5.7 deg are 'impossible' disparities because they could never be generated in natural viewing. Assuming symmetric disparity encoding (±5.7 deg), disparity would provide mice useful binocular depth information over a range of distances from 5 cm to infinity. This range of disparities is significantly larger than the disparity ranges encoded by the primate and cat visual systems (Fig. 6.2B), but it is the range that provides binocular depth information over a useful range of distances for mice.

The range of disparities that the mouse visual system is stimulated with in natural viewing can be used predict the range of spatial frequencies that disparity sensitive neurons are selective for. To determine the spatial frequencies that carry useful information about disparities between ±5.7 deg, we examined the disparity signals that would result from a binocularly viewed high contrast luminance edge positioned at or behind the preferred binocular viewing distance. We use a binocularly

viewed edge because each eye's image of the edge has a spatial frequency spectrum that approximates the 1/f contrast fall−off that is characteristic of natural images (Field, 1987). The difference between the left and right eye images of the edge is the binocular difference signal. At each spatial frequency, the binocular difference signal is sinusoidal with contrast amplitude given by:

$$A_B\left(f\middle|\delta_k\right)=\sqrt{A_L(f)^2+A_R(f)^2-2A_L(f)A_R(f)\cos\left(2\pi f\delta_k\right)} \qquad (3)$$

Here f is the spatial frequency, δ_k is a particular disparity, A_L and A_R are the left and right eye retinal amplitudes, and $A_B(f \mid \delta_k)$ is the amplitude of the binocular difference signal (Burge & Geisler, 2012). Fig. 6.2C shows the amplitude of this difference signal for seven disparities (−6 to 0 deg) spanning the range of uncrossed disparities to which mice are predicted to be sensitive. The shape and magnitude of the spectra differ systematically as a function of disparity between 0.01 and 0.1 cpd. At higher spatial frequencies, the binocular difference signals are barely distinguishable. Thus, the pattern of binocular contrasts in this spatial frequency range (0.01 to 0.1 cpd) contains the information that is most useful for estimating disparities between −5.7 and 5.7 deg.

This analysis suggests that individual neurons are insufficient to accurately estimate binocular disparity from natural stereo−images. Individual V1 binocular neurons are sensitive only to a narrow band of frequencies (e.g. 1.5 octaves), whereas disparity information is contained in the pattern of binocular contrast across spatial frequencies. Thus, in natural images, disparity must be estimated from the pattern of population activity of many V1 neurons with different spatial frequency preferences.

Interestingly, the spatial frequency range that carries useful disparity information (0.01 to 0.1 cpd) is very similar to the spatial frequency range that mouse

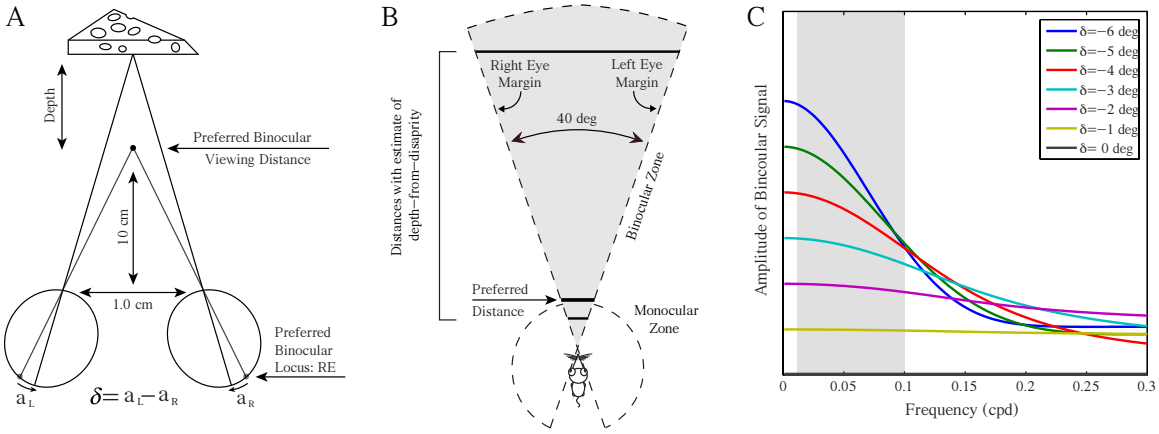

Figure 6.2: Stereo−geometry, spatial frequencies with disparity information in mouse

(A) Stereo−geometry of the mouse visual system. A point on an object of interest projects to the left and right eyes. If the object is not at the preferred binocular viewing distance, binocular disparity results. The preferred binocular locus is the pair of retinal locations where disparity estimates are most precise. (B) Mouse monocular and binocular visual fields. Mouse binocular visual fields subtend ~40 deg (Heesy, 2004). Each monocular visual field subtends ~180 deg. (C) The spatial frequencies that are useful for estimating disparities in the predicted range. Amplitude spectra of binocular difference signals (eq. 3) after being filtered by 1.5 octave bandwidth filters. Shaded region indicates the spatial frequencies (0.01 to 0.10 cpd) that provide the best information for estimating the disparities that are predicted to be ecologically relevant for mouse stereopsis. Higher spatial frequencies provide little information about disparity.

visual cortex selects for (Niell and Stryker, 2008; Vreysen et al., 2012). We therefore used drifting sine−wave gratings of low spatial frequency (0.03 − 0.06 cycles per deg) to characterize disparity selectivity of individual neurons in mouse V1.

Binocular integration in mouse and cat

We observed a variety of response patterns from V1 neurons in mouse and cat under binocular stimulation. The spiking activity of individual neurons was measured in response to eight binocular disparities (Fig. 6.3A, left column), to monocular stimulation of the left and right eyes, and to no stimulation (Fig. 6.3A, right column). Spiking activity to each stimulus was cycle−averaged and the peak response amplitude (F1+DC, Appendix A) was measured for each condition (Fig. 6.3A, bottom right panel). We initially classified cells as simple and complex on the basis of the relative response modulation to monocularly−presented drifting gratings (Appendix A). Among simple cells we observed a variety of responses patterns which indicate little relationship between ocular dominance and disparity tuning. The first subset of simple cells was characterized as binocular based on their ocular dominance (Fig. 6.3A,B). Responses from these binocular simple cells were modulated by disparity during binocular stimulation. The second subset of simple cells were characterized as monocular by ocular dominance. Surprisingly, responses from these simple cells were also modulated by binocular disparity (Fig. 6.3C,D). A third subset of simple cells were characterized as binocular by ocular dominance, but did not show a response modulation to the binocular stimulus (Fig. 6.3E,F). These three subsets of simple cells show that binocularity based on ocular dominance and binocular disparity are not necessarily linked (LeVay and Voigt, 1988; Chino et al., 1994).

Complex cells of mouse and cat showed the same variety of response patterns as simple cells. Neurons that were classified as either binocular or monocular by ocular dominance could exhibit disparity tuning (Fig. 6.4A−D). In addition, we found complex cells that appeared binocular by ocular dominance, but exhibited little response modulation to changes in binocular disparity (Fig. 6.4E,F). The lack of relationship between binocularity defined by ocular dominance and by disparity sensitivity shown in these example neurons suggests that these two measures of binocularity reflect distinct neural computations.

To quantify the relationship between binocularity defined by ocular dominance and binocularity defined by disparity selectivity, we quantified the degree of binocularity for both monocular and binocular stimulus conditions across our population of neurons. For ocular dominance we used the spiking ocular dominance index (ODI_R) which compares the degree to which neurons respond to the contralateral and ipsilateral eye based on the monocular stimuli (Appendix B). ODI_R values of 0 indicate equal responses to each eye (Figs. 6.3A,B, 6.4A,B), while values of −1 and 1 indicate the dominance of the ipsilateral and contralateral eyes (Figs. 6.3C,D, 6.4C,D). As previously shown, mouse V1 neurons exhibit a pronounced ocular dominance bias for the contralateral eye (mean $ODI_R = 0.35 +/- 0.54$, s.d.) (Gordon and Stryker, 1996) (Fig. 6.5A).

To quantify the degree of response modulation induced by binocular stimulation we computed a disparity selectivity index (DSI) which describes the degree of response modulation evoked by changes in spatial phase for binocular stimuli. The disparity selectivity index is based on similar measurements of orientation selectivity (Ringach et al., 2002; Tan et al., 2011; Appendix B). DSI values range between 0 and 1, where 0 indicates a lack of modulation by binocular disparity (Figs. 6.3E,F, 6.4E,F) and higher values indicate greater degrees of modulation by disparity (Figs. 6.3A−D, 6.4A−D).

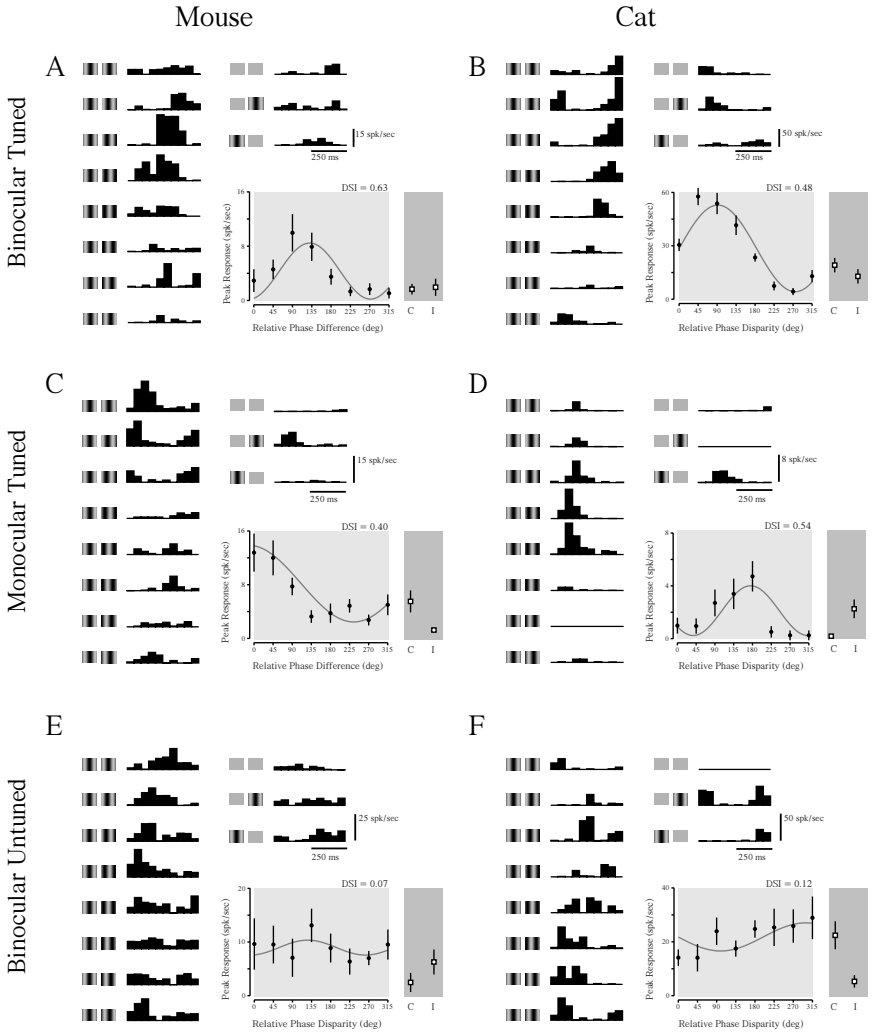

Figure 6.3: Simple cell disparity selectivity in mouse and cat

(A) Binocular neurons in mouse V1 show a modulation of peak response to different spatial phase combinations of binocular stimuli. Binocular cycle−averaged responses are shown in the left column. Illustration of each stimulus condition is shown next to each response. Spontaneous activity and monocular responses are shown in the right column. Binocular tuning is plotted from peak response amplitudes of binocular responses (black dots), alongside monocular responses (squares). (B) Same as in A for a neuron in cat V1. (C) Same as in A for a monocular neuron. (D) Same as in C for a neuron in cat V1. (E) Neurons in mouse V1 can show no modulation in response amplitude despite responding to stimulation of either eye. (F) Same as E for a neuron in cat V1.

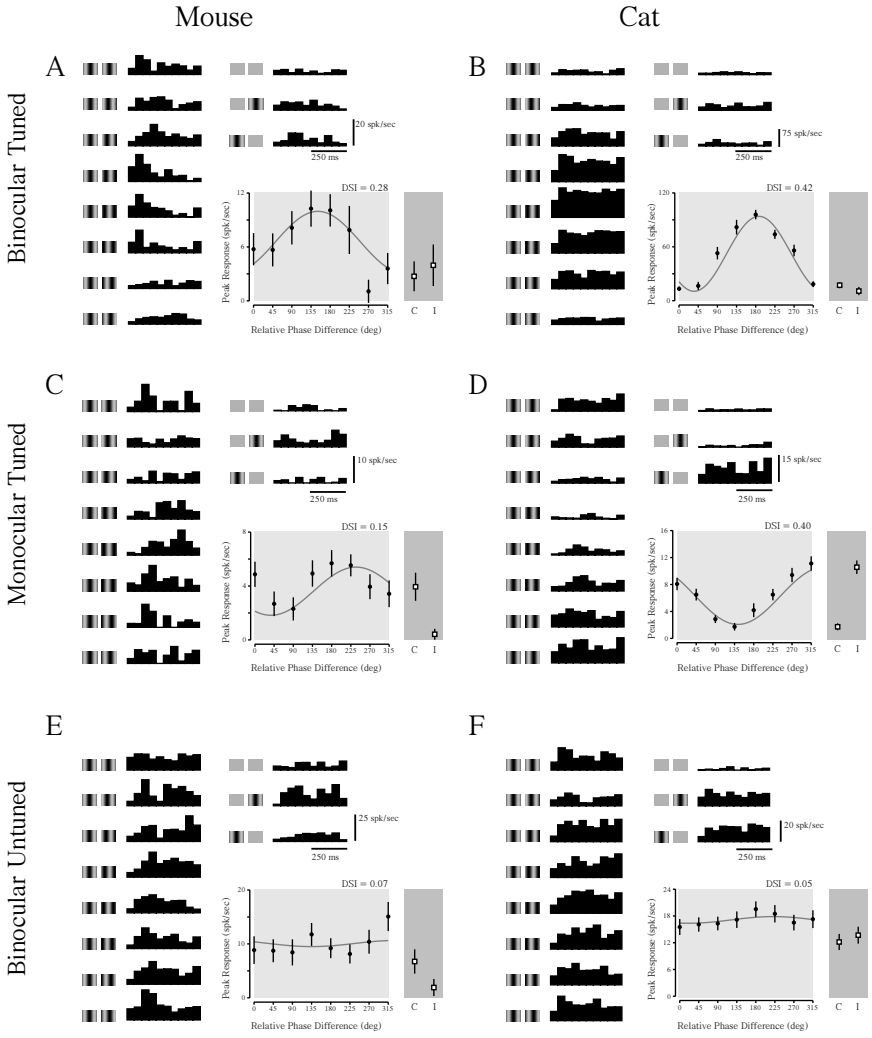

Figure 6.4: Complex cell disparity selectivity in mouse and cat
(A–F) Same layout as in Figure 6.3 for complex cells.

Mouse V1 neurons are modulated by binocular stimulation, exhibiting a similar range of DSI values to that found in the cat (mouse DSI range = 0 to 0.7, cat range = 0 to 0.75). On average, however, mouse neurons were modulated less by disparity than cat neurons (mouse: mean DSI = 0.18 ± 0.18 SD; cat: mean DSI = 0.30 ± 0.18 SD, significant difference between mouse and cat, $P < 0.001$, t−test). Across mouse V1 neurons, there was no significant difference in DSI values between simple and complex cells (Fig. 6.5, light and dark symbols, respectively; Student's t−test, $p < 0.4$), but across cat neurons, there was a difference between these classes of cells (simple cell mean = 0.37 ± 0.18, complex cell mean = 0.2 ± 0.14, Student's t−test, $p < 0.005$), which has been reported previously (Chino et al., 1994). Computing disparity selectivity with only the modulation response component in simple cells and mean response component in complex cells did not change the difference in DSI between cell classes (simple cell mean = 0.36 ± 0.24, complex cell mean = 0.22 ± 0.17, Student's t−test, $p < 0.005$).

To compare the degree of binocularity based on ocular dominance to the degree of disparity selectivity we compared the ODI_R to the DSI metrics. We first transformed the ODI_R by taking the absolute value so that a value of 0 indicates a binocular neuron and 1 a monocular neuron. No systematic relationship is evident between the two metrics in the mouse (Fig. 6.5A, slope = 0.01 ± 0.07, principal component analysis with bootstrapped standard error, Sokal and Rohlf, 1995) or in the cat (Fig. 6.5B, slope = 0.08 ± 0.09, principle component analysis with bootstrapped standard error, Sokal and Rohlf, 1995) (LeVay and Voigt, 1988; Chino et al., 1994). The failure to observe a relationship between the absolute value of ODI_R and DSI might be due to the nonlinear relationship between the inputs a neuron receives and its spiking ouput. For example, a neuron could receive strong synaptic inputs from both eyes, but because of spike

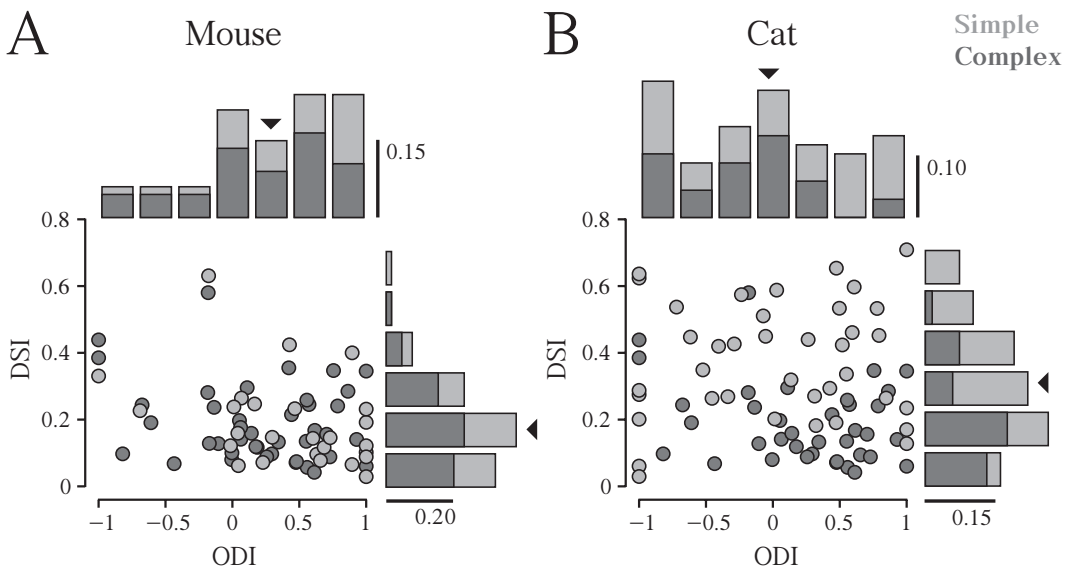

Figure 6.5: Relationship between ocular dominance and disparity selectivity
(A–B) ODI_R and DSI plotted for each simple (light gray) and complex (dark gray) cell in mouse V1 (A) and cat V1 (B). Distributions for each index are shown along the same axis. Scale bars indicate proportion of cells in histograms.

threshold only monocular stimulation to the dominant eye elicits a spiking response. In this case, the spiking ODI_R value would be near 1, indicating monocularity, despite receiving input from both eyes (Priebe, 2008). Though our extracellular recordings revealed no relationship between the degree of disparity selectivity and ocular dominance there may nonetheless exist a relationship between these two metrics at the subthreshold level.

Threshold–linear model of the binocular disparity tuning

Our observation that mouse V1 neurons are sensitive to binocular disparity suggests that similar computations are being performed in V1 across mammals. This raises the question about how comparisons between left and right eye inputs occur. The dominant framework for describing how disparity selectivity arises in primate and cat V1 is the disparity–energy model, which proposes that binocular complex cells responses result by summing and squaring binocular simple cell outputs (Ohzawa, 1998) (but see Burge & Geisler, 2014). In simple cells, binocular integration is modeled as a linear combination of left– and right–eye signals, followed by an output threshold nonlinearity. If the computation underlying disparity selectivity in mouse simple cells is the same as in the cat, the same model should provide accurate fits to mouse disparity tuning curves. Further, this model could provide predictions of the synaptic inputs underlying monocular and binocular responses, which may reveal a relationship between ocular dominance and disparity selectivity that is not evident in spiking responses (Fig. 6.5).

To determine how effectively this model can account for the responses of mouse and cat V1 simple cells, we fit a threshold–linear model to the monocular and binocular responses of individual neurons (Appendix B). The gain represents the slope

of the supra−threshold input to spiking transformation. The summed input from each eye is then passed through a threshold nonlinearity to generate a predicted spike rate. This model provides good fits to both the response amplitude and phase that occurs in both mouse and cat V1 neurons for both monocular and binocular stimulation, even for neurons that are classified as monocular by ODI_R (Fig. 6.6A, mouse, $r^2 = 0.68$; Fig. 6.6B, cat, $r^2 = 0.71$). To account for the binocular response of these neurons, synaptic input from both eyes is required. The threshold−linear model (Appendix B) fits these extracellular data by using a substantial degree of nonpreferred eye synaptic input, but not so much that a spiking response is observed to monocular stimulation (Fig. 6.6A,B, monocular column). Binocular stimulation, however, reveals the impact of the synaptic input from the nonpreferred eye (Fig. 6A,B, binocular column). Many mouse V1 neurons appear to be biased for the contralateral eye (Fig. 6.6A, monocular column), but weak input from the ipsilateral eye nonetheless strongly influenced responses during binocular stimulation (Fig. 6.6A, binocular column). The threshold−linear model is also able to capture simple cell disparity tuning from neurons that were classified as binocular by ocular dominance (data not shown).

In simple cells, the threshold−linear model accounted for binocular responses and disparity tuning in both mouse ($r^2 = 0.33 \pm 0.35$ SD) and cat ($r^2 = 0.60 \pm 0.52$ SD). To illustrate how well the model accounted for disparity selectivity, we plotted the predicted spiking responses (Fig. 6.6, *middle*) against the measured spiking responses (Fig. 6.6, *top*) for all simple cells, color−coded by the absolute value of ODI_R (gray shading, Fig. 6.7A,B). In simple cells, the threshold−linear model predicts the measured spiking responses, so much of the data lies along a unity line. The threshold−linear model is better able to capture the responses of cat than mouse simple cells, but this discrepancy is partly due to the overall differences in response modulation with

disparity: for mouse neurons with DSI greater than 0.15, the threshold−linear model captures far more of the response variance ($r^2 = 0.45 \pm 0.25$ SD).

We also fit the complex cell responses using the threshold linear model. While the linear−threshold model could predict some binocular responses in mouse ($r^2 = 0.24 \pm 0.43$ SD), it was a poor predictor of response modulation in cat ($r^2 = 0.07 \pm 0.58$ SD). This model predicts response modulation to drifting gratings, while complex cells, by definition, do not modulate to drifting gratings. At the level of spiking responses we did not observe a relationship between these two metrics of binocularity (ODI_R and DSI) (Fig. 6.8A, mouse: slope $= -0.07 \pm 0.08$; cat: slope$=-0.12 \pm 0.12$, principle component analysis with bootstrapped standard error, Sokal and Rohlf, 1995), but such a relationship potentially exists at the subthreshold level and could be obscured in our extracellular measures. A strong prediction of the threshold−linear model is that a greater similarity in the gain of inputs from each eye, quantified by ODI based on synaptic inputs (ODI_V), should lead to a greater degree of disparity selectivity. To examine whether a relationship between the ocular dominance binocularity and disparity selectivity exists at the subthreshold level, we defined ODI_V as ocular dominance based on the synaptic input gains from the threshold−linear model (Appendix B). This comparison of ODI_V and DSI reveals a clear relationship across V1 simple cells (mouse: slope $= -0.30 \pm 0.12$; cat: slope $= -0.48 \pm 0.14$, principle component analysis with bootstrapped standard error, Sokal and Rohlf, 1995). This finding indicates that, at a subthreshold level, the amount of input between the two eyes in response to a monocular stimulus is related to response modulation during binocular stimulation (Fig. 6.8B).

We considered whether the difference in the degree to which binocular disparity modulated the responses in mice and cats might be due to the differences in the

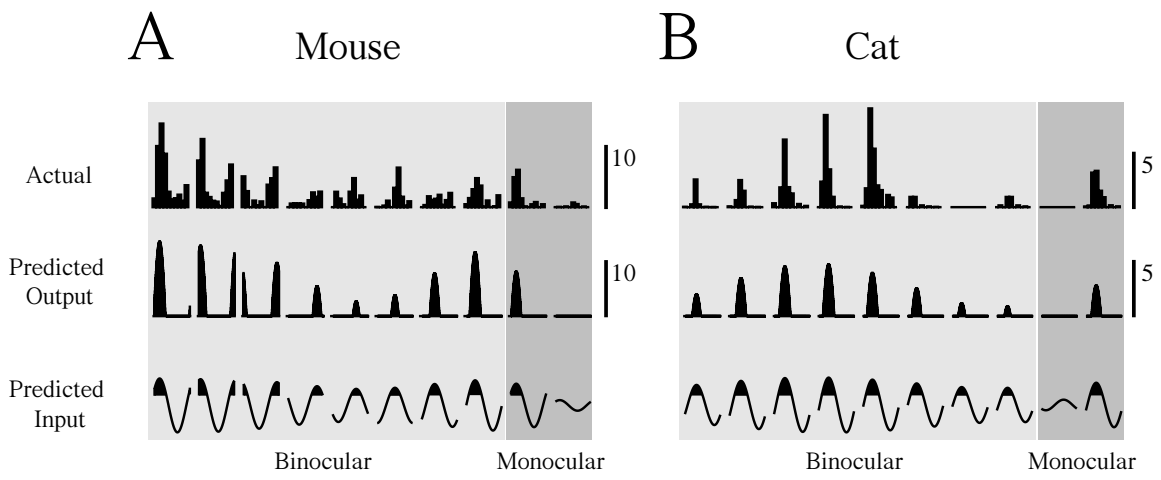

Figure 6.6: A simple linear model predicts responses to dichoptic stimulation
(A–B) Estimating input from each eye and using a threshold nonlinearity to model monocular responses in simple cells generates accurate predictions of binocular responses in mouse and cat. Example cells from Figures 6.3C (A) and 6.3D (B) are shown. Measured responses (top) are shown with predicted responses (middle) and predicted subthreshold inputs (bottom) for both binocular and monocular responses. Scale bars indicate spike rate (spk/sec) for measured and predicted output.

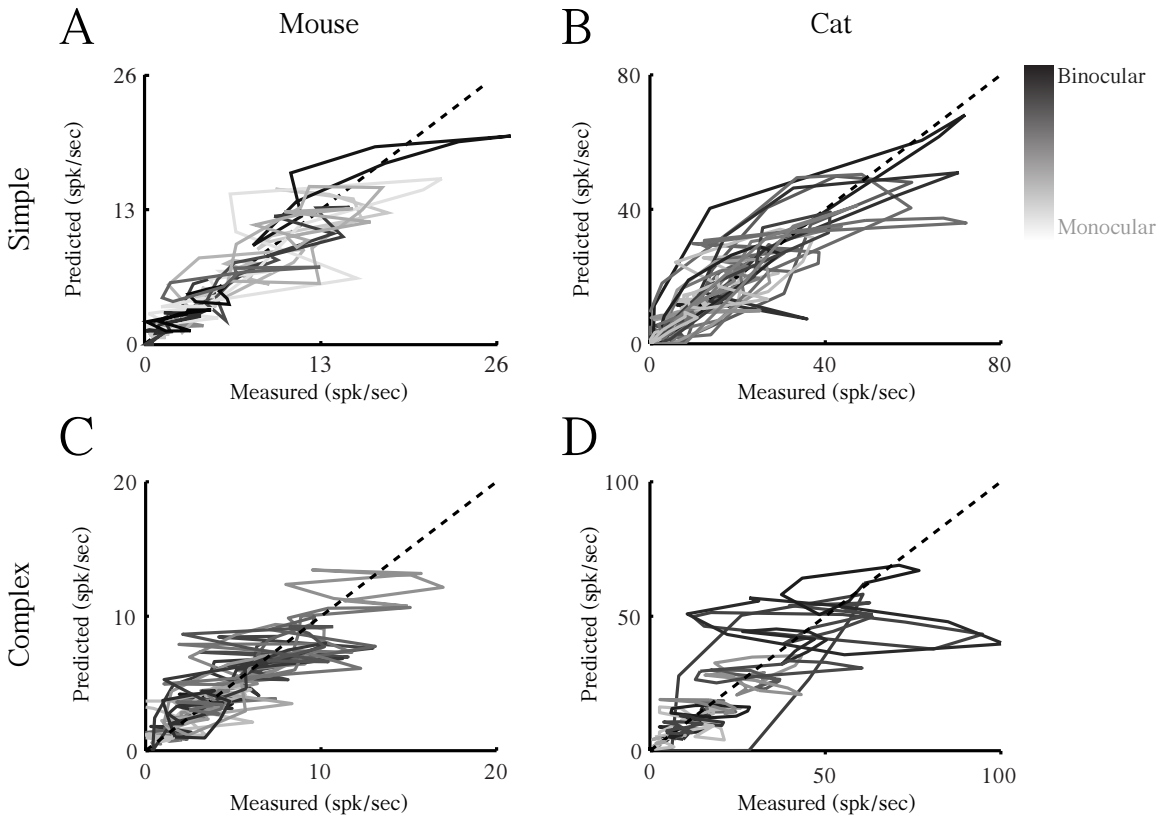

Figure 6.7: Relationship between predicted and measured binocular responses

A simple linear−threshold model predicts binocular responses across simple cells recorded in mouse (A) and cat (B). Each cell is plotted and shaded relative to binocularity measured by monocular stimulation (absolute value of ODI). The dashed line represents unity.

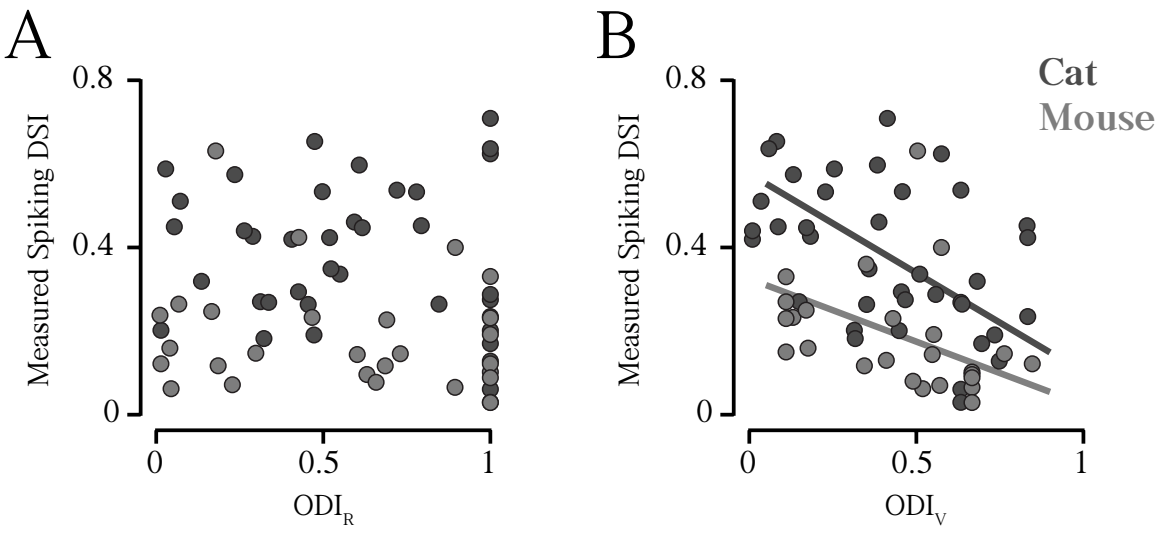

Figure 6.8: Relationship of ODI from predicted inputs and measured DSI
(A) The absolute value of the ODI_R of spiking responses is plotted with DSI for simple cells in cat (dark gray) and mouse (light gray). No clear relationship is evident. (B) The absolute value of the ODI_V, based on predicted subthreshold inputs, is plotted with DSI for simple cells in cat and mouse. Cells with predicted subthreshold inputs showing a greater degree of binocularity are also more selective for binocular disparities as measured by the spiking DSI. In both, the absolute value of ODI is plotted so that a value of 0 indicates a binocular neuron and a value of 1 indicates a monocular neuron.

binocularity of inputs: mice V1 neurons are more contralaterally–biased than cat neurons than cat neurons. But we find that mouse V1 neurons with matching degrees of input ocular dominance to cat neurons exhibit less disparity selectivity (Fig. 6.8B). Neurons with a substantial amount of binocular input ($ODI_V = 0 - 0.25$) were vastly different in disparity selectivity between the cat (mean = 0.49 ± 0.11 SD) and mouse (mean = 0.23 ± 0.06 SD) (Student's t–test $p<0.001$). Therefore the difference in the degree of disparity selectivity found in mouse and cat cannot solely reflect the contralateral bias of mouse neurons.

Subthreshold and suprathreshold binocular integration in mouse and cat

To directly test predictions of the threshold–linear model (Figs. 6.6 & 6.8) we preformed *in vivo* whole–cell patch–clamp recordings (Pei et al., 1991; Ferster and Jagadeesh, 1992; Margrie et al., 2002) from the binocular zone of mouse V1 and cat V1. Binocular disparity and ocular dominance were measured using the same methods as for extracellular recordings (Appendix A). Here we report intracellular records from 13 mouse simple cells and 33 cat simple cells. We focus only on simple cells, because this cell type is the recipient of direct thalamocortical input and the first stage of visual processing (Skottun et al., 1991; Hirsch et al., 1998; Priebe et al., 2004; Martinez et al., 2005). Further, our threshold–linear model requires phase–sensitive subthreshold inputs to generate predictions (Fig. 6.6); a property of simple cell receptive fields, but not complex cells which are phase–insensitive. The role of simple cells in mouse visual processing is less clear, but we focus on these cells because of their phase–sensitive properties.

In mouse V1, simple cells show membrane potential and spiking responses that depend on stimulus disparity. From cycle–averaged responses of an example neuron

(Fig. 6.9A, *top*), the preferred disparity (45−90° phase difference) evoked large membrane potential fluctuations, while the null disparity (225−270° phase difference) showed smaller fluctuations. A similar pattern of disparity selectivity was observed in spike rate (Fig. 6.9A, *top*). The large fluctuations at the preferred disparity suggest a phase alignment of ocular inputs. Plotting peak subthreshold and suprathreshold responses (F1 + DC; Appendix A) shows response modulation by binocular phase differences, and binocular responses that were much stronger than the response to either eye alone (Fig. 6.9A, *bottom*). The difference in modulation between subthreshold and suprathreshold responses is a consequence of the membrane potential−to−spike rate transformation, also been shown to enhance orientation tuning, direction selectivity and ocular dominance (Priebe and Ferster, 2008). The example cell in Figure 6.9A receives strong input from both eyes, but binocular response modulations were also evident in weakly binocular simple cells from mouse V1 (Fig. 6.9B). In cat V1, simple cells were often strongly binocular at the level of membrane potential evoked by either eye alone (Fig. 6.9 C−D; see also Chapter 7). We also observed large changes in response amplitude to binocular disparities, evident in the modulations of membrane potential and spike rate (Fig. 6.9 C−D; see also Chapter 7).

The simple threshold−linear model predicts that ocular dominance of subthreshold membrane potential is correlated with disparity selectivity (Fig. 6.8). From our intracellular recordings of simple cells in mouse and cat V1, we computed the ocular dominance of subthreshold membrane potential (ODI_{Vm}, Appendix B) and the disparity selectivity of both subthreshold membrane potential and suprathreshold spiking (DSI_{Vm} and DSI_{Spk}, respectively; Appendix B). In cat V1 records, we observed a significant relationship between the ocular dominance and disparity selectivity of subthreshold inputs (Fig. 6.10A; PCA slope = −0.11 ± 0.04 SE, $r^2 = 0.13$, n = 33).

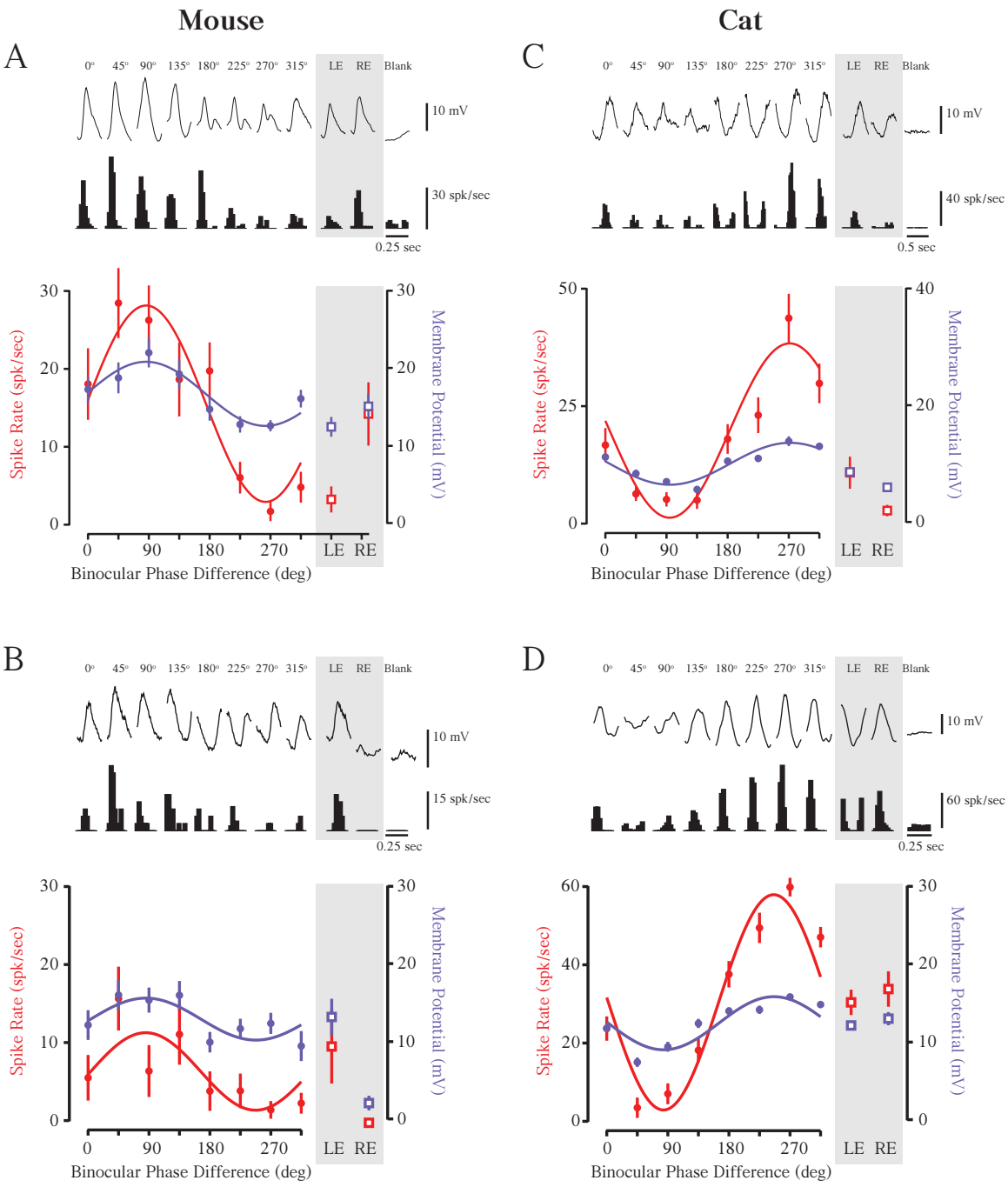
Mouse
Cat
A
B
C
D
0° 45° 90° 135° 180° 225° 270° 315°
LE RE
Blank
10 mV
30 spk/sec
15 spk/sec
40 spk/sec
60 spk/sec
0.25 sec
0.5 sec
Spike Rate (spk/sec)
Membrane Potential (mV)
Binocular Phase Difference (deg)
0 90 180 270
LE RE

Figure 6.9: Binocular disparity selectivity of membrane potential and spiking responses in simple cells of mouse and cat V1

(A) Binocular mouse simple cell cycle−averaged responses to 8 binocular phase combinations of optimal drifting gratings (*top*). Shown is subthreshold membrane potential and evoked spiking responses. Binocular stimuli were interleaved with monocular stimulation. This example cell has a preferred binocular phase difference around 45−90 deg, evident in the membrane potential fluctuations and strong modulation of spiking responses. Note the strong subthreshold responses to both eyes individually. Full extent of disparity tuning plotted for membrane potential (purple) and spiking (red) peak responses (F1 + DC) (*bottom*). Mean and standard error are shown for binocular (circles) and monocular (squares) conditions. Solid curves are cosine fits used to illustrate disparity tuning. (B) Same as in (a) for another example mouse neuron. Unlike in (a), monocular membrane potential responses in this neuron are dominated by the left eye, evident in the large fluctuations. (C−D) Same as in (a) for two binocular cat simple cells strongly modulated by binocular stimuli.

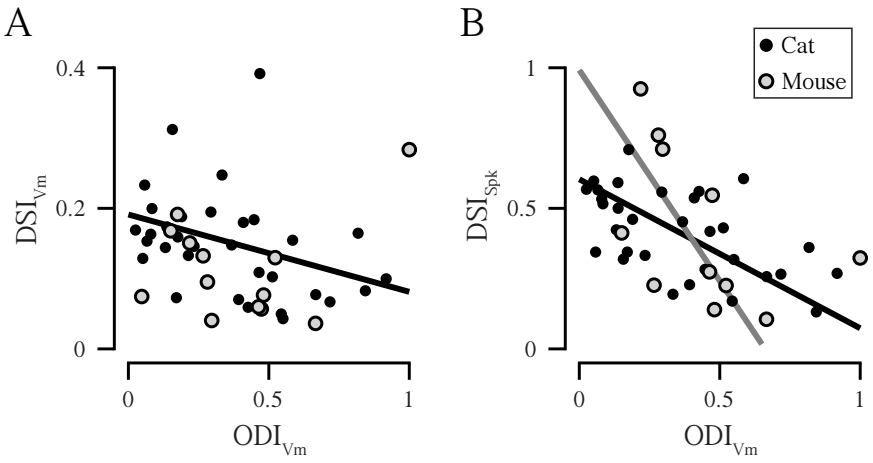

Figure 6.10: Relationship between ocular dominance and disparity selectivity for membrane potential and spiking

(A) Comparison of ocular dominance index (ODI) and disparity selectivity index (DSI) values for subthreshold membrane potential from simple cells in mouse (*gray open circles*) and cat (*black circles*). Line indicates PCA slope, significant only for cat data. (B) Comparison of subthreshold ODI with spiking (suprathreshold) DSI from simple cells in mouse and cat. Lines indicate PCA slopes for mouse (*gray*) and cat (*black*).

In mouse V1 records, however, no such relationship was evident (Fig. 6.10A; PCA slope = 0.03 ± 0.16 SE, n = 13). These analyses were restricted to neurons not strictly monocular (ODI_{Vm} > 1) and those which were at least modestly disparity selectivity from spiking activity (DSI_{Spk} > 0.1). When examining ODI_{Vm} and DSI_{Spk} we observed significant relationships in both species (Fig. 6.10B). For cat V1 simple cells, the major slope from PCA (Sokal and Rohlf, 1995) was −0.53 ± 0.16 SE (r^2 = 0.23, n = 32), and for mouse V1 simple cells this slope was −1.5 ± 1.0 SE (r^2 = 0.19, n = 11). To obtain accurate measurements of DSI_{Spk}, we required all neurons to exhibit spiking activity and respond to at least one binocular stimulus. These data from both mouse and cat confirm our predictions of the threshold−linear model and definitively show that in simple cells, the magnitude of synaptic from each individual eye is related to increased disparity selectivity.

DISCUSSION

Neurons in mouse V1 are known to receive inputs from left and right eye sensory streams, and yet it has been unclear how these two representations are integrated. By systematically changing the binocular disparity of left and right eye stimuli within an ecologically−relevant range, we found that binocular integration in V1 neurons exhibited responses modulated by disparity. Indeed, disparity tuning in mouse V1 neurons is similar to that found in cat V1 neurons, but differed in degree of modulation. A simple threshold−linear model accounted for the disparity selectivity of simple cells in both the cat and mouse, suggesting that a substantial subthreshold input from the weaker eye significantly modulates responses during normal binocular viewing. Model predictions were confirmed by intracellular recordings of subthreshold

membrane potential and suprathreshold spiking responses in both animals. Our recordings demonstrate that a common computation is being performed by V1 across mammalian species that provides information about the depth of objects.

Our initial experiments revealed an increase in neuronal sensitivity to binocular stimuli, but the increase is less than expected under the assumption of independent sources of noise in the sensory periphery (Simpson et al., 2009). Human psychophysical detection performance generally improves by a factor of $\sqrt{2}$ with binocular vs monocular stimulation. These experiments are generally performed at threshold contrast; sensitivity is generally smaller when the task is to discriminate differences between high contrast gratings (Legge, 1984). Because our measurements in the mouse were performed at high contrast, however, our records may not reveal the expected sensitivity improvement of $\sqrt{2}$. Measuring increases in sensitivity in mouse V1 neurons using low contrast stimuli may better match psychophysical measurements.

A wide variety of binocular interactions are present in mouse V1 neurons, as previously shown in cat V1 neurons (Pettigrew et al., 1968; Ohzawa and Freeman, 1986). One of these interactions is the dramatic response amplitude difference between monocular and binocular responses (Figs. 6.3B–C and 6.6A–B). Many mouse V1 neurons are clearly modulated by binocular stimulation, even though they would be classified as monocular by conventional measures of ocular dominance. A simple explanation is that sub–threshold synaptic inputs exist for both eyes, but monocular input from one eye is not sufficiently weighted to exceed the spiking threshold under monocular stimulation (Priebe and Ferster, 2008). Near spike threshold, small changes in membrane potential or synaptic input generate huge changes in spike rate, so amplitude differences between monocular and binocular synaptic inputs could elicit vastly different spiking responses. This explanation suggests that disparity tuning results from interactions at the level of subthreshold membrane potential, hidden from

our extracellular records (Ohzawa and Freeman, 1986; Ohzawa, 1998). Importantly, this prediction is confirmed from our intracellular recordings of subthreshold and suprathreshold responses (Fig. 6.10). In both mouse and cat we find subthreshold ocular dominance is related to suprathreshold disparity selectivity. Further, at least for cat V1 simple cells, this relationship holds even at the level of membrane potential.

Mammals are not the only vertebrates possessing binocular neurons, but the structure of the mammalian visual system contains elements supporting the generation of binocular neurons. Unlike other vertebrates, not all retinal ganglion cell projections cross at the optic chiasm. Both left and right eye outputs project to the same brain structures, instead of being laterally segregated. In the primate, for example, approximately 40% of the ipsilateral retinal projections do not cross at the optic chiasm, allowing for information streams from both eyes to innervate the same side of the lateral geniculate nucleus (LGN) (Perry et al., 1984; Chalupa and Lia, 1991). The percentage of retinal ganglion cell projections not crossing the optic chiasm in the mouse is very small, around 3−4%, but that small percentage of uncrossed retinal output innervates 10% of mouse LGN (Dräger, 1974; Godement et al., 1984). Although ipsilateral and contralateral retinal ganglion cells project to the LGN, those projections remain segregated. The second structural change in the visual system of mammals is the presence of a six layer cerebral cortex where left and right eye signals converge. Like the expansion of the ipsilateral representation in the LGN from few ipsilateral retinal ganglion cells, mouse binocular zone occupies approximately one−third of V1 despite an ipsilateral representation of only 10% in the LGN (Leamey and Protti, 2008). In the mouse it appears that a small basis for binocularity, in terms of uncrossed ipsilateral retinal projections, is amplified greatly to generate binocularity in V1.

Throughout our study we find less prominent disparity tuning in mouse V1 neurons compared to those in cat (Fig. 6.5), even when examining only simple cells (Fig. 6.8B).

In general, mouse V1 neurons are modulated to a lesser degree than cat neurons, although the potential exists for large disparity selectivity as we find DSI values share a similar range (mouse: 0 − 0.7, cat: 0 − 0.75; see also Fig. 6.10). One reason for these differences could be the lack of ocular dominance columns in mouse V1, where instead, there is a single binocular region receiving inputs from the ipsilateral eye. At the edges of this region neurons could be weakly binocular even at the level of synaptic input. Another difference is the extent of receptive fields relative to the binocular zone. Since receptive field sizes in mouse V1 vary greatly (5 − 30 deg) and the binocular field of view in mice is only 40 degrees (Fig. 6.2B), it is possible that binocular overlap in many neurons is too small in order to generate striking binocular response interactions observed in cat. In addition, simple−cell receptive fields in mouse V1 neurons are shown to differ from those in cat, as there is substantial overlap between ON− and OFF− subregions (Liu et al., 2010). In cat V1, simple cells of layer 4 receive direct input from the LGN and are thought to form the basis of disparity selectivity, which is inherited by complex cells in layer 2/3 through the integration of inputs across simple cells (Ohzawa, 1998). Simple and complex cells of mouse V1 are found throughout cortical layers (Niell and Stryker, 2008), suggesting that the emergence of disparity sensitivity could occur through a number of mechanisms and may not require direct thalamocortical input. In fact, synaptic mechanisms underlying binocular integration in mouse V1 are completely unknown, as these properties could result from combining thalamocortical, intracortical, and inhibitory synaptic input. Another possibility is that there exists mostly nonlinear summation of subthreshold input even in simple cells of mouse V1, as linear summation cat V1 is shown to generate robust disparity tuning (Ohzawa and Freeman, 1986). Finally, regarding synaptic inputs underlying visual responses of simple cells, it is known that mouse V1 neurons possess a push−push excitation−inhibition mechanism (Liu et al., 2010; Tan et al, 2011) while cat V1

neurons exhibit a push−pull mechanism (Hirsch et al., 1998; Priebe and Ferster, 2006). It may be that the binocular combination of these mechanisms is important in generating differences in simple cell disparity selectivity.

Other vertebrates besides mammals have evolved visual systems with binocular neurons. One prominent example, the barn owl (*Tyto alba*), has binocular depth perception that is quite similar to human binocular depth perception (van der Willigen, 2011). Binocular neurons in the barn owl's Wulst visual area have a high degree of binocularity and disparity tuning (Pettigrew and Konishi, 1976a; Nieder and Wagner, 2000; Nieder and Wagner, 2001) and exhibit a number of similar properties as shown in mouse (and primate and cat) V1 binocular neurons: strong disparity tuning, enhancement and suppression of responses to binocular stimulation, and ocular dominance plasticity during the critical period (Pettigrew and Konishi, 1976b). Given these similarities, it is interesting to note that binocularity in birds evolved independently from mammals (Pettigrew, 1986). Indeed, disparity selectivity in the barn owl emerges from a visual pathway that is completely different from that in mammals. In contrast to mammals, all projections from the two eyes in the barn owl cross at the optic chiasm and remain segregated until they converge within the Wulst.

Many animals with binocular depth perception use multiple depth cues to estimate depth (Landy et al., 1995; Hillis et al., 2004). These signals include but are not limited to figure−ground cues (Burge, Fowlkes, Banks, 2010), defocus blur (Burge and Geisler, 2011; Held and Cooper, 2012), motion parallax (Wallace, 1959), and looming (Beverley, 1973a; 1973b). Binocular disparity is thus not the only source of information relevant for estimating depth, but it is a source of information that many animals exploit.

The convergent evolution of binocular depth perception suggests that stereopsis confers important evolutionary advantages. Binocular neurons that underlie this

perceptual ability across phyla have similar properties despite differences in the neuroanatomical pathways and the (presumed) different mechanisms that give rise to them. This suggests that binocular neurons subserving depth perception extract similar information from the retinal images and that a common computation, independent of a particular mechanism, may underly all visual systems with stereopsis (Burge & Geisler, 2014). It is not yet known whether, or how, rodents use disparity to estimate depth in natural viewing. The necessary psychophysical studies have not been performed. For example, binocular cues located in the upper and overhead retinotopic regions of mouse vision could play an important in predator avoidance behaviors. Nonetheless, our recordings demonstrate that mouse V1 neurons are sensitive to binocular disparities consistent with an ecologically relevant range of object depths. The cross−species similarities between mouse, owl, cat, and primate suggest that the integration of left− and right−eye image information underlying disparity selectivity is an example of a common computation performed across visual systems. This computation is an important example of how visual systems select for and integrate useful information from multiple sensory sources to constrain estimates of behaviorally relevant properties of the natural environment.

Chapter 7: Strabismus disrupts binocular synaptic integration in cat primary visual cortex[1]

ABSTRACT

Visual disruption early in development dramatically changes how primary visual cortex neurons integrate binocular inputs. The disruption is paradigmatic for investigating the synaptic basis of long−term changes in cortical function, because the primary visual cortex is the site of binocular convergence. The underlying alterations in circuitry by visual disruption remain poorly understood. Here we compare membrane potential responses, observed via whole cell recordings *in vivo*, of primary visual cortex neurons in normal adult cats with those of cats in which strabismus was induced prior to the developmental critical period. In strabismic cats, we observed a dramatic shift in the ocular dominance distribution of simple cells, the first stage of visual cortical processing, towards responding to one eye instead of both, but not in complex cells, which receive inputs from simple cells. Both simple and complex cells no longer conveyed the binocular information needed for depth perception based on binocular cues. There was concomitant binocular suppression such that responses were weaker with binocular than with monocular stimulation. Our estimates of the excitatory and inhibitory input to single neurons indicate binocular suppression that was not evident in synaptic excitation, but arose de novo because of synaptic inhibition. Further constraints on circuit models of plasticity result from indications that the ratio of excitation to inhibition evoked by monocular stimulation decreased mainly for non−preferred eye stimulation. Although we documented changes in synaptic input

[1] Published article: Scholl B., Tan A.Y.Y., and Priebe N.J. (2013). Strabismus disrupts binocular synaptic integration in primary visual cortex. *Journal of Neuroscience* 33(43): 17108−17122.

throughout primary visual cortex, a circuit model with plasticity at only thalamocortical synapses is sufficient to account for our observations.

INTRODUCTION

Binocular information about the visual world first converges in mammals in primary visual cortex (V1). The cortical circuitry which integrates binocular information develops normally only with requisite visual experience (Katz and Crowley, 2002; Hensch, 2004; Huberman et al., 2008). Strabismus, a misalignment in the visual axes of the two eyes, is a disorder in humans preventing appropriate fusion of the two retinal images (Levi et al., 1979; Von Noorden and Campos, 2002; Economides et al., 2012). Rearing animals with strabismus induced prior to the critical period leads to three major differences in V1 response properties. First, neurons are more monocular, responding more strongly to a stimulus presented to one eye than to the other (Hubel and Wiesel, 1965; Blakemore, 1976; Shatz et al., 1977; Lowel, 1994; Lowel et al., 1998; Engelmann et al., 2002). Second, neurons are less disparity selective, responding more uniformly regardless of the disparity between stimuli presented simultaneously to both eyes, leading to a loss of ability to estimate object depth visually (Chino et al., 1994; Smith et al., 1997). Third, neurons are binocularly suppressed, responding more weakly to binocular than to monocular stimulation (Sengpiel and Blakemore, 1994; Sengpiel et al., 1994).

While the effects of strabismus on V1 neuron response properties have been extensively studied using extracellular recordings, the underlying changes in cortical circuitry remain poorly understood (Hubel and Wiesel, 1965; Blakemore, 1976; Crewther et al., 1985; Chino et al., 1994; Roelfsema et al., 1994; Sengpiel and Blakemore, 1994; Sengpiel et al., 1994; Fries et al., 1997; Smith et al., 1997; Schmidt et al., 2004; Sengpiel et al., 2006; Ranson et al., 2012). We accordingly performed

whole−cell recordings *in vivo* to characterize the differences in synaptic input to V1 neurons of normal and strabismic cats. We observed that strabismus increased the monocularity of membrane potential in V1 simple cells, the first stage of visual cortical processing, but not in V1 complex cells, which receive inputs from simple cells. In strabismic animals, membrane potential and spiking responses of both simple and complex cells were less disparity selective, and no longer conveyed binocular information needed for depth perception from binocular cues. There was accompanying binocular suppression such that membrane potential and spiking responses were weaker during binocular than monocular stimulation. Estimates of excitatory and inhibitory input onto single neurons indicated binocular suppression that was not evident in synaptic excitation, but arose due to changes in the amount of excitatory and inhibitory synaptic drive: excitatory inputs were more monocular than inhibitory inputs. Although we documented changes in synaptic input in both simple and complex cells, a circuit model with plasticity at only thalamocortical synapses is sufficient to account for our observations (Khibnik et al., 2010).

RESULTS

To characterize changes in synaptic input onto V1 neurons associated with strabismus during development, we obtained whole−cell patch clamp recordings *in vivo* (Pei et al., 1991; Ferster and Jagadeesh, 1992; Margrie et al., 2002) from cats after artificially inducing exotropic strabismus prior to the critical period of visual cortex development, and compared those with recordings from litter−matched control animals and normal animals (Hubel and Wiesel, 1965; Chino et al., 1983; Chino et al., 1994) (Appendix A).

Ocular dominance of membrane potential and spike rate

We first verified that our procedure for inducing an ocular misalignment produced the changes in V1 spike rate ocular dominance found previously (Hubel and Wiesel, 1965; Yinon and Auerbach, 1975; Chino et al., 1983; Freeman and Tsumoto, 1983; Klalil et al., 1984; Chino et al., 1994; Löwel et al., 1998; Engelmann et al., 2001), by obtaining extracellular recordings in the strabismic animals and their litter–matched controls. Dichoptic stimulus presentation was used to identify the dominant eye for each neuron, after which we then characterized orientation selectivity, spatial frequency tuning, and receptive field location (Appendix A) (Ohzawa and Freeman, 1986a, b).

We characterized the ocular dominance of subthreshold (membrane potential) and suprathreshold (spiking) responses in V1 neurons of normal and strabismic animals, using optimal drifting gratings presented to each eye separately (Fig. 7.1A–D). We quantified ocular dominance profiles with an ocular dominance index (ODI; Appendix B). The ocular dominance index for spike rate (ODI_{spk}) in normal animals, which includes data from both intracellular and extracellular recordings, is characterized by a uniform distribution (Fig. 7.1E, *right*). In strabismic animals, however, the ODI_{spk} distribution is peaked at high and low values, indicating markedly decreased binocularity, with many neurons spiking in response only to stimuli presented to one eye (Fig. 7.1G, *right*). The ODI_{spk} distributions for normal and strabismic animals are similar to those previously reported (Hubel and Wiesel, 1965; Chino et al., 1994).

A complete loss of spiking responses to stimulation of one eye indicates a loss of synaptic input from that eye, but latent inputs may persist which evoke only subthreshold responses. To uncover the extent of synaptic changes that occur in strabismic animals we examined the ocular dominance of the membrane potential for

individual V1 neurons. Membrane potential ocular dominance was different between strabismic and normal animals. The ODI_{vm} distribution was peaked at 0 in normal animals (Fig. 7.1E), but was flat in strabismic animals (Fig. 7.1G). The distribution of ocular dominance for membrane potential was also significantly different than that of the spike responses (Fig. 7.1E,G). In both normal and strabismic animals, membrane potential responses were more binocular than spike rate, as shown by the increased number of neurons with ODI_{vm} values near 0 relative to ODI_{spk}. The membrane potential records thus indicate that a total loss in spiking responses to stimulation of one eye is undergirded by only a partial loss of synaptic input.

Apart from changes in synaptic input, additional factors such as differences in intrinsic properties could play a role in the spike rate ocular dominance shift caused by strabismus. We did not, however, find a statistically significant change in the resting membrane potential between V1 neurons in normal and strabismic animals (Normal: $V_{rest} = -61.6 \pm 9.7$ mV, n = 76; Strabismic: $V_{rest} = -60.7 \pm 8.6$ mV, n = 79; mean ± s.d., $p > 0.30$, Welch's t−test). We also measured the nonlinear relationship between membrane potential and spike rate using a power−law fit (Priebe et al., 2004) for intracellular records with sufficient spiking activity (Appendix A), and did not find a difference in the fit exponent between V1 neurons in normal and strabismic animals (normal: $p = 3.0 \pm 0.9$, n = 52; strabismic: $p = 2.9 \pm 1.2$, n = 57; mean ± s.d., $p > 0.25$, Welch's t−test). The relationships between ODI_{vm} and ODI_{spk} in normal and strabismic animals were also similar, consistent with the transformation of membrane potential into spike rate being unaffected by strabismus (Fig. 7.1F, H) (Priebe, 2008; Priebe and Ferster, 2008). Differences in ocular dominance between normal and strabismic animals thus depend mainly on changes in synaptic input. Because the ODI distributions are approximately symmetric about 0 in normal and strabismic animals

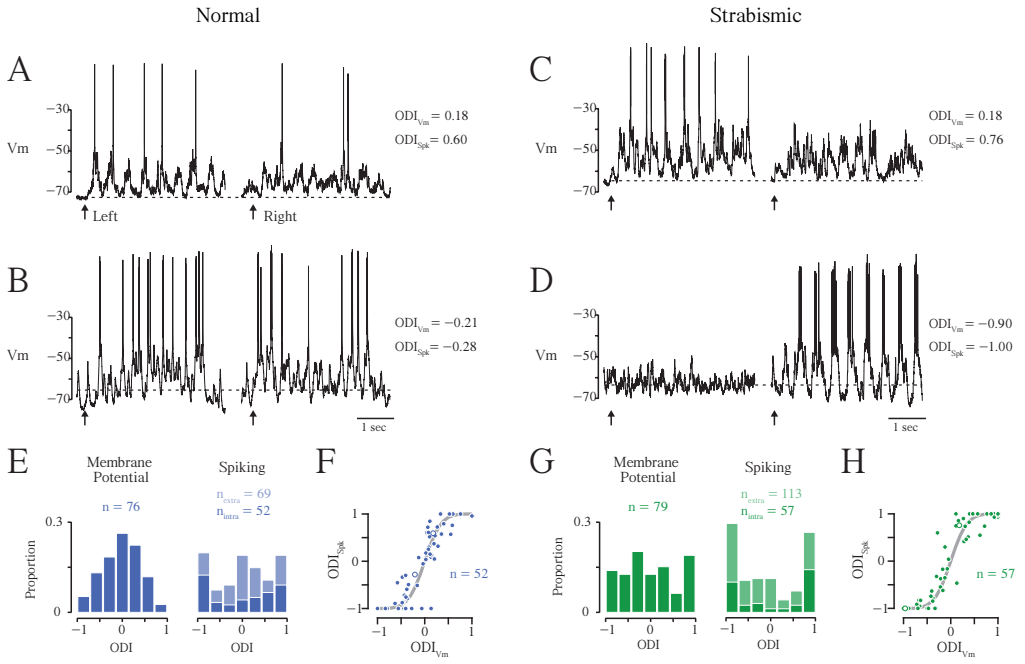

Figure 7.1: Strabismus alters ocular dominance of neurons in primary visual cortex

(A) Intracellular recording of a V1 neuron from a normal animal responding to a drifting grating of preferred orientation, spatial frequency, and spatial size presented independently to each eye. Arrows indicate stimulus onset time. Stimulation of either eye evoked subthreshold responses, but action potentials were evoked more for left eye stimulation. (B) Same as in (a) for a significantly binocular neuron. (C) Intracellular record from a V1 neuron in a strabismic animal. Strong subthreshold responses were evoked by both eyes, like in (a), however action potentials were evoked only for dominant eye stimulation. (D) Example of a severely monocular neuron in V1 of a strabismic animal. (E) Ocular dominance distribution for all V1 neurons recorded in normal animals. Subthreshold membrane potential (*left*) is more binocular than for suprathreshold spiking activity (*right*). Spiking responses include intracellular (dark shading) and extracellular (light shading) records. (F) Relationship between membrane potential and spiking ocular dominance in V1 neurons from normal animals. (G) Same as in (e) for V1 neurons recorded in strabismic animals. Membrane potential ocular dominance is less binocular and spiking activity shows dramatic monocularity. (H) Same as in (g) for strabismic animals. The relationship between subthreshold and suprathreshold ocular dominance is unaffected by an ocular misalignment. Curves were generated with typical power−law exponent (p = 3) (Appendix A, Priebe et al., 2004).

(Fig. 7.1E,G), it is also convenient to use a monocularity index (MI), defined as the absolute value of ODI. MI is 0 when equal responses are elicited from both eyes; MI is 1 when responses are evoked by only one eye. We found that membrane potential was more binocular in normal (mean MI_{vm} = 0.33 ± 0.24 s.d., n = 76) than in strabismic animals (mean MI_{vm} = 0.64 ± 0.34 s.d., n = 79; mean ± s.d., $p < 0.001$, Mann−Whitney test). The same trend was evident in spike rate from extracellular records and intracellular records with spikes (normal MI_{spk} = 0.53 ± 0.35, n = 121; strabismic MI_{spk} = 0.68 ± 0.33, n = 170; mean ± s.d., $p < 0.001$, Mann−Whitney test). Because normal animals included litter−matched sham controls and non−litter−matched, non−sham animals we compared MI from spiking records from extracellular records and intracellular records with spikes in each group; we found no statistical difference (mean MI_{spk} = 0.48 ± 0.36 s.d., n = 56, mean MI_{spk} = 0.57 ± 0.34 s.d., n = 65, respectively, $p = 0.14$, Mann−Whitney test).

Strikingly, the increase in monocularity due to strabismus depended on neuron type. Simple cells are primarily found in layer 4 of V1, receive direct input from the lateral geniculate nucleus, and modulate in response to drifting gratings (Fig. 7.2A,B) (Skottun et al., 1991; Hirsch et al., 1998; Priebe et al., 2004; Martinez et al., 2005). Simple cells in strabismic animals exhibited a large increase in membrane potential monocularity (normal MI_{vm} = 0.35 ± 0.25, n = 52; strabismic MI_{vm} = 0.62 ± 0.33, n = 48; mean ± s.d., $p < 0.001$, Mann−Whitney test). In contrast, complex cells, which are typically found in superficial and deep layers of V1 and have stimulus−evoked responses which are dominated by an unmodulating component (Fig. 7.2C,D), exhibited only slight changes in membrane potential ocular dominance

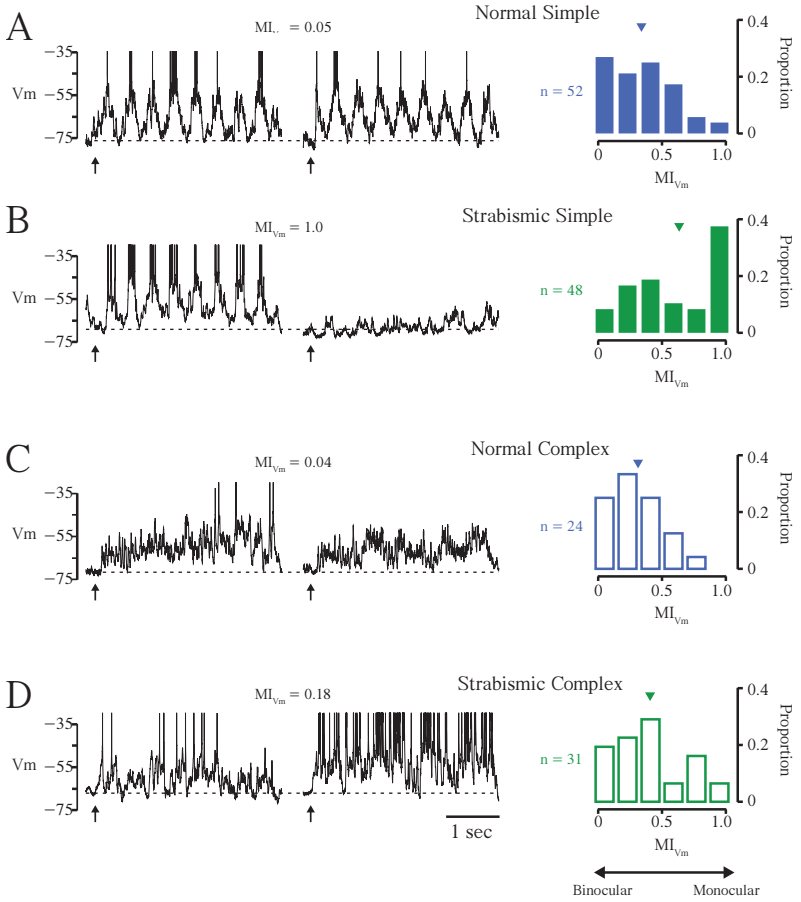

Figure 7.2: Monocularity of subthreshold input to simple and complex cells in primary visual cortex

(A) Example of intracellular record from a V1 simple cell in the normal animal (*left*). Strong synaptic input evoked by stimulation of either eye, reflected in low monocularity index (MI) values (absolute value of ocular dominance). Spikes have been truncated to visualize subthreshold input. Distribution of membrane potential MI across all V1 simple cells in normal animals show that most receive binocular synaptic input (*right*) (B) Example simple cell from a strabismic animal is severely monocular, similar to the example shown in Figure 1D. Simple cells from strabismic animals show dramatic increase in MI for subthreshold input (*right*). (C) Example complex cell from V1 of a normal animal. Complex cells in normal animals receive binocular subthreshold input (*right*). (D) Example complex cell from a strabismic animal. Across the population, complex cells are slightly more monocular, but not to the degree found in simple cells, shown in (b).

(normal: $MI_{vm} = 0.30 \pm 0.20$, n = 24; strabismic: $MI_{vm} = 0.40 \pm 0.27$, n = 31; mean ± s.d., p = 0.17, Mann−Whitney test).

A difference in monocularity between simple and complex cells was also seen in spike rate. Spike rate monocularity shifts were larger in simple cells across extracellular records and intracellular records with spikes (normal: $MI_{spk} = 0.62 \pm 0.34$ n = 70; strabismic: $MI_{spk} = 0.83 \pm 0.26$, n = 84; mean ± s.d., $p < 0.001$, Mann−Whitney test) than in complex cells (normal: $MI_{spk} = 0.41 \pm 0.33$, n = 51; strabismic: $MI_{spk} = 0.54 \pm 0.33$, n = 86; mean ± s.d., p = 0.028, Mann−Whitney test), which has also been observed previously (Chino et al., 1988; Chino et al., 1994).

We detected a monocularity shift in the spike responses but not the membrane potential responses of complex cells, because the nonlinearity relating spike rate and membrane potential acts to enhance small differences in membrane potential responses (Priebe, 2008; Priebe and Ferster, 2008) (Fig. 7.1F,H). Our measurements of spiking responses from intracellular and extracellular records corroborate previous reports that complex cell spiking responses are more binocular than those of simple cells in both normal and strabismic cat V1 (p = 0.002, p = 0.001, respectively, Mann−Whitney test) (Chino et al., 1988; Chino et al., 1994). Heightened binocularity in complex cells might account for the more subtle change in spiking monocularity we observed. Nonetheless, a clear loss of binocular spiking responses in complex cells is evident in strabismic animals, while binocularity of subthreshold inputs remains unchanged (Fig. 7.2). Simple cells receive most of their input from the thalamus, but complex cells receive input mainly from other cortical neurons (Ferster et al., 1996; Chung and Ferster, 1998). Accordingly, the dramatic increase in simple cell monocularity apparent in membrane potential responses and the subtle change in complex cell monocularity apparent only

in spike rate, are consistent with strabismus driving synaptic plasticity primarily at thalamocortical synapses.

These results indicate that a dramatic increase in the monocularity of simple cells accompanies strabismus. This enhanced monocularity, however, is not accompanied by a hyperpolarization elicited by stimulation of the non−preferred eye. Across monocular simple and complex cells (MI_{vm} > 0.75) the mean cycle−averaged response to the nonpreferred eye was −0.17 ± 1.20 mV (mean ± s.d.), and in only 7/24 neurons were responses significantly hyperpolarized relative to the resting membrane potential (bootstrap analysis, Sokal and Rohlf, 1995). Since these values are near zero, membrane potential responses are very near rest during blank periods and constitute effectively no sensory response. Therefore it does not appear that strabismus induces an inhibitory antagonism between neurons selective for the opposite eyes.

Our measurements of peak responses are calculated after removing the response to the first stimulus cycle, as we attempted to analyze steady−state responses and ascertain receptive field properties. It is possible, however, that the initial transient component of neuron response conveys important visual information (Celebrini et al., 1993; Gawne et al., 1996; Reich et al., 2001; Müller et al., 2001; Frazor et al., 2004; Palmer et al., 2007; Chen et al., 2008; Shriki et al., 2012). We examined whether including the first response cycle or using only the first response cycle changed our MI measurements, particularly in complex cells which are phase insensitive. Across all measurements of membrane potential and spiking responses in both simple and complex cells from either control or strabismic animals, inclusion of the first cycle did not significantly change measurements of MI ($p > 0.40$, Mann−Whitney test). Using only the first response cycle also did not alter MI across all records ($p > 0.10$, Mann−Whitney test).

An additional factor that may bias our results is the side of the brain recorded from relative to the deviated eye. The majority of our records are from the left hemisphere, the side contralateral to the deviated eye, but we obtained records from both hemispheres. In both hemispheres a bimodal distribution of ODI was present for spike rate (Hartigan's Dip Test, $p < 0.05$). The monocular indices for both the right and left hemispheres of strabismic animals were significantly higher than the monocular indices in normal animals but the indices between left and right hemispheres were not significantly different from one another (median $MI_{spk} = 0.68$ and 0.82, respectively, Rank−Sum test). Because we find no significant differences in ocular dominance patterns between hemispheres, the data from both hemispheres have been grouped together.

Binocular integration and disparity selectivity

Thus far we have only described V1 neuron responses to stimuli presented separately to each eye, but normally V1 neurons integrate binocular signals to extract information about the depth of objects in the world (Ohzawa et al., 1990; DeAngelis et al., 1991; Cumming and Parker, 1997; Cumming and DeAngelis, 2001). In normal animals, V1 neurons signal object depth through their selectivity for disparity, the spatial difference between right and left eye images. To determine how strabismus alters this binocular integration, we measured disparity selectivity by systematically varying the phase difference between drifting gratings presented dichoptically (Ohzawa and Freeman, 1986a, b).

In normal animals, simple cells show membrane potential and spiking responses that depend on stimulus disparity. In cycle−averaged responses from an example neuron (Fig. 7.3A), the preferred disparity (270^{o} phase difference) evoked large membrane

potential fluctuations, while the null disparity (90° phase difference) evoked little change in membrane potential. A similar pattern of disparity selectivity was observed in the spike rate of neurons (Fig. 7.3A). The large fluctuations at the preferred disparity suggest a phase alignment of ocular inputs. Plotting peak subthreshold and suprathreshold responses (F1 + DC; Appendix A) shows response modulation by binocular phase differences, and binocular responses that were much stronger than the response to either eye alone (Fig. 7.3A, *bottom*). To quantify response selectivity for binocular phase difference we computed a disparity selectivity index (DSI) (Swindale, 1998; Ringach et al., 2002; Scholl et al., 2013; Appendix B). Although membrane potential was tuned to similar disparities as spiking responses in normal animals, DSI values were greater for spike rate than membrane potential (DSI_{vm} = 0.18, DSI_{spk} = 0.46 Fig. 7.3a, *bottom*). This difference is a consequence of the membrane potential–to–spike rate transformation that has also been shown to enhance orientation tuning, direction selectivity and ocular dominance (Priebe and Ferster, 2008).

Simple cells in strabismic animals exhibited a loss of disparity selectivity in membrane potential and spike rate. There was a lack of disparity tuning (Fig. 7.3B, DSI_{vm} = 0.05, DSI_{spk} = 0.07) even in the few simple cells that maintained binocular membrane potential responses (Fig. 7.3B, MI_{vm} = 0.37, MI_{spk} = 0.52). In addition, most binocular responses for membrane potential and spike rate were smaller than responses to stimulation of the preferred eye. Across all simple cell intracellular records from strabismic and normal animals, we found a systematic decrease of DSI in membrane potential and spiking responses (Fig. 7.4A). DSI values for membrane potential were modest (normal: DSI_{vm} = 0.12 ± 0.08, n = 52, strabismic: DSI_{vm} = 0.09 ± 0.08, n = 48, mean ± s.d.), but the decrease in DSI was statistically significant (p = 0.05, Mann–Whitney test). A decrease in disparity sensitivity was also evident in spiking

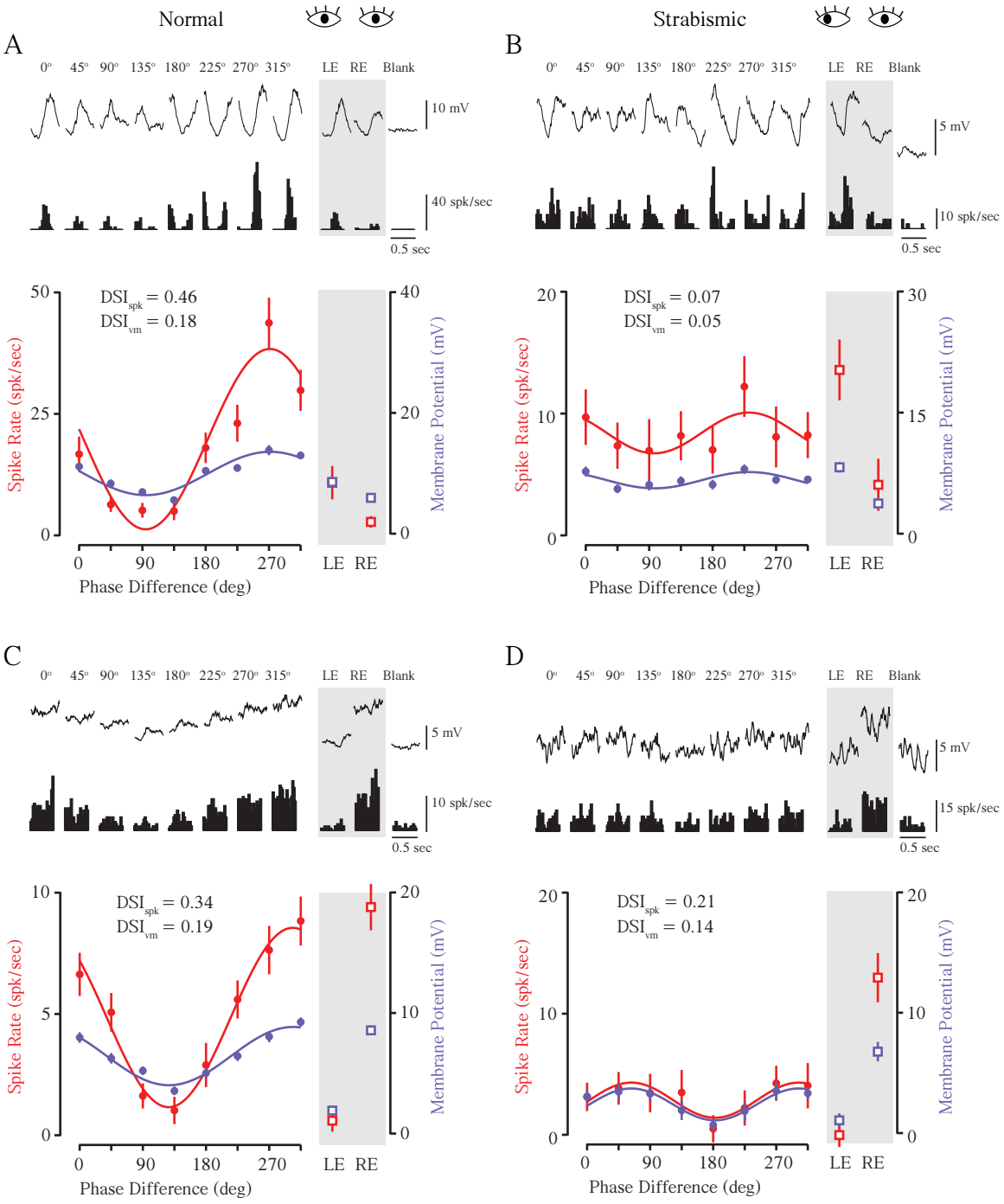
Normal
Strabismic
A
B
C
D
0° 45° 90° 135° 180° 225° 270° 315°
LE RE Blank
10 mV
40 spk/sec
5 mV
10 spk/sec
15 spk/sec
0.5 sec
DSI$_{spk}$ = 0.46
DSI$_{vm}$ = 0.18
DSI$_{spk}$ = 0.07
DSI$_{vm}$ = 0.05
DSI$_{spk}$ = 0.34
DSI$_{vm}$ = 0.19
DSI$_{spk}$ = 0.21
DSI$_{vm}$ = 0.14
Spike Rate (spk/sec)
Membrane Potential (mV)
Phase Difference (deg)
0 90 180 270
LE RE

Figure 7.3: Binocular disparity selectivity of membrane potential and spiking responses in primary visual cortex

(A) Simple cell cycle−averaged responses to a random sequence of 8 binocular phase combinations of optimal drifting gratings presented dichoptically (*top*). Shown for subthreshold membrane potential and evoked spiking responses. Binocular stimuli were interleaved with monocular stimulation (gray shading) and a blank (mean−luminance) period. This example simple cell has a preferred binocular phase difference of 270 deg, evident in the large membrane potential fluctuations and strong modulation of spiking responses. Responses at the preferred disparity can be larger than responses from the stimulation of either eye alone, particularly for evoked spiking activity. Little response was evoked at the null phase (90 deg). Full extent of disparity tuning plotted for membrane potential (purple) and spiking (red) peak responses (F1 + DC) (*bottom*). Mean and standard error are shown for binocular (circles) and monocular (squares) conditions. Solid curves are sine−wave fits used to illustrate disparity tuning. Strong modulation of peak responses by different disparities is reported by a vector strength index (DSI). **(b)** Same as in (a) for simple cell recorded in a strabismic animal. Despite strong membrane potential fluctuations and spiking responses evoked by stimulation of either eye (gray), simple cells were not disparity tuned. Peak responses plotted across all disparities also show suppression in during binocular stimulus conditions (*bottom*). **(c)** Same as in (a) for an example complex cell. **(d)** Same as in (b) for a complex cell. Binocular suppression and lack of disparity tuning in membrane potential and spiking responses is evident for both cycle−averaged responses and tuning curves.

responses across extracellular and spiking−intracellular records (normal: DSI_{spk} = 0.35 ± 0.18, n = 70, strabismic: DSI_{spk} = 0.24 ± 0.18, n = 84; mean ± s.d., $p < 0.001$, Mann−Whitney test).

Similar changes in disparity selectivity were observed in V1 complex cells. In normal animals, complex cell membrane potential and spike rate responses were disparity selective. In an example neuron (Fig. 7.3C), few membrane potential fluctuations are evident as compared to simple cell. Instead, large DC (mean) depolarizations shape disparity preference and underlie selectivity observed in spiking responses. For example, the membrane potential at the null phase (135°) is only slightly larger than the nonpreferred eye (~4 mV), while at the preferred phase (315°) the subthreshold response is much larger (~10 mV). As with simple cells, the preferred disparity of membrane potential and spike rate were matched, but the disparity selectivity was greater for spike rate (DSI_{vm} = 0.19, DSI_{spk} = 0.34). Complex cells from strabismic animals, like simple cells, were weakly disparity selective (Fig. 7.3D). Across all complex cell records, strabismus caused a large decrease in spike rate disparity selectivity (normal: DSI_{spk} = 0.23 ± 0.14, n = 51, strabismic: DSI_{spk} = 0.15 ± 0.13, n = 86; mean ± s.d., $p < 0.001$, Mann−Whitney test) (Fig. 7.4B). There was, however, no significant difference in DSI_{vm} (normal: DSI_{vm} = 0.08 ± 0.06, n = 24; strabismic: DSI_{vm} = 0.12 ± 0.09, n = 31; mean ± s.d., $p = 0.16$, Mann−Whitney test, Fig. 7.4B).

Since we removed responses to the first stimulus cycle, which could potentially contain important sensory information in complex cells, which are phase insensitive, we also examined DSI in responses to the first stimulus cycle. Similar to measurements of MI, this did not change our results for subthreshold or suprathreshold responses. Complex cells from normal animals were significantly more selective for disparity than

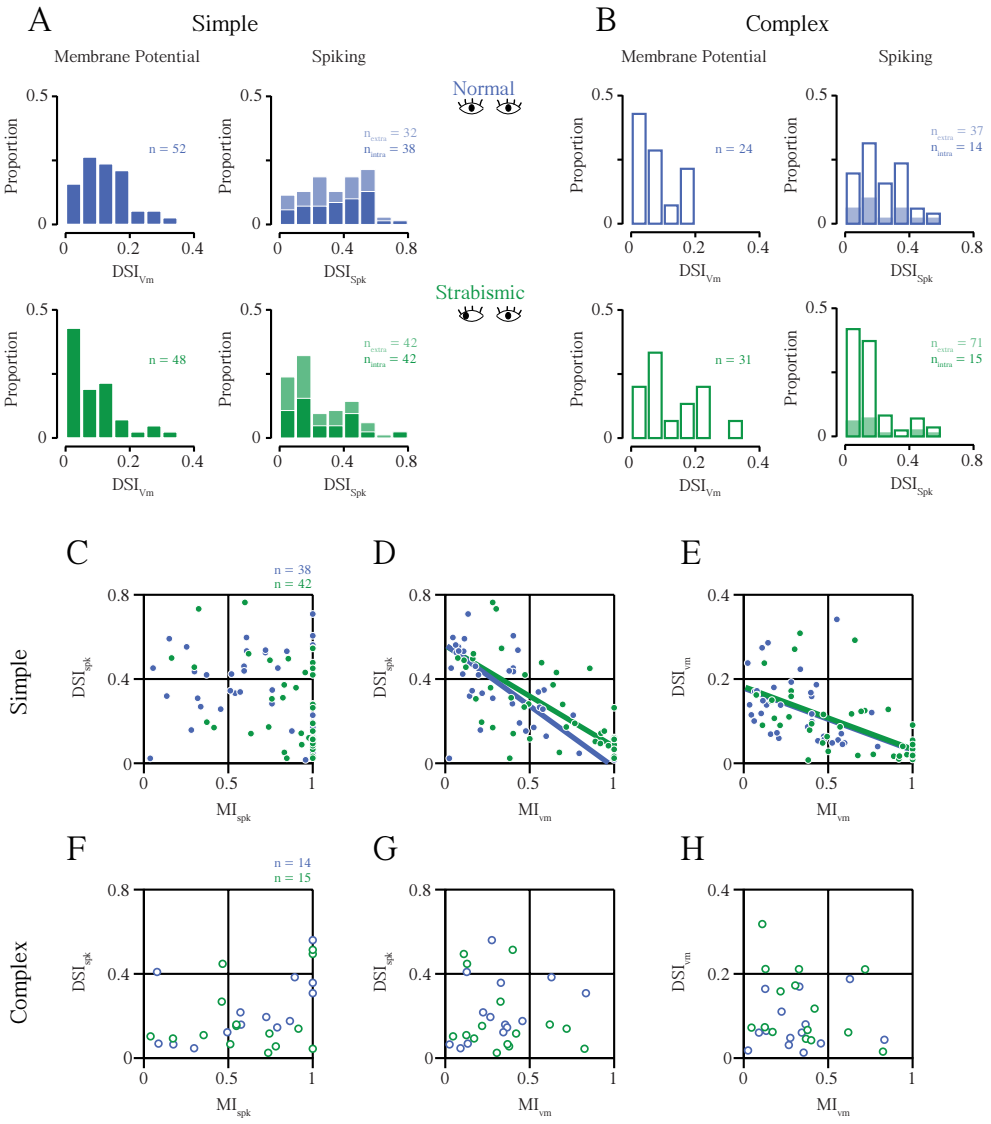

Figure 7.4: Effect of strabismus on disparity selectivity

Distributions of disparity selectivity index (DSI) values for simple cell subthreshold membrane potential and suprathreshold spiking responses in normal (blue) and strabismic (green) animals. Spiking responses include intracellular (dark shading) and extracellular (light shading) records. (B) Same as in (a) for complex cells. (C) Relationship between spiking monocularity index (MI) (absolute value of ocular dominance) and spiking DSI in simple cells from normal and strabismic animals. (D) Same as in (c) for subthreshold MI and spiking DSI. (E) Same as in (c) for subthreshold MI and subthreshold DSI. (F) Same as in (c) for complex cells. (G) Same as in (d) for complex cells. (H) Same as in (e) for complex cells.

those from strabismic animals (median DSI = 0.22 and 0.15, respectively, p = 0.02, Mann−Whitney test). Although DSI values were higher for membrane potential, there was, again, no difference between normal and strabismic animals (median DSI = 0.13 and 0.16, respectively, p = 0.20, Mann−Whitney test).

Response suppression by binocular stimulation, relative to the response to monocular stimulation, was evident in many records (Fig. 7.3B,D) and will be discussed in detail below. This suppression suggests that factors aside from a mismatch of excitatory inputs from each eye are involved in the changes to cortical circuitry associated with strabismus (Levi et al., 1979; Sengpiel and Blakemore, 1994; Sengpiel et al., 1994; Sengpiel et al., 2006) (Fig. 7. 4A−B).

We have thus far described mainly the average effects of strabismus. There was, however, considerable diversity in the effects of our procedure for inducing strabismus on the degree of monocularity and disparity in different animals. The range of DSI values observed (0 − 0.75) was similar between normal and strabismic animals (Fig. 7.4A−B). Although MI and DSI values calculated for each animal overlapped for strabismic and control animals, when MI and DSI were considered separately, there was minimal overlap when both MI and DSI were jointly considered (Fig. 7.5). In each litter there were at least several strabismic animals with large differences in MI and DSI from control animals, indicating that the within−litter variability was as large as that across litters. We do not know if the variability was due to differences in our procedure for inducing strabismus or to variability in environmental and genetic factors.

We have focused on the degree of binocular selectivity in normal and strabismic animals, but strabismus could also alter the response amplitude of neurons. We therefore examined the peak spiking activity and membrane potential responses from records in each population. In normal animals, spiking responses to the preferred binocular stimulus were greater than to the preferred eye in simple cells (20.2 ± 21.4

spk/sec and 14.9 ± 2.0 spk/sec, respectively, n = 70, mean ± s.d., p = 0.05, Mann−Whitney test). This trend was not significant for complex cells (binocular = 15.8 ± 17.1 spk/sec, monocular = 12.4 ± 4.7 spk/sec, respectively, n = 51, mean ± s.d., p = 0.40, Mann−Whitney test), however, membrane potential responses at the preferred binocular phase for complex cells were significantly larger than those evoked by the preferred eye (7.8 ± 2.8 mV, 6.5 ± 9.3 mV, respectively, n = 24, mean ± s.d., p = 0.05, Mann−Whitney test). Simple cell subthreshold responses showed a similar trend (binocular = 10.3 ± 4.8 mV, monocular = 9.2 ± 4.7 mV, n = 52, mean ± s.d., p = 0.29, Mann−Whitney test). In contrast to normal animals, suprathreshold and subthreshold records from strabismic animals showed no differences in both simple (spikes: binocular = 17.6 ± 16.7 spk/sec, monocular = 17.9 ± 7.1 spk/sec, n = 84 mean ± s.d., p = 0.86, Mann−Whitney test; membrane potential: binocular = 10.7 ± 5.5 mV, monocular = 10.5 ± 5.4 mV, n = 48, mean ± s.d., p = 0.75, Mann−Whitney test) and complex cells (spikes: binocular = 11.4 ± 13.1 spk/sec, monocular = 11.8 ± 12.1 spk/sec, n = 86, mean ± s.d., p = 0.87, Mann−Whitney test; membrane potential: binocular = 6.7 ± 4.4 mV, monocular = 6.5 ± 4.3 mV, n = 31, mean ± s.d., p = 0.70, Mann−Whitney test). The increase in peak binocular responses in normal animals, but not strabismic animals, is expected given the loss of disparity selectivity and evidence for binocular response suppression.

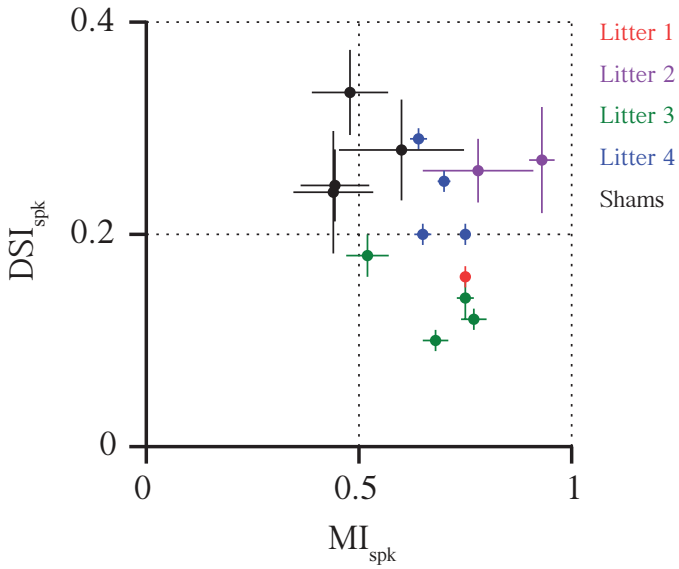

Figure 7.5: Comparison of spiking monocularity and disparity selectivity across animal litters

Mean and standard error of monocularity and binocular disparity selectivity from spiking responses of neurons recorded in each animal from each litter. Strabismic animals are color−coded by litter. Sham control animals shown in black.

Relationship between ocular dominance and disparity selectivity

Strabismus alters both ocular dominance and disparity selectivity, but it is not clear whether a single mechanism can account for these changes. Establishing a link between disparity selectivity and ocular dominance has remained difficult (LeVay and Voigt, 1988; Chino et al., 1994; Read and Cumming, 2004) suggesting that these two changes may reflect multiple circuit changes. On the other hand, for a neuron to be disparity selective, it must receive input from both eyes. This requirement was insufficient to enforce a relationship between spiking ocular dominance and spiking disparity selectivity (Fig. 7.4C,F), for V1 neurons recorded in either normal or strabismic animals (normal: mean PCA slope = 0.06 ± 0.13, strabismic: mean PCA slope = −0.20 ± 0.23, bootstrapped standard error, Sokal and Rohlf, 1995).

However, a relationship between monocularity and disparity selectivity at the level of synaptic input can be obscured by the threshold nonlinearity (Priebe and Ferster, 2008). We therefore compared membrane potential monocularity (MI_{vm}) to disparity selectivity based on spiking (DSI_{spk}) and membrane potential responses (DSI_{vm}). Simple cells from normal animals showed a significant correlation between MI_{vm} and DSI_{spk} (mean PCA slope = −0.59 ± 0.09, n = 38, bootstrapped standard error, Sokal and Rohlf, 1995), and MI_{vm} and DSI_{vm} (mean PCA slope = −0.15 ± 0.04, bootstrapped standard error, Sokal and Rohlf, 1995) (Fig. 7.4D−E, *blue*). These correlations demonstrate that disparity selectivity in simple cells depends strongly on the amount of binocular synaptic input a neuron receives.

Surprisingly, these trends were also found in strabismic animals (Fig. 7.4C−E, *green*). Simple cells in strabismic animals showed a significant correlation between MI_{vm} and DSI_{spk} (mean PCA slope = −0.48 ± 0.08, n = 42, bootstrapped standard

error, Sokal and Rohlf, 1995), and MI_{vm} and DSI_{vm} (mean PCA slope = −0.15 ± 0.03, bootstrapped standard error, Sokal and Rohlf, 1995). In contrast, complex cells showed no significant relationship between subthreshold input and disparity sensitivity in either strabismic or normal animals (Fig. 7.4F−H). The relationship between DSI_{vm} and DSI_{spk} in normal and strabismic animals was similar (Fig. 7.6), consistent with differences between normal and strabismic animals being driven by changes in synaptic input.

The similar relationship between monocularity and disparity tuning for normal and strabismic animals suggests that simple cells in strabismic animals have the potential to be disparity selective if provided with substantial binocular input. The link we established between disparity selectivity and monocularity indicates that the same mechanism could account for the changes in both response properties of simple cells, and is consistent with plasticity of simple cell inputs occurring mainly at thalamocortical synapses, with remaining binocular inputs generating disparity selectivity in the expected manner.

Suppression of binocular responses and synaptic inhibition

We frequently observed response suppression during binocular stimulation in records from strabismic animals. Suppression was evident both in neurons which received binocular synaptic input (Fig. 7.3B) and in those which were monocular (Fig. 7.3D), indicating not only a disruption of binocular integration, but a possible neural mechanism for quenching binocular information in visual cortex. To quantify suppression we measured binocular response Gain (Appendix B). Gain less than 0 indicates that the peak binocular response is less than the response to preferred eye stimulation alone. Gain greater than 0 indicates binocular responses are greater than the preferred monocular response.

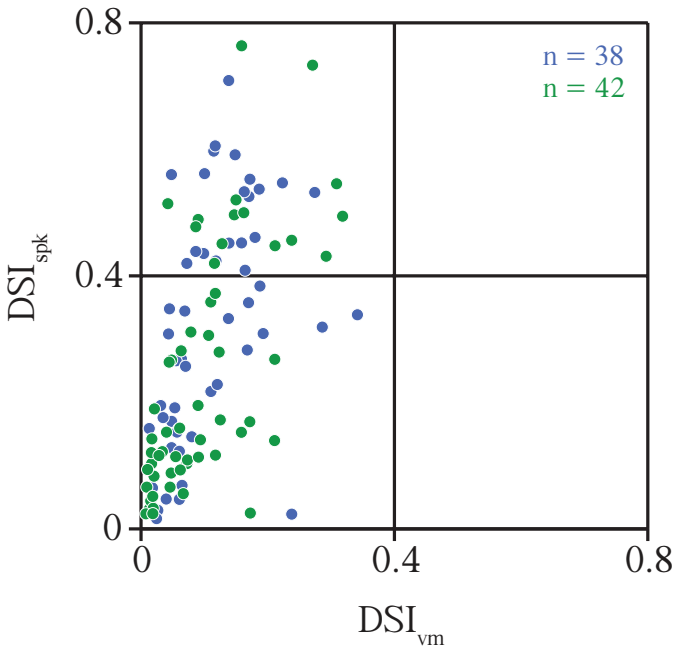

Figure 7.6: Relationship between subthreshold and suprathreshold disparity selectivity

Disparity selectivity index (DSI) plotted for membrane potential and spiking responses in neurons from normal (blue) and strabismic (green) animals.

Many V1 simple and complex cells from normal animals have binocular membrane potential and spike rate responses that are greater than those evoked by stimulation of either eye alone (Fig. 7.7A−B). These correspond to large Gain values (Fig. 7.7A, $Gain_{vm} = +0.28$, $Gain_{spk} = +0.81$). In contrast, neurons from strabismic animals had binocular responses smaller than those evoked by the preferred eye (Fig. 7.7C−D, $Gain_{vm} = -0.09$, $Gain_{spk} = -0.23$). Simple and complex cells exhibiting subthreshold and suprathreshold binocular suppression (Gain < 0) were more prevalent in strabismic animals than in normal animals (Fig. 7.7E−F). The proportion of simple cells displaying binocularly suppressed membrane potential and spike rate responses was larger in strabismic animals (membrane potential strabismic: 40%, normal: 25%; spike rate strabismic: 37%, normal: 19%). For complex cells, the proportion of neurons demonstrating suppression was also more pronounced in strabismic animals (membrane potential strabismic: 45%, normal: 10%; spike rate strabismic: 47%, normal: 22%). Increased binocular suppression caused by strabismus was also reflected in average Gain values for subthreshold responses in simple and complex cells (Fig. 7.7E,G) that were smaller in strabismic animals (simple strabismic: 0.02 ± 0.10, $n = 48$, normal: 0.10 ± 0.12, $n = 52$; mean ± s.d, $p = 0.004$; complex strabismic: 0.06 ± 0.15, $n = 31$, normal: 0.08 ± 0.08, $n = 24$; mean ± s.d, $p = 0.10$; Mann−Whitney test). Average Gain values for spiking responses from extracellular records and intracellular records with spikes were also smaller in strabismic animals (Fig. 7.7F,H) (simple strabismic: 0.12 ± 0.26, $n = 84$, normal: 0.32 ± 0.38, $n = 70$; mean ± s.d, $p = 0.001$; complex strabismic: 0.06 ± 0.26, $n = 86$, normal: 0.23 ± 0.35, $n = 51$; mean ± s.d, $p = 0.001$, Mann−Whitney test).

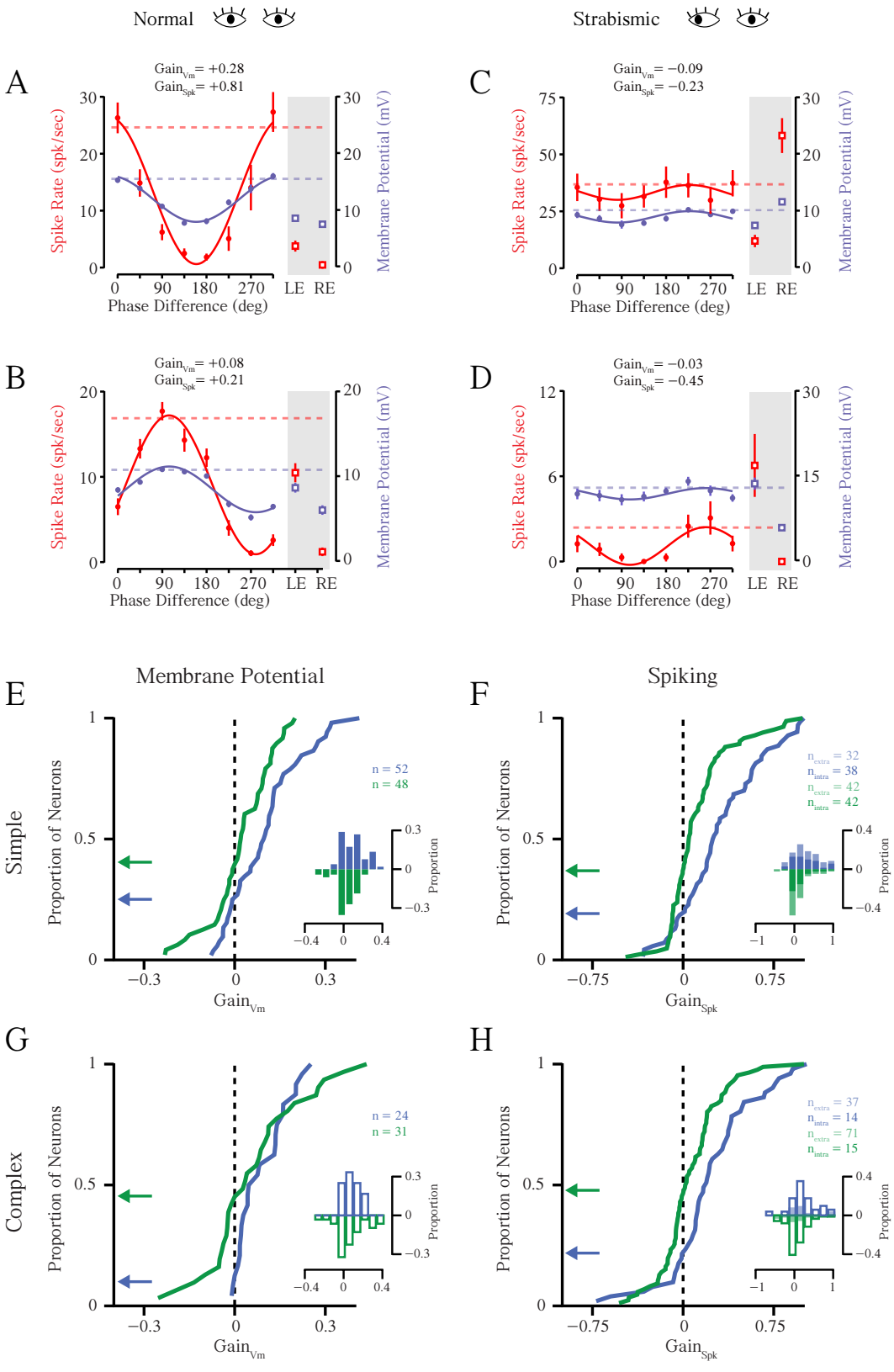
Normal
Strabismic
A
B
C
D
Gain$_{Vm}$ = +0.28
Gain$_{Spk}$ = +0.81
Gain$_{Vm}$ = +0.08
Gain$_{Spk}$ = +0.21
Gain$_{Vm}$ = −0.09
Gain$_{Spk}$ = −0.23
Gain$_{Vm}$ = −0.03
Gain$_{Spk}$ = −0.45
Spike Rate (spk/sec)
Membrane Potential (mV)
Phase Difference (deg)
LE RE
Membrane Potential
Spiking
Simple
Complex
E
F
G
H
Proportion of Neurons
Gain$_{Vm}$
Gain$_{Spk}$
Proportion
n = 52
n = 48
n = 24
n = 31
n$_{extra}$ = 32
n$_{intra}$ = 38
n$_{extra}$ = 42
n$_{intra}$ = 42
n$_{extra}$ = 37
n$_{intra}$ = 14
n$_{extra}$ = 71
n$_{intra}$ = 15

Figure 7.7: Binocular response suppression of membrane potential and spiking responses in neurons of primary visual cortex

(A) Example neuron disparity tuning curve for subthreshold membrane potential (purple) and spiking (red) peak responses from a normal animal. Responses at preferred disparities (0 and 270 deg) are much larger than response from the preferred eye (gray shading). Dashed lines indicate amplitude of summed mean and modulation components of disparity tuning. Positive gain values (Appendix A) reflect the large increase in binocular responses relative to stimulation of the preferred eye. (B) Same as in (a) for another unsuppressed neuron from a normal animal. (C) Same as in (a) for an example neuron from a strabismic animal. Slight suppression of membrane potential responses and large suppression of spiking responses are evident, represented by respective negative gain values. (D) Same as in (c) for another example neuron. (E) Cumulative distribution of gain values for subthreshold membrane potential in simple cells from normal (blue) and strabismic (green) animals. Gain values below 0 (dashed line) indicate binocular suppression. Arrows indicate proportion of neurons suppressed by binocular stimulation. Gain value distributions also shown (inset). (F) Same as in (e) for spiking responses. Spiking distributions include intracellular (dark shading) and extracellular (light shading) records. (G) Same as in (e) for complex cells. (H) Same as in (f) for complex cells.

Given a clear increase in binocular suppression, we asked whether these neurons showed antagonism between the two eyes that may be revealed by monocular stimulation. Similar to the increased monocularity induced by strabismus, binocular suppression was not accompanied by hyperpolarization evoked by the nonpreferred eye. Suppressed neurons from strabismic animals ($Gain_{vm} < 0$) had small depolarizing responses from stimulation of the nonpreferred eye (mean = 1.5 ± 2.3 mV s.d., n = 32). However, simple and complex cell responses were different. Simple cells with binocular suppression had nonpreferred eye responses which were much closer to spontaneous activity, and less than that of complex cells (simple = 0.96 ± 2.3, n = 19, complex = 2.4 ± 2.1, n = 13, mean ± s.d, p = 0.02, Mann−Whitney test). The difference in strength of nonpreferred eye input between simple and complex cells might reflect differences in monocularity (Fig. 7.2). Despite these differences, nonpreferred eye responses from both simple and complex cells indicate that binocular suppression cannot be predicted by a linear summation of right and left eye membrane potential responses. These membrane potential records suggest that synaptic inhibitory mechanisms, activated by binocular stimulation, may contribute to suppression induced by strabismus.

Synaptic inhibition has been the hypothesized cause of binocular suppression (Levi et al., 1979; Sengpiel and Blakemore, 1994; Sengpiel et al., 1994). Pharmacological experiments have provided strong evidence that inhibition underlies binocular suppression (Sengpiel et al., 2006). However, as the pharmacological agent in those experiments caused a large and widespread increase in spike rates, the experiments were unable to rule out that a loss of binocular suppression was due to a global increase in neuronal excitability (Sengpiel et al., 2006). We therefore sought a complementary test of the hypothesis by estimating excitatory and inhibitory inputs to single neurons without drastically affecting spike rates of surrounding neurons. In a few

neurons we estimated excitatory and inhibitory inputs from membrane potential responses recorded at different levels of injected current (Borg−Graham et al., 1998; Hirsch et al., 1998; Anderson et al., 2000).

In neurons from normal animals, membrane potential depolarization evoked by the preferred binocular stimulus was greater than for stimulation of the preferred eye alone (Fig. 7.8A, *left*, Fig. 7.3A, Fig. 7.7A−B). Likewise, peak synaptic excitation and inhibition evoked by the binocular stimulus was greater than that evoked by monocular stimulation (Fig. 7.8A, *middle panels*). A similar trend was evident across a population of neurons (n = 17) from normal animals (Ge: binocular = 2.00 ± 1.71 nS, preferred eye = 1.19 ± 1.13 nS, $p < 0.05$, paired t−test; Gi: binocular = 1.55 ± 1.51 nS, preferred eye = 1.12 ± 1.18 nS, $p < 0.05$, paired t−test, n = 17, mean ± s.d.). Membrane potential, synaptic excitation, and synaptic inhibition did not exhibit binocular suppression and the ratio of excitation to inhibition was generally unchanged across stimulus conditions, yielding no significant change across our sample population whether the mean, median or geometric mean is compared (Fig 8A, *right*). In contrast, in strabismic animals membrane potential depolarization evoked by the preferred binocular stimulus was less than that evoked by the preferred eye (Fig. 7.8B−C, *left*). Conductance estimates across our small population of neurons (n = 9) indicate an increase in inhibition for the preferred binocular stimulus, accompanied by little change in excitation (Ge: binocular = 2.08 ± 0.88 nS, preferred eye = 2.10 ± 0.82 nS, p = 0.97, paired t−test; Gi: binocular = 3.37 ± 2.26 nS, preferred eye = 2.84 ± 1.45 nS, p = 0.31, paired t−test, mean ± s.d.). For neurons in which membrane potential measurements demonstrated binocular suppression (Fig. 7.8B−D), the difference between excitation and inhibition in monocular and binocular conditions is more

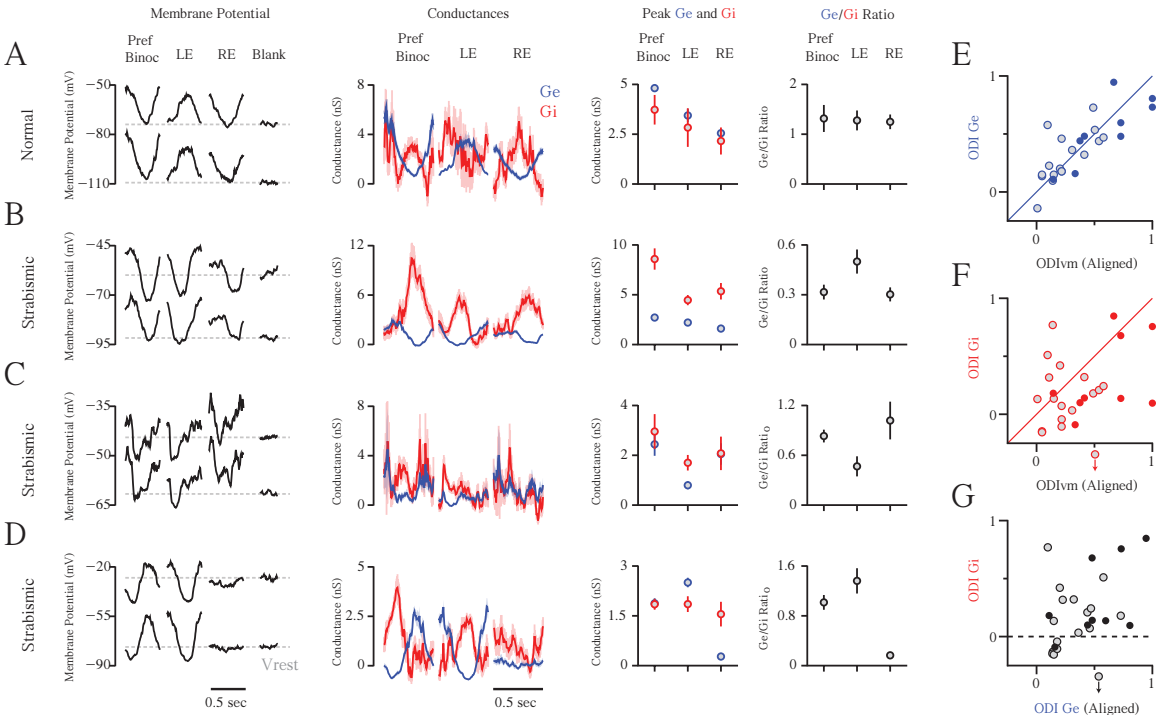

Figure 7.8: Subthreshold binocular suppression due to synaptic inhibition
(A) Mean cycle−averaged membrane potential responses at two levels of current injection, excitatory (blue) and inhibitory (red) synaptic conductances, peak excitatory and inhibitory conductances, and ratio of excitation to inhibition for the preferred binocular disparity and monocular stimulation in an example neuron from the normal animal. (B−C) Same as in (a) for binocular neurons from the strabismic animal. (D) Same as in (b−c) for monocular neuron. Gray dashed line represents resting membrane potential during mean−luminance (blank) periods for each level of current injection. Conductance traces, peak values, and excitation to inhibition ratios are plotted as mean and bootstrapped standard error (Sokal and Rohlf, 1995). (E) The ocular dominance index for the peak excitatory conductance is plotted relative to the ocular dominance index based on the peak membrane potential. Each symbol indicates a different neuron. Filled symbols indicate neurons recorded from strabismic animals, which are more monocular than neurons from normal animals, indicated by open symbols. The ocular dominance for Vm was aligned such that 0 indicates binocular and 1 indicates monocular, for the dominant eye (either contralateral or ipsilateral). This convention for ocular dominance is followed for the ordinate as well. Negative values on the ordinate therefore indicate preference for the opposite eye (F−G) The format follows that in (e), except that the ocular dominance index for inhibition is plotted relative to

membrane potential (f), or inhibition is plotted relative to excitation (g). One neuron, indicated by the arrow, has a very negative ocular dominance score (−0.78).

pronounced. For this subset of neurons (4/9), inhibition is dramatically increased by binocular stimulation relative to excitation (Ge/Gi: binocular = 0.70 ± 0.26, preferred eye = 0.98 ± 0.36, $p < 0.05$, paired t−test, mean ± s.d., Fig 8B−D, *right panels*).

These results suggest that inhibition is playing a direct role in producing binocular suppression. Such inhibition could be generated by an antagonism between the representations of the two eyes, in which case the eye preference for inhibition should be opposite of that for excitation. Alternatively, inhibition may simply be less monocular than excitation, such that binocular stimulation drives inhibition strongly. Our estimates of excitatory conductance indicate that the eye dominance evident in membrane potential is closely related to that found in the resulting membrane potential for neurons recorded in both normal and strabismic animals (Fig. 7.8E, not significant, $p = 0.27$, paired t−test). Inhibition, in records from strabismic animals, is more binocular than either the resulting membrane potential (Fig. 7.8F, mean $MI_{Gi} = 0.33$, $MI_{Vm} = 0.60$, paired t−test, $p < 0.05$) or excitation (Fig. 7.8G, mean $MI_{Ge} = 0.53$), although there is considerable variability on a cell−by−cell basis. While inhibition is more binocular than excitation it nonetheless shares overall eye preference with excitation. Therefore, the decline in the excitatory to inhibitory ratio observed in suppressed neurons (Fig. 7.8B−D) results from inhibition being more broadly tuned for eye preference and being driven better by binocular stimulation instead of an antagonism between the two eye representations. Our conductance measurements therefore suggest that increased inhibition evoked by the preferred binocular stimulus could account for binocular response suppression and facilitate the loss of binocular convergence observed in strabismic animals. These indications from our limited sample must be tested by more extensive measurements.

DISCUSSION

Primary visual cortex (V1) is the first site of binocular integration leading to seamless visual perception and stereoscopic depth perception (Ohzawa et al., 1990; DeAngelis et al., 1991; Cumming and Parker, 1997; Cumming and DeAngelis, 2001). The effects of strabismus in V1 were previously studied by extracellular recording of spiking responses, leaving the underlying subthreshold synaptic inputs unknown (Hubel and Wiesel, 1965; Blakemore, 1976; Crewther et al., 1985; Chino et al., 1994; Roelfsema et al., 1994; Sengpiel and Blakemore, 1994; Sengpiel et al., 1994; Fries et al., 1997; Smith et al., 1997; Schmidt et al., 2004; Sengpiel et al., 2006; Ranson et al., 2012). Using intracellular recordings we found that strabismus increased monocularity in simple cells, but not in complex cells. Simple and complex cells both exhibited decreased disparity selectivity, and an increased occurrence of binocular suppression. Finally, our estimates of excitatory and inhibitory synaptic input onto single neurons indicate that binocular suppression was the result of an imbalance in the ratio of excitation and inhibition. Inhibition shared eye preference with excitation, but was more binocular than excitation. Inhibition therefore increased to greater degree than excitation in response to binocular stimulation, which leads to an overall response suppression.

We outline a diagrammatic circuit model for the changes induced by strabismus based on the disparity energy model (Anzai et al., 1999b, a) (Fig. 7.9). In normal animals, simple cells receive thalamic excitatory input from left and right eyes (Fig. 7.9, *left*). Net excitation from each eye is selective for spatial phase, and thus temporally modulated by sinusoidal stimuli. Disparity selectivity with binocular stimulation results because the two eyes provide correlated excitation only at a particular relative spatial phase. Complex cells receive excitatory input from multiple

simple cells with a wide range of spatial phase selectivity and a narrow range of disparity selectivity, and have responses that are not temporally modulated by sinusoidal stimuli but are disparity tuned. Because simple cell inputs to complex cells do not have identical disparity selectivity, net synaptic input to a complex cell is less disparity selective than spiking responses from simple cells. Neurons in normal animals also receive synaptic inhibition that contains components with various degrees of selectivity for spatial phase (Azouz et al., 1997; Borg–Graham et al., 1998; Hirsch et al., 1998; Hirsch et al., 2003; Monier et al., 2003; Cardin et al., 2008; Nowak et al., 2008).

In this model, strabismus causes each simple cell to lose excitatory input from one of the eyes as a result of Hebbian or Hebbian–like spike timing–dependent plasticity (Miller et al., 1989; Song et al., 2000; Gutig et al., 2003) (Fig. 7.9, *right*). Because of the loss of excitatory input from one eye, simple cells become more monocular and less disparity tuned. Complex cells remain binocular because they receive inputs from left and right eye–preferring simple cells, but are less disparity selective because those simple cells that provide feedforward drive are less disparity tuned. Because the input to inhibitory neurons is unchanged, inhibition onto simple cells remains. The increased ratio of inhibition to excitation results in binocular suppression of simple cells. As simple cells provide input to complex cells, the latter also exhibit binocular suppression. If thalamic input is lost in all simple cells, an alternative model in which inhibition is recurrent rather than feedforward would exhibit similar behavior. We therefore argue that plasticity only at thalamocortical synapses is sufficient to account for our observations.

Notably, each neuron's disparity selectivity depends on the spatial selectivity of its inputs and a variety of weights are needed to generate the full range of disparity tuning observed (Anzai et al., 1999a, b; Schmidt and Löwel, 2006; Schmidt and Löwel,

2008; Jaffer et al., 2012). In our simple model, the general nature of strabismus is the same regardless of the differences in synaptic strength, spatial selectivity, and spatial phase between inputs from each eye to each neuron. It is possible that the quantitative extent of induced changes by strabismus does depend on such initial differences, but we do not have the data to determine these dependencies. Our simple model is thus only qualitative with respect to such possible dependencies.

The plausibility of strabismus causing changes mainly at thalamocortical synapses is consistent with evidence that the thalamocortical synapse is also the site of plasticity following monocular deprivation (Khibnik et al., 2010; Wang et al., 2013), but differs from conclusions from other groups. For example, monocular deprivation is known to induce changes in the spiking responses first of supragranular neurons and then subsequently of thalamorecipient neurons (Diamond et al., 1994; Trachtenberg et al., 2000), indicating that plasticity emerges through cortical interactions first. One potential resolution to this apparent discrepancy is that supragranular neurons receive input from several thalamorecipient neurons and perform an effective averaging that renders weak changes in thalamorecipient neurons more visible. Further, thresholding synaptic inputs in the supragranular neurons would further enhance any slight change in their subthreshold ocular dominance (Priebe, 2008; Priebe and Ferster, 2008). Another argument against the minimal model we diagrammed is the observation of changes in the inhibitory network following monocular deprivation, as shown by changes in visual responses of inhibitory neurons (Yazaki−Sugiyama et al., 2009) and the potentiated inhibitory synapses onto excitatory neurons after monocular deprivation (Maffei et al., 2004; Maffei et al., 2006). The net inhibition onto excitatory neurons might be unchanged if thalamic input onto inhibitory neurons is weakened, but is compensated by strengthened inhibitory inputs onto excitatory neurons (House et al., 2011). Finally, the rules of plasticity responsible for such changes may be different than the simple

Hebbian rule we assumed for thalamocortical synapses onto excitatory simple cells (Bell et al., 1997; McBain et al., 1999; Holmgren and Zilberter, 2001; Woodin et al., 2003; Tzounopoulos et al., 2004; Haas et al., 2006; Lu et al., 2007; Caporale and Dan, 2008; Kullmann et al., 2012). Indeed, monocular deprivation experiments indicate that even Hebbian plasticity may be inadequate over long time scales, and changes are supplemented with homeostatic mechanisms (Mrsic−Flogel et al., 2007; Maffei and Turrigiano, 2008; Ranson et al., 2012).

Not only is ocular misalignment a primary example of experience−dependent learning, but it is a common visual disorder found in humans. We have demonstrated profound cell−type specific changes in synaptic drive following exotropic strabismus. Along with the disruption of right and left eye integration we also find that inhibitory interactions contribute to the loss of cortical circuitry underlying binocularity. In particular we have found that the inhibitory network associated with strabismus is not solely based on an antagonism between the eyes, but instead acts to suppress binocular integration. A common treatment to preserve cortical responses to both eyes has been to patch the stronger eye, but this may not be helpful in the recovery of stereo vision. Instead, therapies that actively engage both eyes during visual tasks result in improvements of stereo vision (Li et al., 2011; Li et al., 2013). These therapies may in fact be altering the inhibitory network that has developed to prevent diplopia and thus aiding in the recovery of proper depth perception.

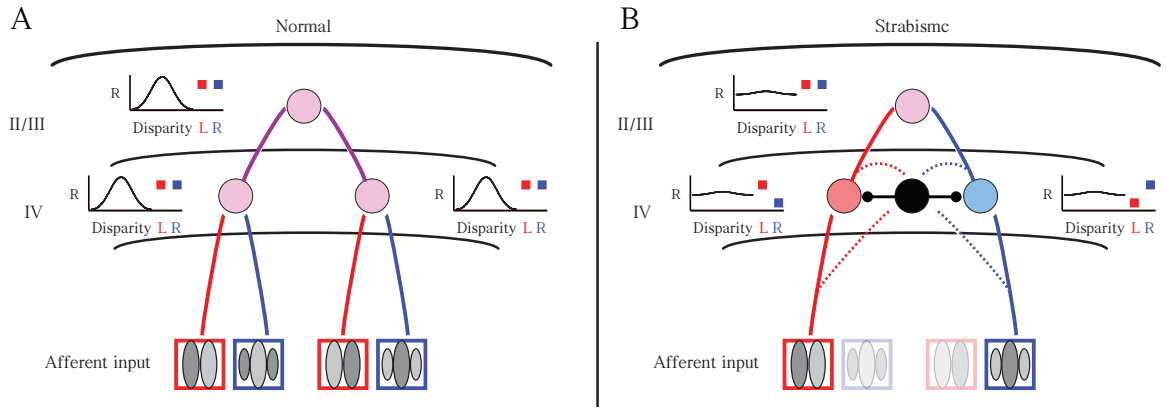

Figure 7.9: Loss of thalamic input in circuit model of strabismus

(A) Left and right eye inputs converge on layer 4 simple cells, generating disparity selectivity. Simple cell inputs converge onto complex cells in layer 2/3, which are also disparity selective. **(b)** In strabismic animals, simple cells receive monocular input. A loss of binocularity causes a loss of disparity selectivity, which also occurs in complex cells through feedforward inputs. Complex cells receive inputs from simple cells and thus can be binocular. Suppression of binocular responses is mediated by inhibitory interneurons receiving input from thalamocortical inputs and simple cells. In this simple model, the strabismus−induced changes are qualitatively similar for all neurons regardless of the initial difference in synaptic strength, spatial selectivity and spatial phase between the inputs from each eye to the neuron.

Chapter 8: Loss of binocular disparity selectivity following monocular deprivation in mouse V1

ABSTRACT

Experience dependent plasticity during the critical period of development shapes anatomical and functional elements of cortical circuits. In primary visual cortex (V1) of mice, neurons in binocular zone shift preference toward the ipsilateral eye if the contralateral eye is occluded during the critical period. This shift equalizes the relative contribution of input from each eye. Here we tested how this increased ocular input affects binocular disparity selectivity of V1 neurons, a response property arising from the integration of ocular inputs. Using two-photon calcium imaging we measured ocular dominance (OD) and disparity selectivity of neurons in the binocular zone of mice after occluding one eye during the critical period. Surprisingly, a decrease in disparity sensitivity accompanied increased binocularity in deprived animals. Decreased disparity tuning was most pronounced in moderately binocular neurons, as measured by ocular dominance. These data suggest the enhanced binocularity resulting from OD plasticity is at least partially nonfunctional due to a loss of disparity selectivity, suggesting synaptic input misalignment during deprived visual experience.

INTRODUCTION

Experience-dependent plasticity during the critical period of development shapes anatomical and functional elements of cortical circuits (Katz and Crowley, 2002; Espinosa and Stryker, 2012). In primary visual cortex (V1) of mice, neurons are

contralaterally biased, but following monocular deprivation (MD) of the contralateral eye during the critical period their preferences shift towards the non−deprived (ipsilateral) eye (Gordon and Stryker, 1996). This increased ocular input provides an enticing model to study plasticity of ocular integration. Conventionally, neuronal eye preferences are measured by an ocular dominance (OD) index through independent stimulation of each eye (Dräger, 1975; Wagor et al., 1980; Gordon and Stryker, 1996; Hanover et al., 1999; Tagawa et al., 2005; Mrsic−Flogel et al., 2007; Hofer et al., 2009), but this metric provides little information about integration. Binocular disparity selectivity, the sensitivity to local spatial offsets between retinal images, emerges in V1 through the integration of ocular inputs (Joshua, 1970; DeAngelis et al., 1995; Scholl et al., 2013a). Binocular disparity tuning can be observed in individual neurons as some binocular phase differences between eyes elicit large increases in responses, while others can reduce responses, relative to monocular stimulation alone (Hubel and Wiesel, 1962; Pettigrew et al., 1968; Ohzawa and Freeman, 1986; Longordo et al., 2013; Scholl et al., 2013b). How enhanced binocularity from OD plasticity affects disparity tuning and ocular integration remains unknown.

We hypothesized three basic outcomes, as a consequence of increased binocularity, following critical period MD, on disparity selectivity in mouse V1 neurons, outlined in Figure 8.1. An OD shift could increase excitatory input onto neurons through enhancement of non−deprived eye input, generating greater binocular disparity tuning (Fig. 8.1B). This could result from either modification of the non−deprived eye synaptic weights or formation of new connections, but requires that new inputs possess identical spatial−temporal profiles to original inputs for preserving selectivity. Alternatively, non−deprived eye inputs might arise from wholly new synaptic connections with dissimilar spatial−temporal profiles, generating a decrease in disparity tuning by enhancing untuned binocular excitatory input (Fig. 8.1B). Activity

decorrelation between the two eyes during deprived visual experience might provide a basis for this scenario (Chen et al., 2014). A final possibility is disparity tuning maintenance, potentially resulting from an equal and opposite changes in synaptic weights of each eye (Fig. 8.1B) (Mrsic−Flogel et al., 2007). Here modification of pre−existing inputs containing relevant spatial−temporal information is necessary.

We used *in vivo* two−photon calcium imaging (Stosiek et al., 2003; Kerr and Greenberg, 2005; Ohki et al., 2005; Garaschuk et al., 2006; Golshani and Portera−Cailliau, 2008) of hundreds of superficial neurons in the binocular zone of mouse V1 to determine how OD plasticity shapes binocular integration. In normal mice and those that underwent critical period MD, ocular dominance and disparity selectivity weremeasured. We found classic OD plasticity, with neurons shifting preference to the non−deprived eye, accompanied a loss of disparity selectivity. We also measured changes in disparity tuning for monocular and binocular cells separately and found disparity selectivity was greatest in moderately binocular neurons.

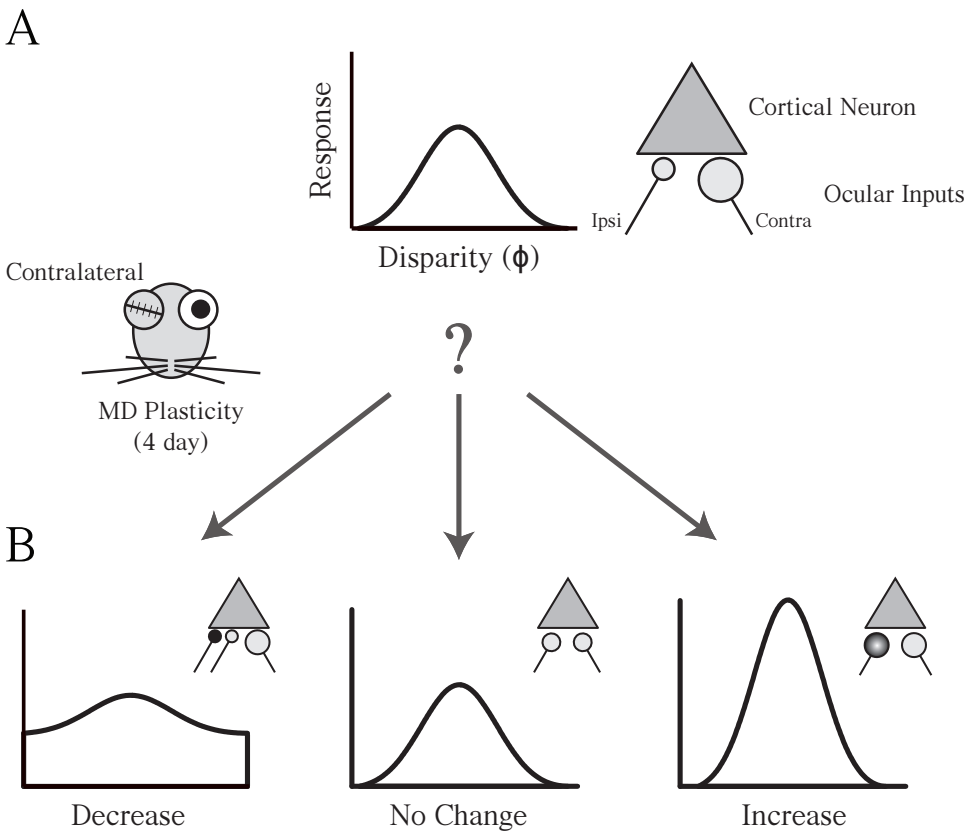

Figure 8.1: Hypothesized changes in disparity tuning after monocular deprivation

(A) Normal adult mouse visual cortical neurons are contralaterally biased, but can receive binocular subthreshold inputs to generate binocular disparity sensitivity through the combination of weak ipsilateral and strong contralateral inputs (*right)*. (B) Monocular deprivation of the dominant eye leads to a shift in ocular preference such that neurons are more binocular. Increased binocularity could affect disparity selectivity via different mechanisms: decreased tuning due to mismatching spatial temporal inputs, no change through proportional plasticity, or increased tuning by enhancement of excitatory input from the weak eye.

RESULTS

We used *in vivo* two−photon calcium imaging to measure the ocular dominance and binocular disparity tuning of neurons in primary visual cortex (V1) of anesthetized normal and monocularly deprived (MD) mice. Deprivation of the contralateral eye was initiated during the critical period (P28−P30) and lasted for 4 days (Gordon and Stryker, 1996; Hanover et al., 1999; Tagawa et al., 2005). In each experiment the binocular zone of V1 was identified from extracellular recordings, receptive fields were carefully mapped in a targeted region within the central 30 degrees of the visual field, and a mirror was placed in front of the contralateral eye to allow for presentation of a dichoptic stimulus (Scholl et al., 2013a). Cortical tissue in the binocular region of interest was bulk loaded with the cell−permeable form of the calcium indicator Oregon Green BAPTA−1 (OGB−1 AM; Appendix A) (Stosiek et al., 2003; Kerr and Greenberg, 2005; Ohki et al., 2005; Garaschuk et al., 2006; Golshani and Portera−Cailliau, 2008), resulting in a stained volume of approximately 150−300 microns in diameter.

To measure monocular responses and binocular disparity selectivity we pseudorandomly dichoptically presented drifting vertical gratings (90 deg) to each eye alone or simultaneously while recording changes in calcium fluorescence. By varying the contralateral stimulus phase, we probed eight binocular disparities (0−315 deg phase difference). During each experiment we imaged multiple focal planes (6−15) at depths ranging from 150 to 460 microns below the pia surface. A rotatable objective was used to position the cortical surface normal to imaging plane. Cells were chosen by hand from an OGB−1 AM structure image (Fig. 8.2, *left*) and an automated algorithm created a mask for denoting pixels to average in each frame (Appendix A). Across normal animals used (n = 6, P35−P60) we identified a total of 3,982 neurons, of which 1,059 neurons were visually responsive for monocular stimuli (27%) and 2,237 neurons

were visually responsive for binocular stimuli (56%). Across MD animals used (n = 4, P33–P35) we identified a total of 2,469 neurons, of which 846 neurons were visually responsive for monocular stimuli (34%) and 1,650 neurons were visually responsive for binocular stimuli (67%). Differences in visual responsiveness between monocular and binocular conditions is in part due to a lack of stimulus parameter optimization. To adequately probe binocular disparities, a single orientation and spatial frequency was used in each experiment. Mouse V1 neurons exhibit a 'salt and pepper' pattern of orientation preferences and a wide range of spatial frequency selectivities (Ohki et al., 2005; Niell and Stryker, 2008), so our monocular stimuli are certainly ineffective at stimulating all potential visually responsive neurons (e.g. those tuned for horizontal gratings).

Fluorescence fluctuations from cells in mouse V1 were strongly modulated by binocular disparities, compared to stimulation of either eye alone or the blank (mean luminance) period, similarly to previous reports of spiking activity (Scholl et al., 2013a) and two–photon calcium imaging in cat V1 (Kara and Boyd, 2009). In an example neuron (Fig. 8.2A, traces), monocular stimulation of either eye evoked nearly equivalent changes in fluorescence (~10% ΔF/F), while the preferred disparity (90^{o} phase difference) evoked even larger fluorescence changes (~30% ΔF/F) and the null disparity (270^{o} phase difference) evoked little change (~5% ΔF/F), all relative to activity during the blank period. Plotting stimulus–averaged peak calcium responses showed response modulation by binocular phase differences, and binocular responses that were as strong or stronger than responses to either eye alone (Fig. 8.2A, see tuning curve). From these neural responses we computed two metrics: an ocular dominance index (ODI) to compare monocular responses from each eye and a disparity selectivity index (DSI) to quantify response selectivity to binocular phase differences

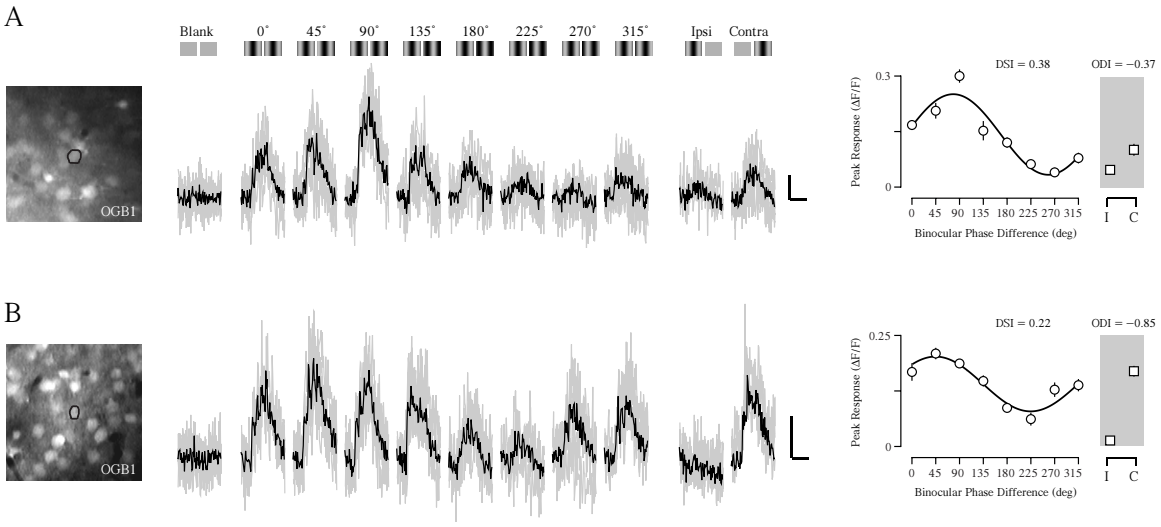

Figure 8.2: Two−photon imaging binocular disparity selectivity of neurons in mouse V1 binocular zone

(A) Example of calcium responses in a binocular neuron evoked by a range of binocular disparities (0 − 315 deg), monocular stimulation of each eye, and a mean luminance screen. Individual traces shown in gray and trial−average mean shown in black. Illustration of each stimulus shown above response traces. Scale bar indicates 10% change in fluorescence (ΔF/F) and 1 sec duration. Mean and standard error of peak ΔF/F shown in a tuning curve. Two−photon images (left) show fluorescence from OGB−1 AM. (B) Same as in (a) for a monocular neuron with strong disparity selectivity.

(Appendix B). In this example (Fig. 8.2A), these metrics depicted a binocular, but contralaterally biased, neuron with strong disparity selectivity (ODI = −0.37, DSI = 0.38). A number of monocular neurons were also observed with moderate disparity tuning (ODI = −0.85, DSI = 0.22, Fig. 8.2b).

Across all neurons with visually−evoked response to monocular stimuli we found a shift in ODI between normal and deprived animals (Fig. 8.3A−C). As reported previously from spiking (Gordon and Stryker, 1996; Hanover et al., 1999; Tagawa et al., 2005) and calcium responses (Mrsic−Flogel et al., 2007; Kameyama et al., 2010), the contralateral bias of neurons in normal mice (Fig. 8.3A) shifts towards more equivalent monocular responses (Fig. 8.3B). Since the ODI is a symmetric index, to quantify the difference in these distributions we computed the absolute value of ODI, such that a value of 0 indicates binocular responses and a value of 1 indicated perfectly monocular responses. Neurons from normal animals were more monocular than those from MD animals (Normal: median |ODI| = 0.54, mean |ODI| = 0.57 ± 0.33 s.d.; MD: median |ODI| = 0.36, mean |ODI| = 0.43 ± 0.31 s.d.; p = 0.0001, Mann−Whitney test). A shift in ODI was also evident in the cumulative distributions normal and deprived animals responses (Fig. 8.3C).

We next investigated differences in disparity selectivity for all neurons with visual responses of binocular stimuli in normal and deprived animals (Fig. 8.3A−C). As proposed earlier, a shift towards greater binocularity in monocular responses might affect binocular disparity tuning in different ways (Fig. 8.1): increased, decreased, or maintained selectivity. Across our population of neurons we found that compared to the distribution of DSI in normal animals (Fig. 8.3D), neurons from deprived animals exhibited a decrease in DSI (Fig. 8.3E). This modest decrease was significant (Normal: median DSI = 0.20, mean DSI = 0.24 ± 0.18 s.d.; MD: median DSI = 0.15, mean DSI

= 0.19 ± 0.14 s.d.; p = 0.0001, Mann−Whitney test), suggesting nonfunctional OD plasticity. Given the differential effects of OD plasticity on binocular and monocular neurons in mouse V1 (Mrsic−Flogel et al., 2007), we also explored the relationship of DSI as a function of the absolute value of ODI. We constrained this analysis to cells with robust visual responses to both monocular and binocular stimuli (Normal: n = 878, MD: n = 752). Here we found the strongest DSI decrease occurred in moderately binocular neurons (0.20 < |ODI| < 0.40, Normal median DSI = 0.20, MD median DSI = 0.14, p = 0.008; 0.40 < | ODI| < 0.60, Normal median DSI = 0.21, MD median DSI = 0.15, p = 0.009; Mann−Whitney test). A similar trend was noted in the most binocular neurons (0 < |ODI| < 0.20, Normal median DSI = 0.13, MD median DSI = 0.12, p = 0.13; Mann−Whitney test), but it was not significant. Our data show that an OD shift by deprivation of the contralateral eye during the critical period causes a loss of binocular disparity selectivity, particular in that of neurons with moderate binocularity.

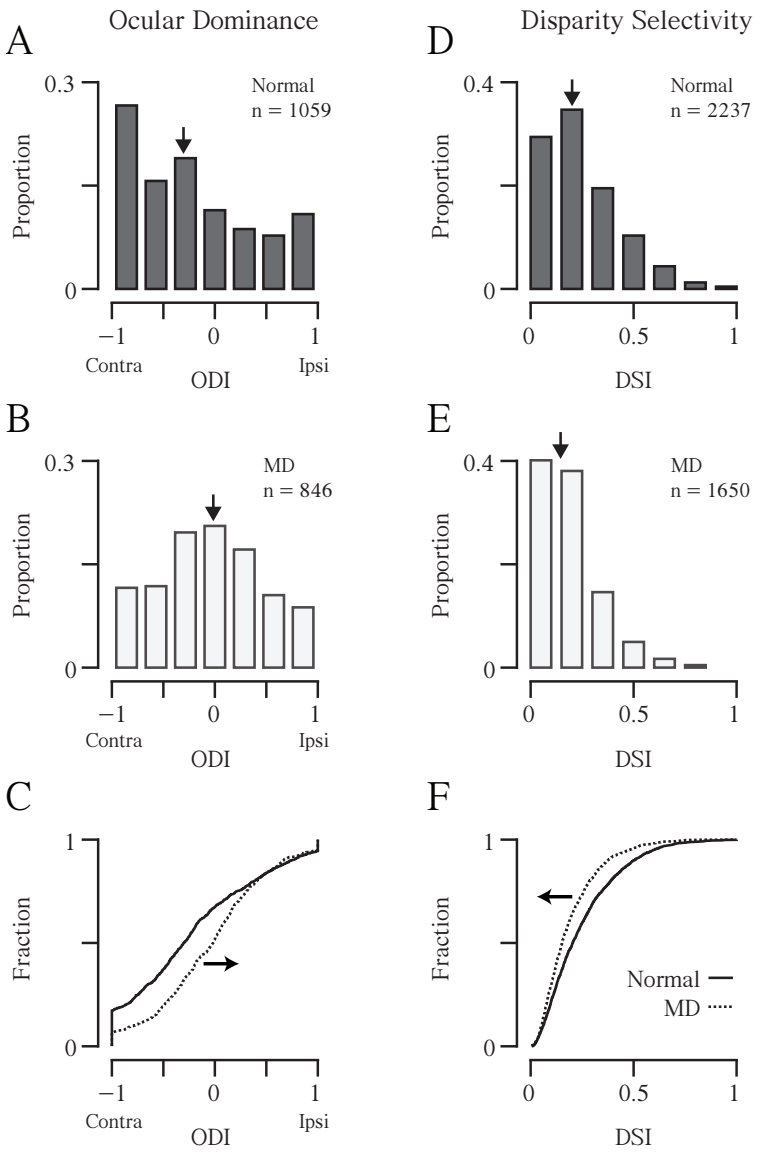

Figure 8.3: Monocular deprivation increases binocularity and decreases disparity selectivity

(A) Distribution of ocular dominance index (ODI) in normals animals. Arrow indicates median. (B) Same as (a) for monocular deprived (MD) animals. (C) Cumulative distributions of ODI in normal and deprived animals. Solid line indicates normal animals and dashed line indicates MD animals. Arrow indicates direction shift. (D) Distribution of disparity selectivity index (DSI) in normal animals. Arrow indicates median. (E) Same as (d) for MD animals. (F) Same as (c) for DSI in normal and MD animals. Arrow indicates direction shift.

DISCUSSION

Experience–dependent plasticity during the critical period guides maturation of sensory cortical circuits, both in anatomy and functional response properties of individual neurons. Neurons in the mouse V1 binocular zone shift their preference toward the ipsilateral eye if the contralateral eye is occluded during the critical period, causing increased binocularity as measured by ocular dominance (OD) (Dräger, 1975; Wagor et al., 1980; Gordon and Stryker, 1996; Hanover et al., 1999; Tagawa et al., 2005; Mrsic–Flogel et al., 2007; Hofer et al., 2009). We assessed how this enhancement in feedforward input transforms ocular integration as measured by binocular disparity selectivity (DSI) using dichoptic stimulation of mouse V1 neurons in the binocular zone (Scholl et al., 2013a). We hypothesized three possible outcomes: increased disparity tuning from enhancement of non–deprived excitatory inputs, maintenance of disparity tuning through proportional changes between each eye, or decreased tuning resulting from newly formed or modified synaptic non–deprived eye inputs with mismatched spatial–temporal profiles. Using two–photon calcium imaging we measured OD and DSI in populations of neurons in both normal and deprived animals. We found the increased binocularity, evident in a OD shift, was accompanied by a decrease in DSI. Further, in deprived animals, moderately binocular neurons displayed the greatest loss of disparity selectivity. Our data suggest OD plasticity mediated enhancement of binocularity drives a misalignment of synaptic inputs from the two eyes.

Here we provide evidence for recruitment of nonfunctional inputs following OD plasticity, suggesting formation of new connections abandoning spatial–temporal profile of existing inputs. Additional evidence for this mechanism is shown in the loss of orientation preference similarity between the two eyes following monocular

deprivation and loss of binocular overlap in receptive field structures with dark rearing (Wang et al., 2010; Sarnaik et al., 2014). It is important to note that other mechanisms are likely involved. For example, the disparity selectivity decrease we observed could be confounded by concurrent proportional synaptic weight changes, as many cells still exhibited strong binocular disparity selectivity in deprived animals (Mrsic−Flogel et al., 2007). Chronic calcium imaging of cellular populations could potentially elucidate these different mechanisms, although calcium reporters can not truly reflect underlying changing in synaptic inputs. To more clearly elucidate these changes, intracellular records are necessary to directly measure subthreshold synaptic input onto neurons and the resulting disparity selectivity. In particular, intracellular measurements in combination with genetic tools silencing (Lien and Scanziani, 2013) cortical input could provide a means to dissect apart thalamocortical synaptic inputs from each eye and intracortical input, in order to identify the dynamics of synaptic plasticity.

Chapter 9: Local integration accounts for weak selectivity of mouse parvalbumin interneurons in mouse V1[1]

ABSTRACT

Dissecting the functional roles of excitatory and inhibitory neurons in cortical circuits is a fundamental goal in neuroscience. Of particular interest are their roles in emergent cortical computations such as the integration of ocular inputs in primary visual cortex. We measured the binocular response selectivity of parvalbumin (PV^+) interneurons relative to the remaining neurons (PV^-). PV^+ interneurons received strong inputs from both eyes, but lacked selectivity for binocular spatial disparity. Because broad selectivity could result from the heterogeneous synaptic input from neighboring neurons, we examined how individual PV^+ interneuron selectivity compared to the local network selectivity. PV^+ neurons, but not PV^- neurons, showed functional similarity to neighboring cell populations over spatial distances resembling *in vitro* measurements of connectivity. Our findings suggest that broad selectivity of PV^+ interneurons results from nonspecific integration within local networks.

INTRODUCTION

Inhibitory interneurons constitute a minority of cortical cells (~20%) (DeFelipe, 2002) and are highly diverse in morphology and molecular composition (DeFelipe et al., 2013; Markram et al., 2004). One particular interneuron subtype, parvalbumin expressing neurons (PV^+), account for a large percentage of interneurons in mouse

[1]Work under review: Scholl B., Pattadkal J.J., Dilly G.A., Zemelmen B.V., and Priebe N.J. (2015) Local integration accounts for weak selectivity of mouse parvalbumin interneurons. *Neuron*.

neocortex (35−40%) (Gonchar et al., 2007). Their prevalence has made them an ideal target to examine the functional connectivity among neocortical excitatory and inhibitory cells. Connectivity measurements from paired intracellular recordings *in vitro* reveal that PV^+ interneurons are densely connected to neighboring excitatory pyramidal neurons, whereas pyramidal cells are weakly connected to one another (Holmgren et al., 2003; Levy and Reyes, 2012; Oswald et al., 2009; Packer and Yuste, 2011; Shepherd and Svoboda, 2005). While these *in vitro* studies have demonstrated distinct connectivity patterns, the functional consequences of these patterns are less clear.

If PV^+ interneurons indiscriminately pool inputs from neighboring neurons with diverse selectivity, they should exhibit broader response selectivity than nearby excitatory neurons. Evidence from *in vivo* two−photon imaging and targeted−extracellular recordings in mouse primary visual cortex (V1) has revealed that inhibitory neurons, and in particularly PV^+ interneurons, exhibit broader orientation selectivity (Atallah et al., 2012; Hofer et al., 2011; Kerlin et al., 2010; Wilson et al., 2012). Such broad selectivity is proposed to result from nearby presynaptic neurons displaying heterogeneous orientation preferences (Dräger, 1975; Sohya et al., 2007; Bock et al., 2011). It is unclear, however, whether inhibitory neurons are broadly selective for other emergent functional properties, or whether this is specific to orientation selectivity.

One emergent functional property in mammalian V1 is the binocularity providing information about the depth of objects in the environment. Different vantage points of the two eyes creates spatial offsets — or disparities — between the retinal images, which may be interpreted by cortical neurons to generate a three−dimensional representation of the visual world (Barlow and Blakemore, 1967; Blakemore, 1969; Hubel and Wiesel, 1973; Joshua, 1970; Nikara and Bishop, 1968; Pettigrew et al., 1968). Individual V1 neurons in primates, carnivores and mice are known to be

selective for binocular disparity (Hubel and Wiesel, 1962; Ohzawa and Freeman, 1986; Pettigrew et al., 1968; Poggio and Fischer, 1977; Poggio et al., 1988; Scholl et al., 2013a), whereby visually evoked responses are strongly modulated by binocular stimuli, relative to monocular stimulation alone. This emergent response property in mice provides an opportunity to explore differences in selectivity of excitatory and inhibitory neurons.

We measured the disparity selectivity of cortical neurons using *in vivo* two–photon calcium imaging in the binocular zone of mouse V1. PV^+ inhibitory interneurons were tagged with a red fluorescent protein through a genetic cross for visual identification. PV^+ inhibitory neurons received greater input from each eye than PV^- neurons, but surprisingly, these neurons also exhibited weaker disparity selectivity. While we find no functional organization for disparity preference in mouse visual cortex, we have uncovered a strong relationship between individual PV^+ cell selectivity and the neighboring network: PV^+ ocular dominance and disparity selectivity biases are predicted by the local population. Our findings suggest that broad selectivity of PV^+ interneurons results from pooling across neighboring cells with heterogeneous functional responses with a spatial length constant less than 100 microns. The similarity in spatial length constants for both disparity and ocular dominance suggests that these responses result from a circuitry pattern in which PV^+ neurons receive inputs from nearby neurons without regard to functional selectivity, whereas PV^- neurons receive functionally–specific inputs.

RESULTS

Measuring responses of PV^+ and PV^- cells in mouse V1 binocular zone

We used *in vivo* two photon calcium imaging to measure the binocular disparity tuning of inhibitory parvalbumin interneurons in primary visual cortex (V1) of anesthetized mice. Parvalbumin expressing (PV^+) interneurons were selectively labeled with red fluorescent protein tdTomato using a *PV−Cre* mouse (Appendix A). Labeling specificity was determined using *post hoc* antibody counterstaining for endogenous PV (Fig. 9.1A−C). There was strong co−localization of tdTomato and PV−immunostaining (Fig. 9.1D−E). In total, cells with both signals (n = 1274) composed a large fraction of the total cells expressing tdTomato (n = 1613, mean fraction = 79.4 ± 7.8% s.d., n = 3 mice). There was also good correspondence between cells with both signals (n = 1274) and the total cells stained for PV (n = 1354, mean fraction = 94.3 ± 3.6% s.d., n = 3 animals).

In each experiment, the V1 binocular zone was identified from extracellular recordings, receptive fields were carefully mapped in a targeted region within the central 30 degrees of the visual field, and a mirror was placed in front of the contralateral eye for dichoptic stimulus presentation (Fig. 9.1F) (Scholl et al., 2013a). Neurons were bulk loaded with the cell−permeable form of the calcium indicator Oregon Green BAPTA−1 (OGB−1 AM, Appendix A) (Garaschuk et al., 2006; Golshani and Portera−Cailliau, 2008; Kerr and Greenberg, 2005; Stosiek et al., 2003), resulting in a stained volume of approximately 150−300 microns in diameter. Light collected from two−photon excitation of fluorescence was split into red and green channels (Appendix A), enabling PV+ and PV− neuron activity to be clearly distinguished (Fig. 9.1G−H). Neurons co−labeled with OGB−1 AM and tdTomato (Fig. 9.1I, *white arrows*) were designated PV^+ and those containing only OGB−1 AM, a mixture of excitatory and remaining inhibitory neurons, were designated PV^-.

To measure binocular disparity selectivity and monocular responses, we randomly presented dichoptic vertical drifting gratings in both monocular and binocular

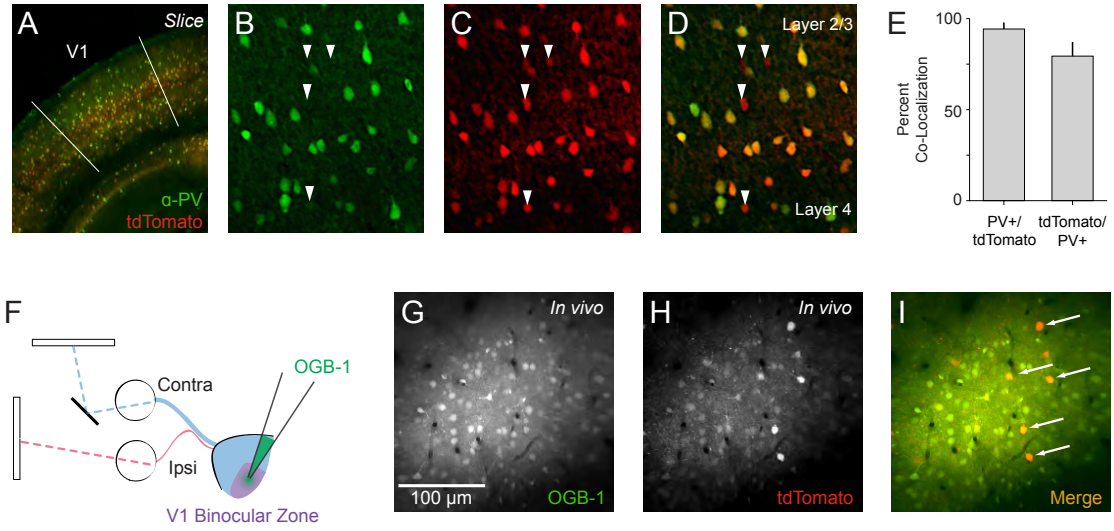

Figure 9.1: Characterization of recombinase−dependent transgene expression in a *PV−Cre* knock−in mouse and *in vivo* two−photon imaging of PV$^+$ interneurons

(A) Representative PV−Cre; Ai14 coronal slice stained for paravelbum (PV) with V1 outlined. Counts obtained from cortical layers 2−5. (B−D) Maximal projections showing co−localization of PV and tdTomato. In these panels all PV$^+$ neurons are tdTomato$^+$. Arrows indicate tdTomato$^+$/PV$^-$ neurons. (E) Summary of PV−tdTomato co−localization. (F) Dichoptic stimulus presentation used to evoke calcium responses. OGB−1 AM bulk loaded in mouse V1 binocular zone. (G) *In vivo* two−photon image of OGB−1 AM. (H) Same as in (g) for tdTomato. (I) Merge of OGB−1 AM and tdTomato. Cells with co−localized fluorescence (putative PV$^+$ interneurons) appear yellow (*arrows*).

conditions while recording changes in calcium fluorescence ($\Delta F/F$) at multiple depths ranging from 150 to 460 microns below the pial surface. Binocular disparity was probed by varying the contralateral stimulus spatial phase, generating eight binocular disparities (0−315 deg phase difference). Across all animals (n = 6, P40 − P60) we identified a total of 338 PV^+ neurons, of which 115 (34%) were visually responsive for monocular stimuli and 236 (70%) were visually responsive for binocular stimuli. We identified 3,982 $tdTomato^-$ (PV^-) neurons, of which 944 (24%) were visually responsive for monocular stimuli and 2001 (50%) were responsive for binocular stimuli. Differences in visual responsiveness between monocular and binocular conditions were in part due to the chosen stimulus parameters. To adequately probe binocular disparities, a single orientation (90° or 270° orientation) and spatial frequency (0.02 or 0.03 cpd) was used in each experiment. Mouse V1 neurons exhibit a 'salt and pepper' pattern of orientation preferences and a wide range of spatial frequency selectivities (Niell and Stryker, 2008; Ohki et al., 2005), so monocular stimuli would be unlikely to stimulate all potential visually responsive neurons (e.g. those tuned for horizontal gratings). Our visual response criterion (Appendix B) required neurons to have significant responses for at least one monocular and binocular stimulus; in some cells, binocular responses were evident despite a lack of monocular responses.

Binocular selectivity of PV^+ and PV^- cells

Calcium signals from mouse V1 cells are strongly modulated by binocular disparities, compared to stimulation of either eye alone or the blank (mean luminance) period, similarly to previous reports of spiking activity (Scholl et al., 2013a). In an example neuron (Fig. 9.2A), fluorescence changes evoked by preferred disparity (135°

phase difference, ~40% ΔF/F, relative to gray screen stimulation) were much larger compared to monocular stimulation of either eye (contra: ~18% ΔF/F, ispi: ~10% ΔF/F), while the null disparity (315^{o} phase difference) evoked little change (~10% ΔF/F). We constructed tuning curves from calcium responses evoked for each binocular stimulus as well as for stimulation of each eye alone (Fig. 9.2A, *right*). From these tuning curves we computed two metrics: an ocular dominance index (ODI) to compare monocular response from both eyes, where −1 indicates responses exclusively to contralateral stimulation and 1 indicates those exclusive to ipsilateral stimulation (Dräger, 1975; Gordon and Stryker, 1996; Hanover et al., 1999; Priebe, 2008); and the disparity selectivity index (DSI) to quantify the degree of response modulation by binocular stimuli, where 0 indicates no modulation and 1 indicates very high selectivity (Scholl et al., 2013a; 2013b) (Appendix B). For the example neuron shown in Figure 9.2A, these metrics describe a binocular, contralaterally biased neuron with robust disparity tuning (ODI = −0.43, DSI = 0.47). We also observed many monocular neurons with strong disparity selectivity as shown in another example (Fig. 9.2B; ODI = −1.0, DSI = 0.54).

From individual traces and tuning curves of stimulus−averaged fluorescence changes, it was evident there were differences between PV^{+} and PV^{-} cells. The calcium responses of PV^{-} neurons were generally modulated by binocular disparities. (Fig. 9.2A−B, *blue*). In contrast, PV^{+} interneurons exhibited weak disparity selectivity, as shown in the lack of calcium response modulations to different binocular phase combinations (Fig. 9.2C−D, *red*). While such insensitivity to binocular disparity might be expected for monocular neurons, we observed this lack of disparity selectivity in PV^{+} neurons responsive to monocular stimulation to either eye (Fig. 9.2C−D).

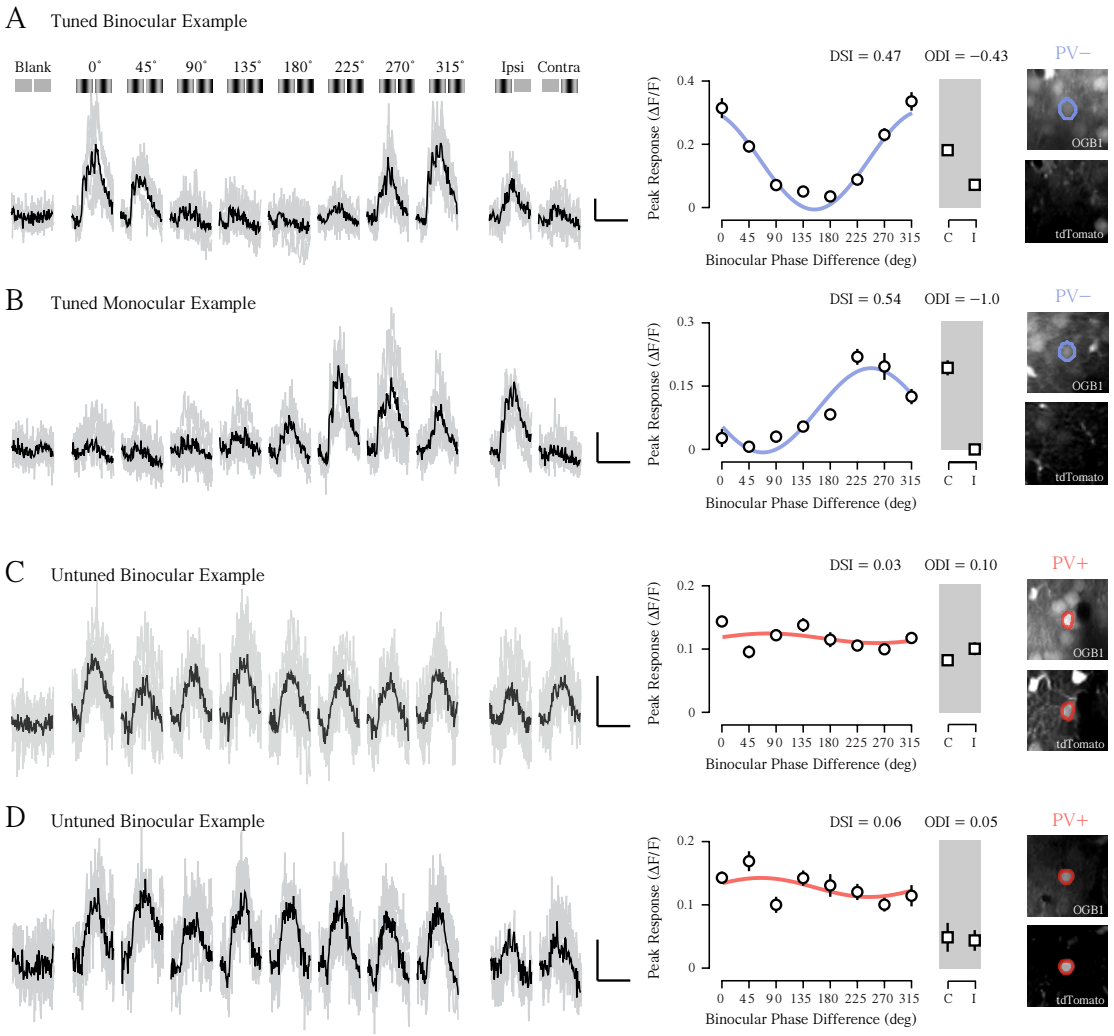

Figure 9.2: Functional two−photon imaging of binocular disparity selectivity
(A) Example calcium responses in a binocular PV− neuron evoked by a range of binocular disparities (0−315 deg), monocular stimulation of each eye, and a mean luminance screen. Individual traces shown in gray and trial−average mean shown in black. Illustration of each stimulus shown above traces. Scale bar indicates 10% change in fluorescence (ΔF/F) and 2 sec duration. Mean ΔF/F and standard error shown in a tuning curve. Tuning curve fit with cosine function. Two−photon images (*right*) show fluorescence from OGB−1 AM (*top*) and tdTomato (*bottom*). Note lack of tdTomato. (B) Same as in (a) for a tuned monocular PV^- neuron. (C−D) Same as in (a) for binocular PV^+ interneurons. Note fluorescence signature for both OGB−1 AM and tdTomato (*right*).

We examined the OD across our sample populations and found that PV^+ interneurons are more binocular than PV^- neurons (Fig. 9.3A–C) (Kameyama et al., 2010). Most PV^+ cells were activated by monocular stimulation of either eye (64%, $-0.5<ODI<0.5$), while many PV^- cells responded mostly to monocular stimulation of a single eye (55%, $-0.5>ODI>0.5$) (Fig. 9.3B). To compare the degree of monocularity in these cell classes we calculated the absolute value of ODI or monocularity index (MI). Here a value of 0 indicates equal responses to stimulation of each eye whereas a value of 1 indicates stimulation to only one eye evoked responses. PV^+ interneurons were significantly more binocular than PV^- neurons (MI PV^-: median = 0.57, mean = 0.58 ± 0.32 s.d.; MI PV^+: median = 0.36, mean = 0.41 ± 0.29 s.d.; p = 0.01, Mann–Whitney test). This trend in the MI was found across different animals or imaging sessions (mean PV^- MI = 0.58 ± 0.04 s.d., mean PV^+ MI = 0.43 ± 0.08 s.d., n = 6). The difference in monocularity between inhibitory and excitatory neurons was also observed by Kameyama et al. (2010), though they examined all layer 2/3 inhibitory neurons instead of just PV^+ neurons. Because PV^+ neurons contribute a significant portion of the layer 2/3 inhibitory neurons it is likely their dataset is dominated by PV + neurons.

Surprisingly, the increased binocularity of PV^+ interneurons was coupled with weak binocular disparity selectivity relative to the disparity selectivity of PV^- neurons (Fig. 9.3D–F; DSI: PV–: median = 0.26, mean = 0.26 ± 0.17 s.d.; DSI; PV+: median = 0.09, mean = 0.12 ± 0.10 s.d.; p = 0.0001, Mann–Whitney test). This is surprising since disparity tuning is a result of the convergence of right and left eye inputs. Despite

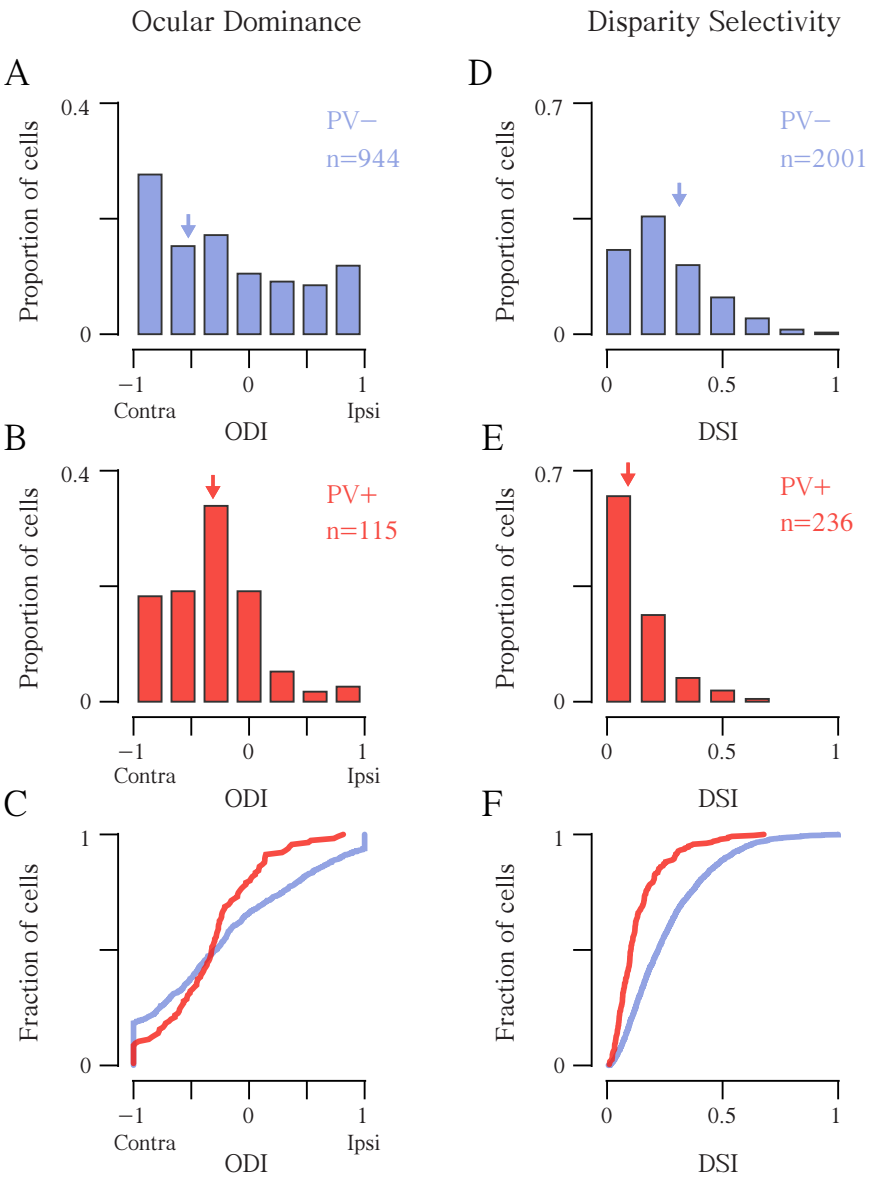

Figure 9.3: PV⁺ interneurons more binocular but lack disparity selectivity compared to PV⁻ neurons

(A) Distribution of ocular dominance index (ODI) for PV⁻ neurons (*blue*). Arrows indicate median value. (B) Same as in (a) for PV⁺ interneurons (*red*). (C) Cumulative distribution of ODI for both populations. (D) Distribution of disparity selectivity index (DSI) for PV⁻ neurons (*blue*). (E) Same as in (d) for PV⁺ interneurons (*red*). (F) Cumulative distribution of DSI for both populations.

receiving more binocular input, PV+ neurons provide fewer signals related to the depth of objects in the world.

The relationship between ocular dominance and disparity selectivity has been obscure (Chino et al., 1994; LeVay and Voigt, 1988; Read and Cumming, 2004; Smith et al., 1997), though it has been shown that increased binocularity is associated with greater disparity selectivity (Scholl et al., 2013a; 2013b; Smith et al., 1997). We examined this relationship by comparing the monocularity index and disparity selectivity index and found no relationship between these measures in PV^+ (mean slope $= 0.04 \pm 0.02$ s.e., Bootstrapped PCA; Appendix B). There was a slight correlation in PV^- neurons (mean slope $= 0.16 \pm 0.03$ s.e., Bootstrapped PCA; Appendix B), but the direction of the relationship is positive, indicating that more monocular neurons are associated with greater disparity selectivity (in contrast to our predictions), and the slope accounts for little variance ($r^2 = 0.08$). Limited evidence exists from spiking data for a relationship between monocularity and disparity selectivity in primates or carnivores (Chino et al., 1994; LeVay and Voigt, 1988; Read and Cumming, 2004; Smith et al., 1997). Since calcium signals reflect underlying spiking activity (Stosiek et al., 2003), our finding of little relationship between these quantities is not unexpected, though may be different from the direct relationship between these parameters observed in intracellular recordings of subthreshold synaptic activity (Scholl et al., 2013b) and models (Scholl et al., 2013a). In summary, PV^+ neurons are more binocular by measures of ocular dominance and exhibit broader disparity selectivity than PV^- neurons.

A functional organization of binocularity

For PV^+ interneurons, the combination of increased binocularity and broad disparity selectivity is puzzling, since binocularity may be associated with greater disparity selectivity (Scholl et al., 2013a; 2013b; Smith et al., 1997). One potential explanation for these seemingly incongruous results is that PV^+ cells receive synaptic inputs from local heterogeneous populations of presynaptic neurons with a variety of stimulus preferences (Bock et al., 2011). Pooling inputs from nearby neurons with distinct eye preferences might produce responses to stimulation of either eye. Further, if neighboring PV^- neurons exhibited diverse disparity preferences then the aggregate input to a target neuron would lack disparity selectivity. While this could account for our PV^+ results, a separate wiring rule would be necessary to account for PV^- neuron selectivity. To test this idea we measured the degree to which neurons are clustered by feature selectivity and the degree to which functional selectivity of individual neurons is related to their neighbors. We first found mouse V1 neurons exhibit a heterogeneous 'salt–and–pepper' organization of eye preference (Fig. 9.4A), similar to previous reports (Mrsic–Flogel et al., 2007), and disparity preference (Fig. 9.4G). To explicitly measure this spatial heterogeneity, we measured the correlation between distance and binocular response similarity and found no relationship (monocularity (MI): Bootstrapped PCA slope = 0.01, p = 1; disparity: circular–linear correlation = 0, p = 1, for cells with DSI > 0.1; Appendix B).

Given this heterogeneity, we tested whether or not there is a correlation between individual PV^+ neuron selectivity and nearby PV^- neurons. For each PV^+ cell we measured the ODI, then defined a spherical volume around that cell's location to encapsulate a population of nearby PV^- cells (Fig. 9.4A, dashed lines; Appendix A). The spherical volume extended across 2–dimensional images and through the multiple

cortical depths at which images were collected. Averaging the ODI of PV^- cells within a 50 micron radius generated predictions of ocular preference in individual PV^+ interneurons, as shown for an example cell (Fig. 9.4C). Here we observe a strong relationship between individual PV^+ cell ODI and the population average (Fig. 9.4D), suggesting that PV^+ cells are integrating inputs from nearby cells.

Because synaptic connections between cortical neurons depend on spatial distance, we next examined the spatial dependency of this relationship by increasing the radii (50 − 150 μm) defining each of PV^- populations. In order for each PV^- population to contain non−overlapping subsets of neurons we used spherical shells for radii greater than 50 microns, such that inner spherical volumes were subtracted away (Fig. 9.4B, Appendix A). As we increased the distance separating PV^+ cells and PV populations, the similarity between individual ODI and population average decreased dramatically. In contrast, we uncovered no relationship between individual ODI of PV^- neurons and local populations of PV^- neurons (Fig. 9.4E). This difference was evident particularly for the nearest neighbors (radius = 50 μm; PV^+ mean slope = 0.78 ± 0.25 s.e., n = 86; PV^- mean slope = 0.10 ± 0.02, n = 717; boot−strapped PCA; Appendix B). Across all radii tested, PV^- neuron ODI showed little relationship with population averages and no spatial dependence (Fig. 9.4F). Mean slopes computed for PV^- neurons were also insignificant, as they were indistinguishable from a PCA slopes computed from shuffled populations (mean shuffle = 0.06 +/− 0.05 s.e. boot−strapped PCA; Fig. 9.4F, gray line; Appendix A−B). Even when limiting our analysis to PV^- neurons with an ODI similar to PV^+ neurons (−0.5 < ODI < 0), we found no significant trends with population averages (Bootstrapped PCA slope; Appendix B). Individual PV^+ neurons, on the other hand, strongly matched the population ODI average in a spatially dependent manner that was significantly greater than shuffled averages (Fig. 9.4F). From these

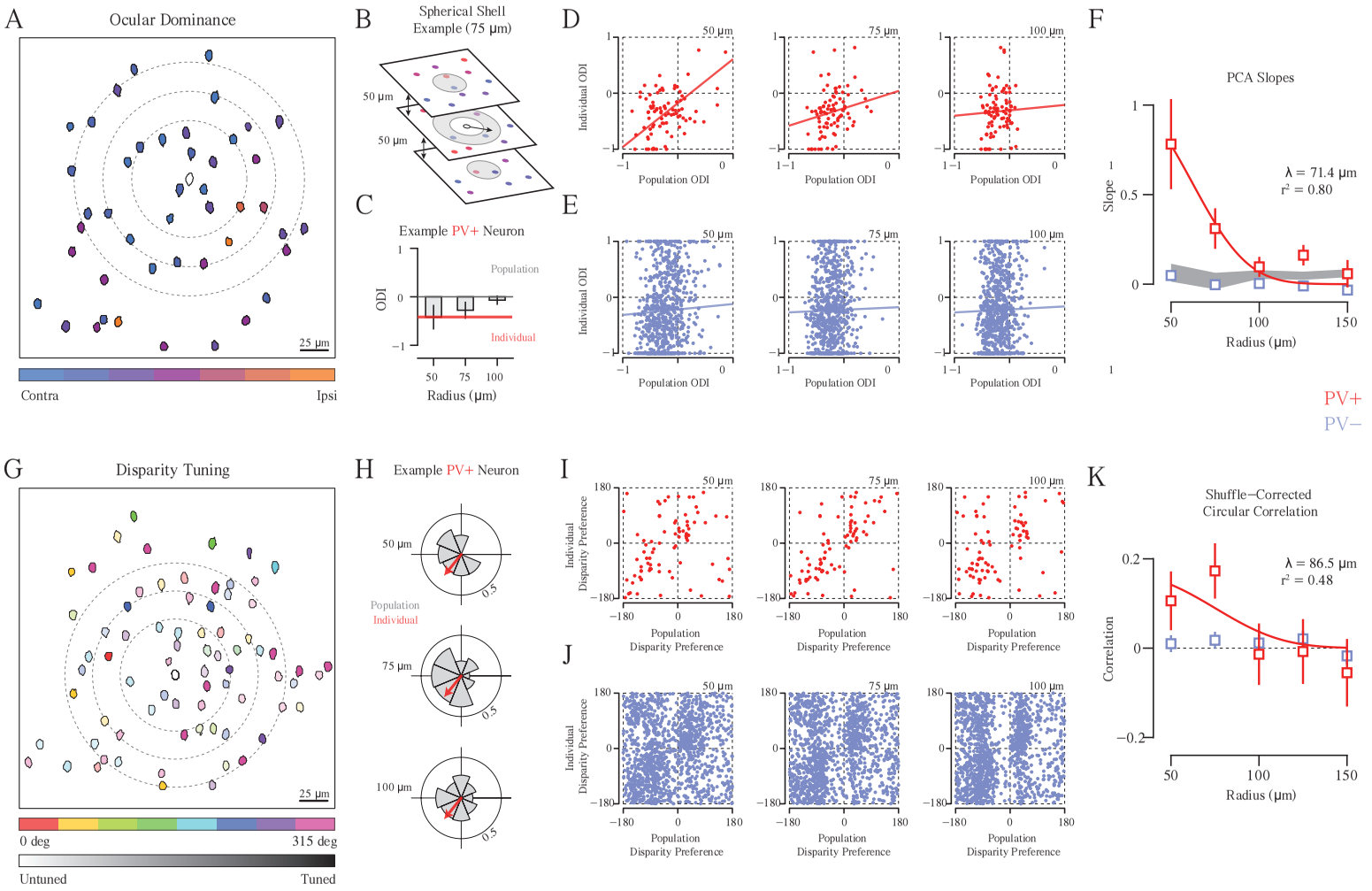
A
Ocular Dominance
25 μm
Contra
Ipsi
B
Spherical Shell
Example (75 μm)
50 μm
50 μm
C
Example PV+ Neuron
ODI
Population
Individual
Radius (μm)
D
50 μm
75 μm
100 μm
Individual ODI
Population ODI
E
F
PCA Slopes
λ = 71.4 μm
r² = 0.80
Slope
Radius (μm)
PV+
PV−
G
Disparity Tuning
25 μm
0 deg
315 deg
Untuned
Tuned
H
Example PV+ Neuron
50 μm
75 μm
100 μm
Population
Individual
I
Individual Disparity Preference
Population Disparity Preference
J
K
Shuffle−Corrected
Circular Correlation
λ = 86.5 μm
r² = 0.48
Correlation
Radius (μm)

Figure 9.4: Spatial relationship of PV^+ interneuron functional properties and local population aggregate

(A) Map of ocular dominance at single focal plane (depth = 420 μm). Cell masks color−coded based on eye preference or ocular dominance index (ODI). Example PV^+ interneuron in center (*mask outline*). Rings (*dashed line*) depict subset of radii tested (50−100 μm). (B) Example volume (radius = 75 μm) to generate local PV^- neuron population. Neurons within boundary (*gray shading*) comprise this population. Note at the individual PV^+ interneuron's focal location, volume is shown as ring because the inner sphere volume (radius = 50 μm) is excluded. (C) Example PV^+ interneuron ODI (*orange*) and population average ODI at different radii (*gray*). (D) Plots of individual PV^+ interneuron ODI and local population average for different radii (*red*). Fit slope and y−intercept computed from Bootstrapped PCA (Appendix B). (E) Same as (d) for PV^- neurons (*blue*). (F) Spatial dependence of relationship between individual cell and local populations. PV^+ interneuron (*red*) and PV^- neuron (*blue*) Bootstrapped PCA slopes (Appendix B) across radii. Spatial length constant (λ) computed from exponential fit (*red line*). (G) Map of binocular disparity selectivity at single focal plane (depth = 400 μm). Cell masks color−coded based on disparity preference (0−315 deg). Hue modulated by disparity selectivity index (DSI). Example PV^+ interneuron in center (*mask outline*). Rings (*dashed line*) depict subset of radii tested (50−100 μm). (H) Example PV^+ interneuron disparity vector (*orange*) and polar histogram of population vectors (*gray*). (I) Plots of individual PV^+ interneuron disparity preference and for local population vector average for different radii (*red*). (J) Same as (i) for PV^- neurons (*blue*). (K) Spatial dependence of relationship between individual cell and local populations. PV^+ interneuron (*red*) and PV^- (*blue*) neuron shuffled−corrected circular−correlations shown across radii. Spatial length constant (λ) computed from exponential fit (*red line*).

data, we then extracted a spatial length constant (λ) describing the spatial–dependent functional relationship of PV^+ interneurons with the local network. An exponential fit (Appendix B) yielded a λ of 71.4 microns ($r^2 = 0.80$).

We next asked whether a similar relationship between individual PV^+ interneurons and the local network existed for binocular disparity selectivity. Each neuron's disparity selectivity was decomposed into two components: DSI or normalized tuning strength and binocular phase difference or disparity preference. Given the 'salt and pepper' organization of disparity preference (Fig. 9.4G) we performed the same volumetric population analysis as for ODI. Because disparity preference is a circular variable, we computed a vector average for each sphere or spherical shell to compare with an individual PV^+ interneuron's vector (Fig. 9.4H, Appendix B). Our analyses excluded PV^+ and PV^- neurons with little response modulation to binocular disparities (DSI < 0.1). Even though PV^+ interneurons possess weak binocular tuning, their individual angular biases appeared to match population vectors, at least for populations within 100 microns (Fig. 9.4I). On the other hand, we found little or no relationship for PV^- neurons (Fig. 9.4J). When comparing individual neuron's DSI to population vector amplitudes we found no relationship for either cell type across all radii (Bootstrapped PCA slope; Appendix B). To quantify the relationship between individual PV^+ disparity preference and population vectors we computed a shuffle–corrected circular correlation coefficient (Appendix B). For the most proximal populations, we found PV^+ interneuron disparity preference was significantly more correlated with the population vector average then PV^- neurons (PV^+: $r = 0.11 \pm 0.07$ s.e., $n = 80$; PV^-: $r = 0.01 \pm 0.02$, $n = 1313$; shuffled–corrected circular correlation coefficient). The lack of relationship between individual PV^- neurons and the local populations was unchanged if we

restricted our analysis to those with weak disparity tuning comparable to PV^+ interneurons ($0.1 < DSI < 0.2$). Individual PV^+ neurons, but not PV^- neurons, were correlated to the population average vector angle at radii of 50−75 microns, while all other spatial locations resulted in correlations near 0 (Fig. 9.4K). From these data, we again used an exponential fit to describe the spatial−dependent functional relationship of PV^+ interneurons with the local network. This yielded a λ of 86.5 microns, similar to that from ODI measurements, albeit capturing less variance in the data ($r^2 = 0.48$).

DISCUSSION

Parvalbumin−expressing (PV^+) inhibitory interneurons exhibit a different ocular dominance profile, disparity selectivity and organization from the remaining neuronal population. Similarly to Kameyama et al. (2010), PV^+ neurons respond more equally to each eye and yet, despite that increased binocularity are weakly selective for binocular disparity. The weak selectivity of individual PV^+ interneurons is related to neighboring neuron population, but only within 100 micron radius. We did not find any relationship between the selectivity of PV^- neurons and their local population. Differences in the functional selectivity and relationships to the surrounding PV^- population suggest that PV^+ interneurons play a distinct role in integrating right and left eye inputs, and reveal a connectivity with neighboring cells potentially reflecting a generalized function of this cell type across neocortical circuits.

Characteristics of PV^+ Selectivity

The broad selectivity we observed in PV^+ interneurons is similar to the weak tuning these neurons exhibit for orientation and direction selectivity (Hofer et al., 2011;

Kerlin et al., 2010). Because this selectivity differs from that of excitatory neurons, it has been proposed that PV^+ cells play a specific role in cortical circuitry, integrating sensory information to modulate cortical response gain without affecting individual cell tuning properties (Atallah et al., 2012), potentially through divisive inhibition (Wilson et al., 2012). Our measurements of binocular disparity in PV^+ neurons reveal a lack of selectivity indicating that a similar integration of sensory inputs is occurring. Integration may occur by pooling inputs from nearby cells; in the mouse these cells have distinct disparity preferences (Fig. 9.4G). It is also possible that PV^+ interneurons could pool across innervating thalamocortical inputs from the contralateral and ipsilateral eyes to generate increased binocularity, but do so in a way that is not spatially specific to each eye. It is important to note that it is still unclear how disparity preference in these neurons is shaped by feedforward thalamic inputs, but the direct relationship between the functional responses of PV^+ neurons and the neighboring neurons suggests a role for intracortical connectivity.

Cortical wiring of excitatory and inhibitory cells

Our measurements provide evidence for the hypothesis that PV^+, but not PV^- cells, receive synaptic inputs from a heterogeneous proximal population of neurons. Our data, in corroboration with previous studies using paired recordings *in vitro*, suggest that PV^+ interneurons integrate synaptic inputs from nearby neurons without regard for the functional selectivity of those inputs (Holmgren et al., 2003; Levy and Reyes, 2012; Oswald et al., 2009; Packer and Yuste, 2011; Shepherd and Svoboda, 2005). Excitatory neurons integrate inputs within a similar cortical distance, but with a lower connection probability. One critical feature appearing to guide connection probability is whether excitatory neurons share functional selectivity (Ko et al., 2013; 2011). Whereas the

cortical pattern of connectivity for excitatory neurons is built upon functional specificity, PV+ interneuron connectivity appears to be built upon a lack of specificity (Bock et al., 2011). These differential connectivity patterns suggest distinct wiring rules for excitatory and inhibitory cells (Fig. 9.5A–B).

The functional spatial length constant (λ) reported here is the first of its kind from two–photon imaging. Not only was λ for ocular dominance and binocular disparity preference comparable (71.5 μm and 86.5 μm, respectively), but these values are similar to estimates of spatial dependence of synaptic connection probability from slice physiology. Levy & Reyes (2012) recover a λ of 92 μm for the probability of an excitatory pyramidal cell synapsing onto a PV^+ interneuron in the auditory cortex. They also determine that the inverse connection has an almost identical λ (90 μm). This second measurement has been derived by another group in visual cortex (Packer and Yuste, 2011), but they reported a slightly higher value (124 μm) and did not measure synaptic connectivity of excitatory neurons onto PV^+ interneurons.

The link between our functional λ and that measured in slice suggests PV^+ cells have a generalized role within neocortical circuitry. These neurons appear to pool the overall activity of local populations (Fig. 9.5B), which could act as a gain control on responses of postsynaptic targets. Because mouse V1 lacks functional organization beyond retinotopy, PV^+ interneurons only provide a signal reflecting the population activity for a spatial location. Because orientation selectivity and disparity selectivity are spatially organized across V1 in carnivores (Hubel and Wiesel, 1963; Kara and Boyd, 2009; Nauhaus et al., 2012a; Ohki et al., 2005; 2006), PV^+ cells should also be selective for orientation and disparity (Fig. 9.5C). The same could be expected for PV^+ interneurons in primate V1, at least for orientation selectivity and spatial frequency

(Bosking et al., 1997; Essen and Zeki, 1978; Hubel and Wiesel, 1963; Nauhaus et al., 2012b). This selectivity may depend, however, on their location within the cortical map. For example, it is possible that PV+ neurons located near pinwheels centers would be less selective, and may contribute to excitatory neuron responses in a manner distinct from PV^+ interneurons within iso−orientation domains (Schummers et al., 2002). In this way, the same spatial connectivity rule for PV^+ cells could result in diverse functional consequences in carnivore and primate V1 as compared to rodents.

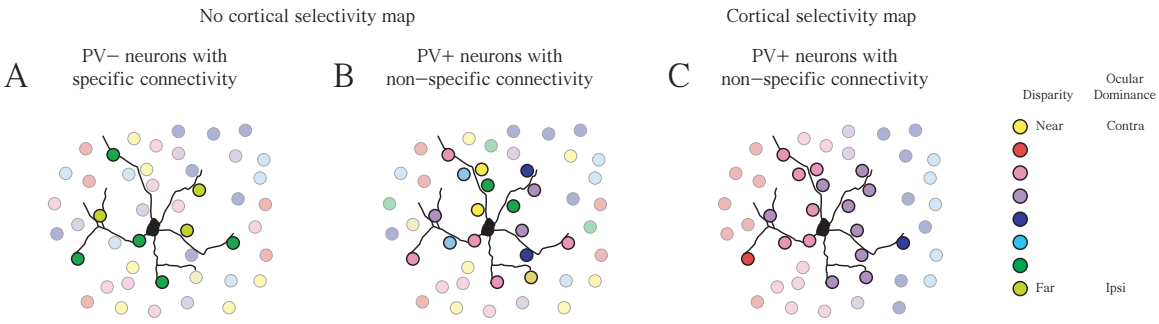

Figure 9.5: Differential connectivity patterns for excitatory and inhibitory cells

(A) Excitatory neurons (PV^-) are connected to neighboring neurons of similar functional selectivity in a 'salt−and−pepper' network. Colors represent disparity or eye preference. (B) Inhibitory neurons (PV^+) connect broadly to nearby neurons, regardless of functional selectivity, in a 'salt−and−pepper' network. (C) Inhibitory neurons (PV^+) in a functionally organized neocortical circuit could follow the same wiring rule as in (b), but it would result in functionally selective PV^+ neurons.

Chapter 10: Conclusion

The anatomical uniformity and organizational similarity of cerebral cortex across mammalian species suggests a set of common computations underly the emergence of functional response properties in individual cortical neurons. In this dissertation I explored this hypothesis using a comparative approach. Using the primary visual cortex (V1) of carnivores and rodents I focused on two computations in V1: the emergence of orientation selectivity and binocular integration of ocular signals. My measurements of neuron response properties in both species reveal not all cortical computations are common to mammalian species. Orientation selectivity, which is an emergent property of cortical neurons in carnivores, is evident in the subcortical relay cells in the mouse visual system. The presence of oriented receptive fields in subcortical visual areas of the mouse suggests their V1 neurons inherit this information, rather than compute it from thalamic inputs like in cat. While the emergence of orientation selectivity was distinct between these species, V1 binocular integration was remarkably similar. In both species, stereoscopic depth sensitivity or disparity selectivity was a property of cortical neurons. A threshold−linear model accounts for this selectivity and predicts that greater subthreshold synaptic input from each eye should generate stronger depth sensitivity. Intracellular recordings from both species upheld this prediction. In sum, it appears that the integration of signals from the two eyes is common computation of the mammalian visual cortex, while orientation selectivity can arise through different mechanisms across mammalian species.

At first approximation, the cortical computations generating orientation selectivity in carnivores and rodents appear distinct, where mouse orientation selectivity is likely computed in the retina and inherited by cortical neurons. However, the exact computation being performed in mouse V1 is still unknown. Either the

selectivity is already present in the input and lost after recomputing this information, or perhaps, a Hubel & Wiesel style model combining oriented and non−oriented subcortical receptive fields accounts for response properties. If the former is an accurate description, then the computation in cat and mouse might be analogous: both would exhibit spatial summation of subcortical presynaptic receptive fields. However, this model remains to be tested. Future experiments should include paired recordings (LGN and V1), dissection of thalamocortical excitatory inputs using optogentics, and potentially anatomical tracings of functional projections. There is perhaps some evidence in our data: mouse relay cells exhibit greater selectivity than subthreshold input to V1 neurons. This might provide evidence for a recomputation, although, if mouse V1 neurons integrate over a wide range of subcortical receptive fields to generate orientation selectivity, then broadly tuned synaptic input would be expected. To fully elucidate the exact model describing the computation for orientation selectivity in mouse V1, further experiments need to be done.

Work presented in this dissertation suggest that the integration of ocular signals is a common computation of the mammalian visual cortex, however, the classical model describing depth sensitivity in cat V1 (e.g. the hierarchal energy model) may not apply to the mouse. In the classic model, disparity selectivity is initially formed in simple cells in layer 4, those receiving direct thalamocortical input. Complex cells in layer 2/3 thereby integrate across simple cells to form more complicated binocular receptive fields. This laminar processing may not exist in the mouse, as simple cells are found throughout layers 2−4. Further, it is unknown whether simple cells in mouse V1 project to complex cells. Instead of mouse binocularity being exactly the same as that in cat V1, I would propose this is an evolutionary old binocular system. As mammals evolved, the eyes rotated forward, more ganglion cell axons did not cross the optic chiasm, and V1 received stronger binocular input. Perhaps the mouse visual system, with lateral

facing eyes and a small number of uncrossed ganglion cell axons, reflects an evolutionarily–early binocular computations. Computations which are refined and greater exploited in carnivores and primates.

Since binocular integration is a common computation in rodent and carnivore V1, I was able to explore how abnormal visual experience disrupted the cortical circuitry for integration in both species. In cat, I induced an ocular misalignment (e.g. strabismus) during the developmental critical period, which creates greater monocularity in V1 neurons and a loss of disparity selectivity. In mouse, I induced monocular deprivation in the contralateral eye during the development, generating greater binocularity accompanied by a loss of disparity selectivity. It's surprising that these two manipulations, each producing a different effect in individual neuron ocular dominance, cause a loss of binocular integration. Monocular deprivation, like strabismus, could create a decorrelation in synaptic inputs between the two eyes. This might explain the nonfunctional excitatory inputs, which create greater binocularity according to ocular dominance and a loss of disparity selectivity. Although, what mechanism explains the loss of disparity selectivity in both species? In strabismic cats, I find suppression of subthreshold inputs and conductances measurements reveal strong binocular inhibition. Binocular inhibitory input could be common in both species. In cat, nonfunctional convergence of ocular inputs is suppressed by binocular inhibition. In mouse, a similar model would explain the loss of disparity selectivity, whereby inhibitory interneurons become more binocular, alongside other V1 neurons, and provide greater binocular inhibitory input.

In a final study presented in this dissertation I used genetic tools in the mouse to investigate binocular receptive field properties of excitatory and inhibitory V1 neurons. Here I found that paravalbumin–expressing (PV+) inhibitory interneurons are more binocular by ocular dominance, but weakly selective for disparity. On the other hand,

non−PV+ neurons, comprised mostly of excitatory cells, were generally contralaterally biased and exhibited strong modulations to stereoscopic stimuli. Further, nonspecific integration of nearby neighboring neuron's functional properties accounted for the broad tuning of PV+ interneurons. These results are intriguing for two reasons. First, since inhibitory neurons are more binocular and unselective for disparity, they provide a potential cellular mechanism explaining the disruption of binocular integration (see above). Of course, it is unknown whether PV+ interneurons share similar receptive properties in cat V1 and what happens to the binocular response properties of these neurons following developmental plasticity manipulations (e.g. strabismus or monocular deprivation). Second, if nonspecific local integration of PV+ inhibitory neurons is found in cat V1, it might be another common cortical computation. Nonspecific local integration in these neurons could be a ubiquitous property across cortex and across mammalian species. In this way, PV+ inhibitory neurons could provide a cellular mechanisms for local normalization pools in cortical networks. Further experiments in the future will hopefully test this hypothesis and discover similarities and differences in inhibitory interneuron receptive field properties between mammalian species.

Appendix A: Methods

PHYSIOLOGY

Physiological procedures for mouse recordings were based on those previously described (Tan et al., 2011; Scholl et al., 2013a). Experiments were conducted using adult C57BL/6 mice (age 5−8 weeks) or *Onychomys Arenicola* grasshopper mice (ages 8 – 24 months). Both male and female animals were used. Mice were anesthetized with intraperitoneal injection of either 50−80 mg/kg sodium pentobarbital or 1 g/kg urethane and with intramuscular injection of 10 mg/kg chlorprothixene; the dose of sodium pentobarbital or urethane was adjusted during the procedure to eliminate the pedal withdrawal reflex. When necessary, isoflurane (0.25−2.0%) was administered during surgery and the experiment duration to eliminate a pedal withdrawal reflex. Brain edema was prevented by intraperitoneal injection of 20 mg/kg dexamethasone. Animals were warmed with a thermostatically−controlled heat lamp to maintain body temperature between 37−38^{o} C. A tracheotomy was performed. The head was placed in a mouse adaptor (Stoelting) and a craniotomy and duratomy were performed over visual cortex. Eyes were kept moist with either frequent application of artificial tears or a thin layer of silicone oil.

Physiological procedures for cat recordings performed as previously described using anesthetized, paralyzed female and male cats (2−5 kg) (Priebe and Ferster, 2006). Anesthesia was induced with ketamine (5−15 mg/kg) and acepromazine (0.7 mg/kg), followed by intravenous administration of a mixture of propofol and sufentanil (Yu and Ferster, 2010). Once a tracheotomy was performed the animal was placed in a stereotaxic frame for the duration of the experiment. Recording stability was increased by suspending the thoracic vertebrae from the stereotactic frame and performing a pneumothoracotomy. Eye drift was minimized with intravenous infusion of vecuronium bromide. Anesthesia was maintained during the course of the experiment with continuous infusion of propofol and

sufentanil (6–9 mg/kg/hr and 1–1.5 ug/kg/hr, respectively). Body temperature (38.3°C), electrocardiogram, EEG, CO_2 , blood pressure, and autonomic signs were continuously monitored and maintained. The nictitating membranes were retracted using phenylephrine hydrochloride and the pupils were dilated using topical atropine. Contact lenses were inserted to protect the corneas. Supplementary lenses were selected by direct ophthalmoscopy to focus the display screen onto the retina.

All procedures were approved by The University of Texas at Austin Institutional Animal Care and Use Committee.

STRABISMUS SURGERY

Animals were anesthetized with isoflurane (1–3 %) and the medial rectus of the right eye was severed prior to the critical period (9–15 days old) to induce exotropic strabismus (divergent squint) (Hubel and Wiesel, 1965; Yinon and Auerbach, 1975; Chino et al., 1983; Freeman and Tsumoto, 1983; Klalil et al., 1984; Chino et al., 1994; Löwel et al., 1998; Engelmann et al., 2001). Exotropia was chosen over esotropia (convergent squint) for comparison with previous key studies (Hubel and Wiesel, 1965; Chino et al., 1983; Chino et al., 1994). Body temperature, breathing rate, SPO_2, and autonomic signs were continuously monitored and maintained. Antibiotic ophthalmic ointment was placed on the eye and the animal was monitored for at least 24 hours after surgery. Deviation of the right eye was checked throughout the visual critical period. Physiology measurements were made 3–24 months after surgery. Strabismus was generated in 11 animals from 4 litters. In 2 animals, severance of the medial rectus was repeated because the muscle reattached several days after the first procedure. In 3 litters, 2 animals underwent a sham procedure where the ocular muscle was left intact. The 6 sham animals were used in addition to 14 normal adult animals. Throughout the text, strabismic animals are compared to normal animals, which includes both litter–matched shams and controls that underwent no sham surgery. We combined normal and litter–matched shams because we found no difference in ocular dominance or disparity selectivity between these two groups.

All procedures were approved by The University of Texas at Austin Institutional Animal Care and Use Committee.

Transgenic Mouse Construction

PV–Cre knock–in mice were generated using an IRES targeting construct to insert the Cre recombinase coding sequence into the 3′ UTR of the mouse PV gene (Figure 1A). The construct also contained a *PGK1–NeoR* positive selection cassette flanked by *frt* sites within the homologous arms and a *RNAPII–DTA* negative selection cassette following the 3' homologous arm. The targeting construct was electroporated into hybrid C57BL/6J–129/SV stem cells, with correct recombinants selected with G418 and screened by Southern blot. Founders were crossed to *ROSA26–FLP* deleter mice to excise the *NeoR* cassette. F1 progeny were backcrossed repeatedly to C57BL/6J to reproduce the C57BL/6J genetic background. C57BL/6J content of the resulting mice was confirmed by microsatellite testing (Charles River Laboratory). To generate experimental animals, homozygous *PV–Cre* mice were crossed to *ROSA26–tdTomato* Cre–reporter mice (Ai14) (Madisen et al., 2010), selectively labeling PV+ interneurons with tdTomato in the hemizygous *PV–Cre;Ai14* progeny.

Immunohistochemical Analysis of PV–Cre Neurons

Brains of *PV–Cre;Ai14* animals were perfused and post–fixed overnight with 4% paraformaldehyde. Non–consecutive 50 μm sections were incubated for 24 h with mouse anti–PV monoclonal antibodies (PV 235, Swant; diluted 1:1000). tdTomato expressing neurons in 4 independent fields of view within V1 were examined for the presence of PV staining on a fluorescence microscope (Axioscope, Carl Zeiss). Image z–stacks were captured using an Apotome attachment and evaluated for co–localization of red and green signals using ImageJ. Most (94.3%) PV+ neurons expressed tdTomato, whereas ~80% tdTomato neurons were PV+.

This discrepancy could be explained by developmental changes in the level PV expression across neurons of the cortex or by differences in the sensitivities of the two detection methods. Similar variations have been observed in other *PV−Cre* transgenic mouse lines, especially among layer 5 cortical neurons (Madisen et al., 2010). Despite the potential for developmental and other caveats, staining overlap within cortical layers 2−3, where *in vivo* imaging took place, was notably higher (not shown).

EXTRACELLULAR RECORDINGS

Extracellular electrodes (1−2 megaohms, Micro Probes) were advanced into cortex (cat: area 17, ~2 mm lateral of midline; mouse: V1 binocular zone) or into the LGN (cat: 9 mm lateral of midline and 6 mm anterior; mouse: 2.5 mm posterior of bregma and 2 mm lateral of midline) with a motorized drive (MP−285, Sutter Instrument Company). After the electrode was in place, warm agarose solution (2−4% in normal saline) was placed over the craniotomy to protect the surface of the cortex and reduce pulsations. V1 was located and mapped by multi−unit extracellular recordings with parylene−coated tungsten electrodes (Micro Probe). In mouse, the boundaries of V1 and V2 were identified by the characteristic gradient in receptive field locations (Dräger, 1975; Métin et al., 1988; Wagor et al., 1980). Eye drift under urethane anesthesia (for mice) is typically small and results in a change in eye position of less than 2 degrees per hour (Sarnaik et al. 2014).

Mouse LGN was consistently in the same location and at a depth of 2.2 − 2.8 mm (Grubb and Thompson, 2003). Before reaching mouse LGN, the electrode passed through cortical activity, two layers of hippocampal activity, and a quiet space (100−300 μm in depth) (Grubb and Thompson, 2003). Weak and unreliable visual responses indicated that the electrode was located medial of the LGN (Grubb and Thompson, 2003). In some experiments, the retinotopic gradient of mouse LGN could be mapped using multi−unit activity.

In cat, LGN recordings were restricted to layers A and A1. X and Y cells were distinguished by presenting contrast reversing gratings at a spatial frequency higher than the cutoff for drifting gratings (Hochstein and Shapley, 1976). Neurons with a frequency doubling response were labeled Y−cells, and those without were labeled X−cells. In cat V1, recordings were restricted to simple cells between 500 and 1100 microns deep. Action potentials were identified using a dual window discriminator (Bak Electronics, DDIS−1). The time of action potentials as well as the raw extracellular traces were recorded for later analysis.

INTRACELLULAR RECORDINGS

Blind whole−cell recordings were obtained in vivo (Pei et al., 1991; Ferster and Jagadeesh, 1992; Margrie et al., 2002). As a reference electrode, a silver-silver chloride wire was inserted into muscle near the base of the skull, and covered with 4% agarose in normal saline to reduce changes in the surrounding fluid and concomitant changes in associated junction potentials. The potential of the CSF was assumed to be uniform and equal to that of the reference electrode. Pipettes (8−12 MΩ) were pulled from 1.2 mm outer diameter, 0.7 mm inner diameter KG−33 borosilicate glass capillaries (King Precision Glass) on a P−2000 micropipette puller (Sutter Instruments) to record from neurons 250 - 850 μm below the cortical surface. To record membrane potential and spike responses, pipettes were filled with (in mM) 135 K−gluconate, 4 NaCl, 0.5 EGTA, 2 MgATP, 10 phosphocreatine disodium, and 10 HEPES, pH adjusted to 7.3 with KOH (Sigma−Aldrich). Current clamp recordings were performed with a MultiClamp 700B patch clamp amplifier (Molecular Devices). Current flow out of the amplifier into the patch pipette was considered positive. Resting membrane potentials were stable (duration range = 10− 150 minutes) and ranged from −50 to −80 mV. Series resistances ranged from 40 to 120 MΩ. Membrane potential time constants from acceptable recordings, measured with hyperpolarizing current injections, were typical for cortical neurons (range = 6 − 24 ms).

Dye Loading and In vivo Two-Photon Microscopy

Bulk loading of a calcium sensitive dye under continuous visual guidance followed previous protocols (Garaschuk:2006kl Golshani and Portera-Cailliau, 2008; Kerr and Greenberg, 2005; Stosiek et al., 2003). A cortical region with central receptive fields in the V1 binocular zone was mapped with extracellular methods prior to loading. Dye solution contained 0.8 mM Oregon Green 488 BAPTA-1 AM (OGB-1 AM, Invitrogen) dissolved in DMSO (Sigma-Aldrich) with 20% pluronic acid (Sigma-Aldrich) and mixed in a salt solution (150 mM NaCl, 2.5 mM KCl, 10 mM HEPES, pH 7.4, all Sigma-Aldrich). Either 40-80 μM Alexa Fluor 594 (Invitrogen) or 125 μM Sulforhodamine 101 (Sigma-Aldrich) was also included for visualization during and immediately after loading. Patch pipettes (tip diameter 2-5 μm, King Precision Glass) containing this solution were inserted into the cortex to a depth of 250-400 μm below the surface with 1.5% agarose (in saline) placed on top the brain. The solution was carefully pressure injected (100-350 mbar) over 10-15 minutes to cause the least amount of tissue damage. OGB-1 AM is weakly fluorescent before cellular-internalization, so the amount of dye injected was inferred through the red dye visualized through the two-photon microscope. To ensure full loading we waited 1 hr before before adding a glass coverslip for imaging. Metal springs were fastened on the attached head plate to place pressure on the glass coverslip and reduce brain pulsations. Fluorescence was collected with a custom-built two-photon resonant mirror scanning microscope and a mode-locked (900-950 nm) Chameleon Ultra Ti:Sapphire laser (Coherent). Excitation light was focused by a 40x water objective (0.8 numerical aperture, Nikon). Collected light was split into red and green channels with a dichroic prior to the photo-multiplier tubes (PMTs). Images were obtained with custom software (Labview, National Instruments). Two different scanning mirror systems were used to collect data: a galvanometer system scanning at 4 Hz frame rate and resonant mirror system scanning at 30 Hz frame rate. Using the galvanometer system, square

regions of cortex 150 μm wide were imaged at 150x150 pixels. Using the resonant mirror system, a square region of cortex 300 μm wide was imaged at 256x455 pixels. Images in all experiments were obtained from at least three depths separated by 20−25 μm, starting at least 150 μm below the cortical surface.

Stimulus Presentation

Visual stimuli were generated by a Macintosh computer (Apple) using the Psychophysics Toolbox (Brainard, 1997; Pelli, 1997) for Matlab (Mathworks) and presented Sony video monitors (GDM−F520) placed either 50 cm (cat) or 38 cm (mouse) from the animal's eyes. The video monitors had a non−interlaced refresh rate of 100Hz and a spatial resolution of 1024x768 pixels, which subtended 40x30 cm (typically 58x46 deg in mouse, 44x34 deg in cat). The video monitors had a mean luminance of 40 cd/cm^2.

Electrophysiology Stimulus Protocol

Drifting gratings (square wave or sinusoidal in the mouse, only sinusoidal in the cat) were presented for either 1.5 sec (mouse) or 4 sec (cat), preceded and followed by 250 ms blank (mean luminance) periods. Spontaneous activity was measured with blank periods interleaved with drifting grating stimuli and lasting the same duration (1.5−2 sec or 4 sec). Stimulus duration was typical for measurements in mouse (Grubb and Thompson, 2003; Gao et al., 2010; Niell and Stryker, 2008) and cat (Priebe, 2008). Spatial and temporal frequency were optimized for each recording. In mouse, spatial frequencies used were 0.03 − 0.05 cpd and temporal frequencies used were 2−4 Hz. In cat, spatial frequencies used were 0.20 − 1.5 cpd, temporal frequencies used were 2−4 Hz, and receptive field size was 0.5−2 degrees in diameter. Spatial frequencies used to stimulate mouse neurons were low, but are close to typical values of selectivity (Niell and Stryker, 2008). Upon isolating a neuron, stimulus parameters were coarsely mapped manually and then

fine−tuned after systematic measurements of orientation and spatial selectivity. All orientation stimuli from mouse were presented to the contralateral eye.

In a subset of neurons from the mouse LGN, we also mapped receptive fields by presenting a 2−dimensional array of dark or light spots in a random sequence and measuring evoked responses. Spots were presented for 150−300 ms and were separated by 150−300 ms.

Binocular stimuli in strabismic and normal cats were presented dichoptically using the preferred stimulus parameters at 2−4 Hz temporal frequency and 90% contrast. A mirror was placed directly in front of the contralateral eye to reflect receptive field locations onto a separate monitor. The angle and location of the mirror was adjusted to avoid occlusion of the field of view for the ipsilateral eye. To measure binocular interactions we systematically changed the spatial phase of one grating while holding the spatial phase of the other grating constant (Ohzawa and Freeman, 1986a, b). Relative phase disparities used ranged from −180 to 135 degrees. All binocular and monocular stimuli were presented during the same block and pseudo−randomly interleaved.

During two−photon imaging sessions to measure orientation selectivity in rodents, drifting gratings (40 deg diameter, 0.02−0.04 spatial frequency, 100% contrast, 2−4 Hz temporal frequency) were presented for 2−3 sec in both electrophysiology and imaging experiments. Stimuli were preceded and followed by 250 ms or 2−3 sec blank (mean luminance) periods for physiology and imaging, respectively. Spontaneous activity was measured during blank (mean luminance) periods pseudorandomly interleaved with drifting grating stimuli. During imaging sessions, the stimulation protocol was repeated 7−8 times at each focal plane. The microscope objective and photomultipliers were shielded from stray light and the video monitors.

During two−photon imaging sessions to measure binocular disparity selectivity in rodents, drifting gratings (40 deg diameter, 0.02−0.04 spatial frequency, 100% contrast, 2−4 Hz temporal frequency) were presented for 2−3 sec. Spontaneous activity was measured during blank (mean luminance) periods interleaved with binocular and monocular drifting grating stimuli, all presented in a

pseudorandom sequence. Binocular phase differences (disparities) ranged 0–315 deg. During imaging sessions, each stimulation protocol was repeated 6–7 times at each focal plane. The microscope objective and photomultiplier tubes were shielded from stray light and the video monitors.

ELECTROPHYSIOLOGY ANALYSIS

To compare estimates of subthreshold membrane potential and suprathreshold spikes, raw records were low–pass filtered with a cutoff at 100 Hz to remove spikes. Spikes were identified on the basis of the larger deflections in membrane potential. Spiking (from extracellular and intracellular records) and membrane potential responses for each stimulus were cycled–averaged across trials following removal of the first cycle. The Fourier transform was used to calculate the mean (F_0) and modulation amplitude (F_1) of each cycle–averaged response. Each extracellular recording analyzed passed a visual response criterion based on an ANOVA between spontaneous firing rate during blank periods and visual stimuli (Gao et al., 2010). Simple and complex cells were separated by computing the modulation ratio (F_1/F_0) for spiking responses to the preferred monocular stimulus; neurons with modulation ratios larger than 1 are considered simple. Peak responses were defined as the sum of the mean and modulation ($F_0 + F_1$). All peak responses are reported after subtraction of the mean spontaneous activity. Mean spontaneous activity for spiking activity and membrane potential fluctuations were measured during blank (mean luminance) periods. Peak responses across orientations were fit a double Gaussian curve (Appendix B) and peak responses to binocular phase differences were fit with a cosine–wave function for illustration (Appendix B). An individual cell's orientation or disparity preference was represented by the angle from the curve fit. Error bars represent SEM unless otherwise indicated. Excitatory and inhibitory conductances were estimated as previously described (Anderson et al., 2000).

For sparse 2–D noise maps, the average spiking response was measured for each white (ON) and black (OFF) pixel. Spikes were averaged within the time

window of the stimulus presentation (150−300 ms). A difference receptive field map (ON subtracted by OFF responses) was generated and the 2−dimensional Fourier transform was used to recover the average direction across the first and second spatial frequency amplitude components (Gardner et al.,1999).

From peak responses, we characterized eye preference with the standard metric, ocular dominance (Appendix B). To measure monocularity, we took the absolute value of ODI, resulting in a non−symmetric metric of binocularity where 0 is binocular and 1 is monocular. Orientation selectivity was quantified using a normalized vector strength (Appendix B). Disparity selectivity was quantified using a normalized vector strength (Appendix B).

TWO−PHOTON CALCIUM IMAGING ANALYSIS

Images were analyzed with custom Matlab software (Mathworks). Cells were identified by hand from structure images based on size, shape, and brightness. Cell masks were generated automatically following previous methods (Nauhaus et al., 2012). Glia were easily avoided due to their different morphology from both OGB−1 AM filled neurons. Time courses for individual neurons were extracted by summing pixel intensity values within cell masks in each frame.

For each stimulus, the mean change in fluorescence ($\Delta F/F$) was calculated (Appendix B). Visually responsive cells were identified if at least one monocular or one binocular stimulus response passed a signal criterion (Appendix B). Visually responsive cells were also defined by having at least one response significantly larger than spontaneous activity (ANOVA, $p<0.05$). Additionally, identified responses to each monocular and binocular stimulus were required to be larger than neuropil activity (>95% confidence interval) and have distinctly different trial−to−trial fluorescence time courses, so as to not be scaled versions of neuropil activity.

Mean changes in fluorescence from visually responsive neurons were used to generated tuning curves for binocular disparity (Appendix B). To measure ocular dominance we used a standard metric (Appendix B). To measure monocularity, we took the absolute value of ODI, resulting in a non−symmetric metric of binocularity

where 0 is binocular and 1 is monocular. Orientation selectivity was quantified using a normalized vector strength (Appendix B). Disparity selectivity was quantified using a normalized vector strength (Appendix B).

Local Network Analysis of Two-Photon Imaging

Within each imaging session, the total number of visually responsive PV^+ and PV^- (monocular and binocular) were identified along with there spatial location and depth. Spatial positions in x-y were converted from pixels into microns. At each cell's 3-dimensional spatial location, spherical volumes were projected outwards to determine different local populations of PV^- cells to average (Appendix B). We used 5 different radii: 50,75,100,125,150 microns. This was use done to sample from each PV^- neuron only once. There was ~2-fold increase in volume with each subsequent radius (for example: $Vol_{50\mu m} = 1.67x10^5\ \mu m^3$ and $Vol_{75\mu m} = 3.96x10^5\ \mu m^3$). Individual cells were only used for analysis if at least 50 microns from the image edges. At least 3 cells were required to generated a local population within a given volume, otherwise that individual cell was excluded from further analysis.

For ocular dominance, the individual cell's ODI was compared to the population average ODI (Appendix B). The relationship between individual ODI and population average ODI was quantified with a slope and y-intercept measured by principle components analysis (Sokal and Rohlf, 1995). Standard error on PCA slopes was computed with a Bootstrap and sampling with replacement (Sokal and Rohlf, 1995). Shuffle corrections were computed by randomly shuffling positions of PV^- cells for a given imaging session and repeating the analysis above. Standard error on shuffled-corrected PCA slope was computed by Bootstrapping and sampling with replacement (Sokal and Rohlf, 1995).

For binocular disparity, tuning of each cell was converted into a polar vector, where the amplitude was defined by the DSI and the angle was defined by the disparity preference. The relationship between disparity preference difference

and distance (in microns) for pairs of cells was quantified by computing a circular–linear correlation coefficient (Zar, 1999; Berens, 2009). Population vectors were computed with a vector average (Appendix B). The relationship between individual cell's DSI and the population vector amplitude was calculated with a Bootstrapped PCA (Sokal and Rohlf, 1995). The relationship between individual cell's disparity preference and the population vector angle quantified by computing a circular–correlation coefficient (Batschelet, 1981) (Appendix B). Circular–correlations were subtracted by a shuffle–corrected circular–correlation to remove inherent biases in our data. Like for ocular dominance, shuffle corrections were computed by randomly shuffling positions of PV^- cells for a given imaging session and repeating the analysis above. Standard error on shuffled–corrected PCA slope was computed by Bootstrapping and sampling with replacement (Sokal and Rohlf, 1995).

To quantify the spatial dependence of PV^+ interneurons we fit our data (PCA slopes or shuffle–corrected circular–correlation) with an exponential (Appendix B).

STATISTICS

All summary statistical significances were calculated using the Mann–Whitney–Wilcoxon rank sum test for equal medians unless stated otherwise. Welch's t–tests were 2–sided and used only on distributions which were Gaussian, as judged by the Lilliefors test ($p > 0.05$). A bootstrapped principle component analysis was used to calculate relationships of measured quantities (Sokal and Rohlf, 1995). Confidence intervals were also computed with a bootstrap to quantify significance and measure response noise (Sokal and Rohlf, 1995). Bootstrap analyses were preformed using all stimulus trials for each neuron, running 5,000–10,000 iterations and sampling with replacement.

Appendix B: Equations

Gaussian Curve Fits

Peak responses across orientations (Θ) were fit with two Gaussian curves of the same variance (σ^2), but two different amplitudes (α and β):

$$R(\theta) = \alpha e^{-(\theta-\theta_{pref})^2/(2\sigma^2)} + \beta e^{-(\theta-\theta_{pref}+\pi)^2/(2\sigma^2)} + spont$$

The second Gaussian (β) was constrained to be 180° phase–shifted from the preferred orientation (Θ_{pref}). A DC component (*spont*) was also included to account for cells with high spontaneous firing rates.

Ocular Dominance Index

To measure ocular dominance we used a standard metric (Dräger, 1975; Gordon and Stryker, 1996; Hanover et al., 1999):

$$ODI = \frac{\left(R_{contra} - R_{ipsi}\right)}{\left(R_{contra} + R_{ipsi}\right)}$$

Here R_{contra} and R_{ipsi} represent calcium responses from the contralateral and ipsilateral eyes, respectively. To measure monocularity, we took the absolute value of ODI, resulting in a non– symmetric metric of binocularity where 0 is binocular and 1 is monocular.

Direction Selectivity Index

Direction selectivity was measured by comparing the preferred (R_p) and opposite (null, R_n) direction responses at the same orientation to generate the direction selectivity index:

$$DSI = \frac{R_p - R_n}{R_p + R_n}$$

Here a DSI value of 0 indicates no direction selectivity, whereas a DSI value of 1 indicates complete selectivity.

Orientation Selectivity Index

Orientation selectivity was quantified using a normalized vector strength (Swindale, 1998; Ringach et al., 2002; Scholl et al., 2013c):

$$OSI = \frac{\sqrt{\left(\sum_{\phi} R_{\phi} \sin 2\phi\right)^2 + \left(\sum_{\phi} R_{\phi} \cos 2\phi\right)^2}}{\sum_{\phi} R_{\phi}}$$

Here $R(\phi)$ is the response to each orientation (ϕ) presented.

DISPARITY SELECTIVITY INDEX

Disparity selectivity was quantified using a normalized vector strength (Scholl et al., 2013a; 2013b):

$$DSI = \frac{\sqrt{\left(\sum_{\phi} R_{\phi} \sin\phi\right)^2 + \left(\sum_{\phi} R_{\phi} \cos\phi\right)^2}}{\sum_{\phi} R_{\phi}}$$

Here $R(\phi)$ is the response to each binocular phase (ϕ) presented.

BINOCULAR RESPONSE GAIN

To quantify suppression we measured binocular response Gain:

$$Gain = \log_{10}\left(\frac{F^0_{binoc} + F^1_{binoc}}{R_{pref}}\right)$$

Gain is defined as a logarithmic ratio of the sum of disparity tuning mean and modulation divided by the peak response to the preferred eye.

PRINCIPLE COMPONENT ANALYSIS

To quantify the relationship between two−independent (measured) variables we used PCA to uncover the major axis slope (Sokal and Rohlf, 1995):

$$s_x = \frac{\sum_{i=1:n}\left(\left(x_i - \bar{x}\right)^2\right)}{n-1}$$

$$s_y = \frac{\sum_{i=1:n}\left(\left(y_i - \bar{y}\right)^2\right)}{n-1}$$

$$s_{xy} = \frac{\sum_{i=1:n}\left(\left(x_i - \bar{x}\right)\cdot\left(y_i - \bar{y}\right)\right)}{n-1}$$

$$D = \sqrt{\left(s_x + s_y\right)^2 - 4\cdot\left(s_x \cdot s_y - \left(s_{xy}\right)^2\right)}$$

$$\lambda_1 = \frac{\left(s_x + s_y + D\right)}{2}$$

$$slope_{major\ axis} = \frac{s_{xy}}{\left(\lambda_1 - s_x\right)}$$

Here s_x and s_y are the variance or sums of squares of x and y, respectively, and s_{xy} is the covariance between x and y. The random, independent measurements are indicated by x and y. The diagonal of variance−covariance matrix (D) used to compute the first (major−axis) eigenvector (λ_1). Eigenvectors measure variability along the major (λ_1) or minor (λ_1) axis. The major−axis slope is calculated from s_x, s_{xy}, and λ_1.

D–PRIME

Signal detection sensitivity (d') for spiking responses to monocular (contralateral) and binocular visual stimulation:

$$d' = \frac{\mu_{resp} - \mu_{spont}}{(1/2)\sqrt{\sigma^2_{resp} + \sigma^2_{spont}}}$$

Here μ_{resp} and σ_{resp} are the response mean and variance during visual stimulation, and μ_{spont} and σ_{spont} are the spontaneous activity mean and variance during mean luminance periods (Simpson and Fitter, 1973; Swets, 1986).

TRANSFORMATION FROM VM TO SPIKE RATE

To describe the nonlinear transformation between membrane potential and spike rate, we modeled the threshold nonlinearity by fitting the relationship between trial–averaged membrane potential and spike rate with a power law nonlinearity (Anderson et al., 2000b; Hansel and van Vreeswijk, 2002; Miller and Troyer, 2002; Priebe et al., 2004):

$$R(V_m) = k\left[\bar{V}_m - V_{rest}\right]_+^p$$

where R is spike rate, is trial–averaged membrane potential, V_{rest} is resting membrane potential, and the subscript, +, indicates rectification ($R = 0$ for $V_m < V_{rest}$). The power law nonlinearity accounts for the effect of trial–to–trial variability by smoothing the threshold–linear relationship between mean membrane potential and mean spike rate (Anderson et al., 2000b).

Threshold–Linear Model of Binocular and Monocular Responses

Responses of individual neurons modeled with the following equation:

$$R(\phi) = gain\left\lfloor g_{ipsi}L_{ipsi}(\phi) + g_{contra}L_{contra}(\phi) - thresh \right\rfloor_{+}$$

where L_{ipsi} and L_{contra} are the luminance changes caused by the drifting grating for each eye (contralateral and ipsilateral), g_{ipsi} and g_{contra} are the input gains from the ipsilateral and contralateral eyes, and $R(\phi)$ is the response to each orientation (ϕ) presented. The gain represents the slope of the suprathreshold input to spiking transformation. The summed input from each eye is then passed through a threshold nonlinearity to generate a predicted spike rate

Ocular Dominance of Threshold–Linear Model Predictions

Using predicted input gains (g_{ipsi} and g_{contra}) from the previous model:

$$ODI_{v} = \frac{\left(g_{contra} - g_{ipsi}\right)}{\left(g_{contra} + g_{ipsi}\right)}$$

Two-Photon Response Normalization

Responses (F_t) to each stimulus presentation were normalized by the response to the gray screen (F_O) immediately before the stimulus came on:

$$\Delta F/F = \left(F_t - F_o\right)/F_o$$

For each stimulus, the mean change in fluorescence (ΔF/F) was calculated in a 0.5 sec window, centered around the global average peak calculated by averaging responses to all stimulus conditions and trials.

Two-Photon Response Criterion

Visually responsive cells were identified if at least one monocular and one binocular stimulus response had:

$$\left(\mu_{stimulus} - \mu_{blank}\right)/\left(\sigma_{stimulus} + \sigma_{blank}\right) \geq 1$$

Here $\mu_{stimulus}$ refers to the mean stimulus evoked response, μ_{blank} refers to the mean spontaneous activity, $\sigma_{stimulus}$ is the stimulus evoked response standard error, and σ_{blank} spontaneous activity standard error.

Spherical Volume

Each sphere's volume was calculated by:

$$Vol_j = \frac{4}{3}\pi\left(r_j^3 - r_{j-1}^3\right)$$

where *j* indicates the specific radius. In this way, the radius was a sphere and all larger radii were hollowed-shells.

Population ODI Average

An individual cell's ODI was compared to the population average ODI:

$$ODI_{pop} = \sum^{n} ODI_{n}$$

Population Vector Average

Population vectors were computed with a vector average:

$$v_{pop} = \frac{1}{n}\sum^{n} \mathrm{R}_{n}\mathrm{e}^{i\psi_{n}}$$

where R_n is the DSI and ψ_n is the disparity preference of each neuron (n) in the population.

Circular–Correlation Coefficient

The relationship between individual cell's disparity preference and the population vector angle quantified by computing a circular–correlation coefficient (Batschelet, 1981):

$$corr = \frac{1}{N}\sqrt{\left(\left(\sum \cos\left(\psi_{n} - \zeta_{n}\right)\right)^{2} + \left(\sum \sin\left(\psi_{n} - \zeta_{n}\right)\right)^{2}\right)}$$

where ψ is the individual cell's disparity preference, ζ is the population vector angle, and N is the total number of neurons (n).

Cosine Function for Tuning Curve Illustration

Tuning curves were fit with a cosine−wave function for illustration:

$$R(\phi) = \frac{\alpha}{2}\left(e^{i(\phi-\phi_{pref})} - e^{-i(\phi-\phi_{pref})} \right) + spont$$

Here *a* is the modulation amplitude, ϕ are the binocular phase differences presented, ϕ_{pref} is the disparity phase preference, and $R(\phi)$ is the fit.

Exponential Decay

To quantify the spatial dependence of PV^+ interneurons we fit our data (PCA slopes or shuffle−corrected circular−correlation) with an exponential curve:

$$y = ae^{-r/\lambda}$$

where *a* is the amplitude, *r* is the spherical radius in microns, and λ is the spatial length constant.

References

Alonso JM, Usrey WM, Reid RC (2001) Rules of connectivity between geniculate cells and simple cells in cat primary visual cortex. J Neurosci 21: 4002–4015.

Anderson JS, Lampl I, Reichova I, Carandini M, Ferster D (2000) Stimulus dependence of two–state fluctuations of membrane potential in cat visual cortex. Nat Neurosci 3: 617–621.

Anderson JS, Carandini M, Ferster D (2000) Orientation tuning of input conductance, excitation, and inhibition in cat primary visual cortex. J Neurophysiol 84: 909–926.

Anderson PA, Movshon JA (1989) Binocular combination of contrast signals. Vis Res 29: 1115–1132.

Antonini A, Fagiolini M, Stryker MP (1999) Anatomical Correlates of Functional Plasticity in Mouse Visual Cortex. J Neurosci 19(11): 4388–4406

Anzai A, Ohzawa I, Freeman RD (1999a) Neural mechanisms for processing binocular information II. Complex cells. J Neurophysiol 82: 909–924.

Anzai A, Ohzawa I, Freeman RD (1999b) Neural mechanisms for processing binocular information I. Simple cells. J Neurophysiol 82: 891–908.

Atallah BV, Bruns W, Carandini M, Scanziani M (2012) Parvalbumin–Expressing Interneurons Linearly Transform Cortical Responses to Visual Stimuli. Neuron 73: 159–170.

Azouz R, Gray CM, Nowak LG, McCormick DA (1997) Physiological properties of inhibitory interneurons in cat striate cortex. Cereb Cortex 7: 534–545.

Barlow HB, Hill RM, Levick WR (1964) Retinal ganglion cells responding selectivity to direction and speed of image motion in the rabbit. J Physiol (Lond) 173: 377–407.

Barlow HB, Blakemore C, Pettigrew JD (1967) The neural mechanism of binocular depth discrimination. J Physio 193: 327–342.

Batschelet E (1981) Circular Statistics in Biology. Academic Press: London.

Bell CC, Han VZ, Sugawara Y, Grant K (1997) Synaptic plasticity in a cerebellum−like structure depends on temporal order. Nature 387: 278−281.

Berens P (2009) CircStat: A MATLAB toolbox for circular statistics. Journal of Statistical Software 31.

Beverley KI, Regan D (1973) Selective adaptation in stereoscopic depth perception. J Physio 232: 40−41.

Blakemore C (1969) Binocular depth discrimination and the nasotemporal division. J Physiol 205:471-497.

Blakemore C (1970) The range and scope of binocular depth discrimination in man. J Physiol (Lond) 211: 599-622.

Blakemore C (1976) The conditions required for the maintenance of binocularity in the kitten's visual cortex. J Neurophysiol 261: 423−444.

Blasdel GG and Fitzpatrick D (1984) Physiological organization of layer 4 in macaque striate cortex. J Neurosci 4: 880−895.

Bock DD, Lee W−CA, Kerlin AM, Andermann ML, Hood G, Wetzel AW, Yurgenson S, Soucy ER, Kim HS, Reid RC (2011) Network anatomy and in vivo physiology of visual cortical neurons. Nature 471: 177-182.

Bonhoeffer T, Grinvald A (1991) Iso−orientation domains in cat visual cortex are arranged in pinwheel−like patterns. Nature 353: 429-431.

Bonin V, Histed MH, Yurgenson S, Reid RC (2011) Local diversity and fine−scale organization of receptive fields in mouse visual cortex. J Neurosci 31:18506-18521.

Borg−Graham LJ, Monier C, Fregnac Y (1998) Visual input evokes transient and strong shunting inhibition in visual cortical neurons. Nature 393: 369−373.

Bosking WH, Zhang Y, Schofield B, Fitzpatrick D (1997) Orientation selectivity and the arrangement of horizontal connections in tree shrew striate cortex. J Neurosci 17: 2112-2127.

Boycott BB and Wässle H (1974) The morphological types of ganglion cells of the domestic cat's retina. J Physiol (Lond) 240: 397–419.

Brainard DH (1997) The Psychophysics Toolbox. Spat Vis 10: 433–436.

Burge J, Fowlkes CC, Banks MS (2010) Natural–scene statistics predict how the figure–ground cue of convexity affects human depth perception. J Neurosci 30: 7269–7280.

Burge J, Geisler WS (2011) Optimal defocus estimation in individual natural images. Proc Natl Acad Sci USA 108: 16849–16854.

Burge J and Geisler WS (2014) Optimal disparity estimation in natural stereo–images. J Vis 14(2): 1–18.

Caporale N, Dan Y (2008) Spike timing–dependent plasticity: a Hebbian learning rule. Ann Rev Neurosci 31: 25–46.

Carandini M and Ferster D (2000) Membrane potential and firing rate in cat primary visual cortex. J Neurosci 20: 470–484.

Cardin JA, Palmer LA, Contreras D (2008) Cellular mechanisms underlying stimulus–dependent gain modulation in primary visual cortex neurons in vivo. Neuron 59: 150–160.

Celebrini S, Thorpe S, Trotter Y, Imbert M (1993) Dynamics of orientation coding in area V1 of the awake primate. Vis Neurosci 10: 811–825.

Chalupa LM, Lia B (1991) The nasotemporal division of retinal ganglion cells with crossed and uncrossed projections in the fetal rhesus monkey. J Neurosci 11:191–202.

Chalupa LM, Williams RW (2008) Eye, retina, and visual system of the mouse. MIT Press.

Chapman B, Stryker MP, Bonhoeffer T (1996) Development of orientation preference maps in ferret primary visual cortex. J Neurosci 16(20):6443–53.

Chen X-J, Rasch MJ, Chen G, Ye C-Q, Wu S, Zhang X-H (2014) Binocular input coincidence mediates critical period plasticity in the mouse primary visual cortex. J Neurosci 34: 2940-2955.

Chen Y, Geisler WS, Seidemann E (2008) Optimal temporal decoding of neural population responses in a reaction-time visual detection task. J Neurophysiol 99: 1366-79.

Cheong SK, Tailby C, Solomon SG, Martin PR (2013) Cortical-like receptive fields in the lateral geniculate nucleus of marmoset monkeys. J Neurosci 33: 6864-6876.

Chino YM, Shansky MS, Jankowski WL, Banser FA (1983) Effects of rearing kittens with convergent strabismus on development of receptive field properties in striate cortex neurons. J Neurophysiol 50: 265-286.

Chino YM, Kaas JH, Smith EL, Langston AL, Cheng H (1992) Rapid reorganization of cortical maps in adult cats following restricted deafferentation in retina. Vision research 32: 789-796.

Chino YM, Smith EL, 3rd, Yoshida K, Cheng H, Hamamoto J (1994) Binocular interactions in striate cortical neurons of cats reared with discordant visual inputs. J Neurosci 14: 5050-5067.

Chisum HJ, Mooser F, Fitzpatrick D (2003) Emergent Properties of Layer 2/3 Neurons Reflect the Collinear Arrangement of Horizontal Connections in Tree Shrew Visual Cortex. J Neurosci 23: 2947-2960.

Chow KL, Masland RH, Stewart DL (1971) Receptive field characteristics of striate cortical neurons in the rabbit. Brain Res 33: 337-352.

Chung S, Ferster D (1998) Strength and orientation tuning of the thalamic input to simple cells revealed by electrically evoked cortical suppression. Neuron 20: 1177-1189.

Cleland BG and Levick WR (1974) Properties of rarely encountered types of ganglion cells in the cat's retina and an overall classification. J Physiol (Lond) 240: 457-492.

Crewther SG, Crewther DP, Cleland BG (1985) Convergent strabismic amblyopia in cats. Exp Brain Res 60: 1–9.

Cronin JE, Sarich VM (1980) Tupaiid and archonta phylogeny: the macromolecular evidence. In: Comparative biology and evolutionary relationships of tree shrews. New York: Plenum.

Cumming BG, DeAngelis GC (2001) The physiology of stereopsis. Ann Rev Neurosci 24: 203–238.

Cumming BG, Parker AJ (1997) Responses of primary visual cortical neurons to binocular disparity without depth perception. Nature 389: 280–283.

de la Cera EG, Rodríguez G, Llorente L, Schaeffel F, Marcos S (2006) Optical aberrations in the mouse eye. Vis Res 46: 2546–2553.

de Nó RL (1949) Cerebral cortex: architecture, intracortical connections, motor projections. Physiology of the Nervous System: 288–330.

DeAngelis GC, Ohzawa I, Freeman RD (1991) Depth is encoded in the visual cortex by a specialized receptive field structure. Nature 352: 156–159.

DeAngelis GC, Ohzawa I, Freeman RD (1995) Neuronal mechanisms underlying stereopsis: how do simple cells in the visual cortex encode binocular disparity? Perception 24: 3–31.

DeFelipe J, Alonso–Nanclares L, Arellano JI (2002) Microstructure of the neocortex: comparative aspects. J Neurocytol 31: 299–316.

DeFelipe J, López–Cruz PL, Benavides–Piccione R, Bielza C, Larrañaga P, Anderson S, Burkhalter A, Cauli B, Fairén A, Feldmeyer D, et al. (2013) New insights into the classification and nomenclature of cortical GABAergic interneurons. Nat Rev Neurosci 14: 202–216.

Diamond ME, Huang W, Ebner FF (1994) Laminar comparison of somatosensory cortical plasticity. Science 265: 1885–1888.

Douglas RJ, Martin KAC (2004) Neuronal circuits of the neocortex. Annu Rec Neurosci 27: 419–451.

Douglas RJ, Martin KAC, Whitterridge D (1989) A canonical microcircuit for neocortex. Neural Comp 1: 480−488.

Dräger UC (1974) Autoradiography of tritiated proline and fucose transported transneuronally from the eye to the visual cortex in pigmented and albino mice. Brain Res 82: 284−292.

Dräger UC (1975) Receptive fields of single cells and topography in mouse visual cortex. J Comp Neurol 160: 269−290.

Economides JR, Adams DL, Horton JC (2012) Perception via the deviated eye in strabismus. J Neurosci 32: 10286−10295.

Elstrott J, Anishchenko A, Greschner M, Sher A, Litke AM, Chichilnisky EJ, Feller MB (2008) Direction selectivity in the retina is established independent of visual experience and cholinergic retinal waves. Neuron 58: 499−506.

Engelmann R, Crook JM, Lowel S (2002) Optical imaging of orientation and ocular dominance maps in area 17 of cats with convergent strabismus. Vis Neurosci 19:39−49.

Espinosa JS, Stryker MP (2012) Development and plasticity of the primary visual cortex. Neuron 75: 230−249.

Essen DC and Zeki SM (1978) The topographic organization of rhesus monkey prestriate cortex. J Physiol (Lond) 277: 193−226.

Ferster D, Chung S, Wheat H (1996) Orientation selectivity of thalamic input to simple cells of cat visual cortex. Nature 380: 249−252.

Ferster D, Jagadeesh B (1992) EPSP−IPSP interactions in cat visual cortex studied with in vivo whole−cell patch recording. J Neurosci 12: 1262−1274.

Field DJ (1987) Relations between the statistics of natural images and the response properties of cortical cells. J Opt Soc Am A 4: 2739−2394.

Fitzpatrick D (1996) The functional organization of local circuits in visual cortex: insights from the study of tree shrew striate cortex. Cereb Cortex 6: 329−341.

Frazor RA, Albrecht DG, Geisler WS, Crane AM (2004) Visual cortex neurons of monkeys and cats: temporal dynamics of the spatial frequency response function. J Neurophysiol 91: 2607–2627.

Freeman RD, Tsumoto T (1983) An electrophysiological comparison of convergent and divergent strabismus in the cat: electrical and visual activation of single cortical cells. J Neurophysiol 49: 238–253.

Fries P, Roelfsema PR, Engel AK, Konig P, Singer W (1997) Synchronization of oscillatory responses in visual cortex correlates with perception in interocular rivalry. PNAS 94: 12699–12704.

Gao E, DeAngelis GC, Burkhalter A (2010) Parallel input channels to mouse primary visual cortex. J Neurosci 30: 5912–5926.

Garaschuk O, Milos R–I, Konnerth A (2006) Targeted bulk–loading of fluorescent indicators for two–photon brain imaging in vivo. Nat Protoc 1: 380–386.

Gardner JL, Anzai A, Ohzawa I, Freeman RD (1999) Linear and nonlinear contributions to orientation tuning of simple cells in the cat's striate cortex. Vis Neurosci 16: 1115–1121.

Gawne TJ, Kjaer TW, Richmond BJ (1996) Latency: another potential code for feature binding in striate cortex. J Neurophysiol 76: 1356–1360.

Gilbert CD (1983) Microcircuitry of the visual cortex. Ann Rev Neurosci 6: 217–247.

Girman S, Lund R (2010) Orientation–specific modulation of rat retinal ganglion cell responses and its dependence on relative orientations of the center and surround gratings. J Neurophysiol 104: 2951–2962.

Godement P, Salaün J, Imbert M (1984) Prenatal and postnatal development of retinogeniculate and retinocollicular projections in the mouse. J Comp Neurol 230: 552–575.

Golshani P, Portera–Cailliau C (2008) In vivo 2–photon calcium imaging in layer 2/3 of mice. JoVE 13: 681.

Gonchar Y, Wang Q, Burkhalter A (2007) Multiple distinct subtypes of GABAergic neurons in mouse visual cortex identified by triple immunostaining. Frontiers Neuroanatomy 1: 3.

Gordon JA, Stryker MP (1996) Experience–dependent plasticity of binocular responses in the primary visual cortex of the mouse. J Neurosci 16: 3274–3286.

Grubb MS and Thompson ID (2003) Quantitative characterization of visual response properties in the mouse dorsal lateral geniculate nucleus. J Neurophysiol 90: 3594–3607.

Gutig R, Aharonov R, Rotter S, Sompolinsky H (2003) Learning input correlations through nonlinear temporally asymmetric Hebbian plasticity. J Neurosci 23: 3697–3714.

Haas JS, Nowotny T, Abarbanel HD (2006) Spike–timing–dependent plasticity of inhibitory synapses in the entorhinal cortex. J Neurophysiol 96: 3305–3313.

Hammond P (1974) Cat retinal ganglion cells: size and shape of receptive field centres. J Physiol (Lond) 242: 99–118.

Hanover JL, Huang ZJ, Tonegawa S, Stryker MP (1999) Brain–derived neurotrophic factor overexpression induces precocious critical period in mouse visual cortex. J Neurosci 19: RC40.

Hansel D, Van Vreeswijk C (2012) The Mechanism of Orientation Selectivity in Primary Visual Cortex without a Functional Map. J Neurosci 32: 4049–4064

Heesy CP (2004) On the relationship between orbit orientation and binocular visual field overlap in mammals. Anat Rec A. 281A: 1104–1110.

Heimel JA, Van Hooser SD, Nelson SB (2005) Laminar organization of response properties in primary visual cortex of the gray squirrel (Sciurus carolinensis) J Neurophysiol 94: 3538–3554.

Held RT, Cooper EA (2012) Blur and disparity are complementary cues to depth. Curr Biol 22: 426–431.

Hensch TK (2004) Critical period regulation. Ann Rev Neurosci 27: 549–579.

Hillis JM, Watt SJ, Landy MS (2004) Slant from texture and disparity cues: Optimal cue combination. J Vis 4: 967−992.

Hirsch JA, Alonso JM, Reid RC, Martinez LM (1998) Synaptic integration in striate cortical simple cells. J Neurosci 18: 9517−9528.

Hirsch JA, Martinez LM, Pillai C, Alonso JM, Wang Q, Sommer FT (2003) Functionally distinct inhibitory neurons at the first stage of visual cortical processing. Nat Neurosci 6: 1300−1308.

Hochstein S, Shapely RM (1976) Linear and nonlinear spatial subunits in Y cat retinal ganglion cells. J Physio 262: 265−284.

Hofer SB, Mrsic−Flogel TD, Bonhoeffer T, Hübener M (2006) Prior experience enhances plasticity in adult visual cortex. Nat Neurosci 9: 127−132.

Hofer SB, Mrsic−Flogel TD, Bonhoeffer T, Hübener M (2009) Experience leaves a lasting structural trace in cortical circuits. Nature 457: 313−317.

Hofer SB, Ko H, Pichler B, Vogelstein J, Ros H, Zeng H, Lein E, Lesica NA, Mrsic−Flogel TD (2011) Differential connectivity and response dynamics of excitatory and inhibitory neurons in visual cortex. Nat Neurosci 14, 1045−1052.

Holmgren CD, Zilberter Y (2001) Coincident spiking activity induces long−term changes in inhibition of neocortical pyramidal cells. J Neurosci 21: 8270−8277.

Holmgren CD, Harkany T, Svennenfors B, Zilberter Y (2003) Pyramidal cell communication within local networks in layer 2/3 of rat neocortex. J Physiol 551, 139−153.

Horner BE, Taylor JM, Padykula HA (1964) Food habits and gastric morphology of the grasshopper mouse. J Mammal 45(4): 513−535.

House DR, Elstrott J, Koh E, Chung J, Feldman DE (2011) Parallel regulation of feedforward inhibition and excitation during whisker map plasticity. Neuron 72: 819−831.

Hubel DH and Wiesel TN (1959) Receptive fields of single neurones in the cat's striate cortex. J Physiol (Lond) 148: 574−591.

Hubel DH, Wiesel TN (1961) Integrative action in the cat's lateral geniculate body. J Physiol (Lond) 155: 385–398.

Hubel DH, Wiesel TN (1962) Receptive fields, binocular interaction and functional architecture in the cat's visual cortex. J Physiol (Lond) 160: 106–154.

Hubel DH, Wiesel TN (1963) Shape and arrangement of columns in cat's striate cortex. J Physiol (Lond) 165: 559–568.

Hubel DH, Wiesel TN (1965) Binocular interaction in striate cortex of kittens reared with artificial squint. J Neurophysiol 28: 1041–1059.

Hubel DH, Wiesel TN (1968) Receptive fields and functional architecture of monkey striate cortex. J Physiol (Lond) 195: 215–243.

Hubel DH, Wiesel TN (1973) A re–examination of stereoscopic mechanisms in area 17 of the cat. J Physio 232: 29–30.

Huberman AD, Feller MB, Chapman B (2008) Mechanisms underlying development of visual maps and receptive fields. Ann Rev Neurosci 31: 479–509.

Huberman AD, Niell CM (2011) What can mice tell us about how vision works? Trends Neurosci 34: 464–473.

Jaffer S, Vorobyov V, Sengpiel F (2012) Effects of different forms of monocular deprivation on primary visual cortex maps. Vis Neurosci 29: 247–253.

Jia H, Rochefort NL, Chen X, Konnerth A (2010) Dendritic organization of sensory input to cortical neurons in vivo. Nature 464: 1307–1312.

Joshua DE (1970) Binocular single vision and depth discrimination. Receptive field disparities for central and peripheral vision and binocular interaction on peripheral single units in cat. Exp Brain Res 10: 389–416.

Joshua, D. and Bishop, P.O. (1970) Binocular single vision and depth discrimination. Receptive field disparities for central and peripheral vision and binocular interaction on peripheral single units in cat. Exp Brain Res 10, 389–416.

Kaas JH (1980) Comparative neurology of the telencephalon: A comparative survey of visual cortex organization in mammals. Plenum Press, New York and London.

Kaas JH (1989) The evolution of complex sensory systems in mammals. J Exp Biol 146: 165–176.

Kalatsky VA, Stryker MP (2003) New paradigm for optical imaging: temporally encoded maps of intrinsic signal. Neuron 38: 529–545.

Kameyama K, Sohya K, Ebina T, Fukuda A, Yanagawa Y, Tsumoto T (2010) Difference in Binocularity and Ocular Dominance Plasticity between GABAergic and Excitatory Cortical Neurons. J Neurosci 30: 1551–1559.

Kara P, Boyd JD (2009) A micro–architecture for binocular disparity and ocular dominance in visual cortex. Nature 458: 627–631.

Kaschube M, Schnabel M, Löwel S, Coppola DM, White LE, Wolf F (2010) Universality in the evolution of orientation columns in the visual cortex. Science 330: 1113–1116.

Katz LC, Crowley JC (2002) Development of cortical circuits: lessons from ocular dominance columns. Nat Rev Neurosci 3: 34–42.

Kerlin AM, Andermann ML, Berezovskii VK, Reid RC (2010) Broadly Tuned Response Properties of Diverse Inhibitory Neuron Subtypes in Mouse Visual Cortex. Neuron 67: 858–871.

Keil W, Kaschube M, Schnabel M, Kisvarday ZF (2012) Response to Comment on "Universality in the Evolution of Orientation Columns in the Visual Cortex ". Science.

Kerr, J., Greenberg, D., Helmchen, F. (2005) Imaging input and output of neocortical networks in vivo. Proc. Natl. Acad. Sci. 102, 14063–14068.

Khibnik LA, Cho KK, Bear MF (2010) Relative contribution of feedforward excitatory connections to expression of ocular dominance plasticity in layer 4 of visual cortex. Neuron 66: 493–500.

Klalil RE, Spear PD, Langsetmo ARNE (1984) Response properties of striate cortex neurons in cats raised with divergent of convergent strabismus. J Neurophysiol 52: 514–537.

Ko H, Cossell L, Baragli C, Antolik J, Clopath C, Hofer SB, Mrsic−Flogel TD (2013) The emergence of functional microcircuits in visual cortex. Nature 496: 96−100.

Ko H, Hofer SB, Pichler B, Buchanan KA, Sjöström PJ, Mrsic−Flogel TD (2011) Functional specificity of local synaptic connections in neocortical networks. Nature 473: 87−91.

Krubitzer L (1995) The organization of neocortex in mammals: are species differences really so different? TINS 18(9): 408−416.

Kuhlmann L, Vidyasagar TR (2011) A computational study of how orientation bias in the lateral geniculate nucleus can give rise to orientation selectivity in primary visual cortex. Front Syst Neurosci 5: 81.

Kullmann DM, Moreau AW, Bakiri Y, Nicholson E (2012) Plasticity of inhibition. Neuron 75: 951−962.

Landy MS, Maloney LT, Johnston EB (1995) Measurement and modeling of depth cue combination: In defense of weak fusion. Vision Res 35: 389−412.

Landry SO (1970) The Rodentia as omnivores. Quarterly Review of Biology: 351−372.

Langley WM (1994) Comparison of predatory behaviors of deer mice (Peromyscus maniculatus) and grasshopper mice (Onychomys leucogaster). J Comp Psychol 108(4): 394.

Leamey CA, Protti DA (2008) Comparative survey of the mammalian visual system with reference to the mouse. Eye, retina, and visual system of the mouse.

Lien AD, Scanziani M (2013) Tuned thalamic excitation is amplified by visual cortical circuits. Nat Neurosci 16:1315−1323.

Legge GE (1984) Binocular contrast summation− I. Detection and discrimination. Vision Res 24: 373−383.

LeVay S, Gilbert CD (1976) Laminar patterns of geniculocortical projection in the cat. Brain Res 113: 1−19.

LeVay S, Voigt T (1988) Ocular dominance and disparity coding in cat visual cortex. Vis Neurosci 1: 395−414.

Leventhal AG, Schall JD (1983) Structural basis of orientation sensitivity of cat retinal ganglion cells. J Comp Neurol 220: 465–475.

Levi DM, Harwerth RS, Smith EL, 3rd (1979) Humans deprived of normal binocular vision have binocular interactions tuned to size and orientation. Science 206: 852–854.

Levick WR (1967) Receptive fields and trigger features of ganglion cells in the visual streak of the rabbits retina. J Physiol (Lond) 188: 285–307.

Levick WR, Thibos LN (1980) Orientation bias of cat retinal ganglion cells. Nature 286: 389–390.

Levick WR, Oyster CW, Takahashi E (1969) Rabbit lateral geniculate nucleus: sharpener of directional information. Science 165: 712–714.

Levy RB, Reyes AD (2012) Spatial profile of excitatory and inhibitory synaptic connectivity in mouse primary auditory cortex. J Neurosci 32, 5609–5619.

Li J, Thompson B, Deng D, Chan LYL, Yu M, Hess RF (2013) Dichoptic training enables the adult amblyopic brain to learn. Curr Bio 23: 308–309.

Li RW, Ngo C, Nguyen J, Levi DM (2011) Video–game play induces plasticity in the visual system of adults with amblyopia. PLoS Biol 9: e1001135.

Li YT, Ma WP, Pan CJ, Zhang LI, Tao HW (2012) Broadening of cortical inhibition mediates developmental sharpening of orientation selectivity. J Neurosci 32: 3981–3991.

Liu B, Li P, Sun YJ, Li Y, Zhang LI, Tao HW (2010) Intervening inhibition underlies simple–cell receptive field structure in visual cortex. Nat Neurosci 13: 89–96.

Longordo F, To M–S, Ikeda K, Stuart GJ (2013) Sublinear integration underlies binocular processing in primary visual cortex. Nat Neurosci 16: 714–723.

Löwel S (1994) Ocular dominance column development: strabismus changes the spacing of adjacent columns in cat visual cortex. J Neurosci 14: 7451–7468.

Löwel S, Schmidt KE, Kim DS, Wolf F, Hoffsümmer F, Singer W, Bonhoeffer T (1998) The layout of orientation and ocular dominance domains in area 17 of strabismic cats. Europ J Neurosci 10: 2629−2643.

Lu JT, Li CY, Zhao JP, Poo MM, Zhang XH (2007) Spike−timing−dependent plasticity of neocortical excitatory synapses on inhibitory interneurons depends on target cell type. J Neurosci 27: 9711−9720.

Luckett WP (1980) The suggested evolutionary relationships and classification of tree shrews: Comparative biology and evolutionary relationships of tree shrews. New York: Plenum.

MacPhee RDE (1993) Primates and their relatives in phylogenetic perspective. New York: Plenum.

Madisen L, Zwingman TA, Sunkin SM, Oh SW, Zariwala HA, Gu H, Ng LL, Palmiter RD, Hawrylycz MJ, Jones AR, et al. (2010) A robust and high−throughput Cre reporting and characterization system for the whole mouse brain. Nat Neurosci 13: 133−140.

Maffei A, Nataraj K, Nelson SB, Turrigiano GG (2006) Potentiation of cortical inhibition by visual deprivation. Nature 443: 81−84.

Maffei A, Nelson SB, Turrigiano GG (2004) Selective reconfiguration of layer 4 visual cortical circuitry by visual deprivation. Nat Neurosci 7: 1353−1359.

Maffei A, Turrigiano GG (2008) Multiple modes of network homeostasis in visual cortical layer 2/3. J Neurosci 28: 4377−4384.

Mangini NJ, Pearlman AL (1980) Laminar distribution of receptive field properties in the primary visual cortex of the mouse. J Comp Neurol 193: 203−222.

Margrie TW, Brecht M, Sakmann B (2002) In vivo, low−resistance, whole−cell recordings from neurons in the anaesthetized and awake mammalian brain. Europ J Physiol 444: 491−498.

Markram H, Toledo−Rodriguez M, Wang Y, Gupta A, Silberberg G, Wu C (2004) Interneurons of the neocortical inhibitory system. Nat. Rev. Neurosci. 5, 793−807.

Marshel JH, Kaye AP, Nauhaus I, Callaway EM (2012) Anterior–posterior direction opponency in the superficial mouse lateral geniculate nucleus. Neuron 4: 713–720.

Martinez LM, Wang Q, Reid RC, Pillai C, Alonso JM, Sommer FT, Hirsch JA (2005) Receptive field structure varies with layer in the primary visual cortex. Nat Neurosci 8: 372–379.

McBain CJ, Freund TF, Mody I (1999) Glutamatergic synapses onto hippocampal interneurons: precision timing without lasting plasticity. Trend Neurosci 22: 228–235.

McLoughlin N, Schiessl I (2006) Orientation selectivity in the common marmoset (Callithrix jacchus): the periodicity of orientation columns in V1 and V2. Neuroimage 31(1):76–85.

Métin C, Godement P, Imbert M (1988) The primary visual cortex in the mouse: receptive field properties and functional organization. Exp Brain Res 69: 594–612.

Miller KD, Keller JB, Stryker MP (1989) Ocular dominance column development: analysis and simulation. Science 245: 605–615.

Monier C, Chavane F, Baudot P, Graham LJ, Fregnac Y (2003) Orientation and direction selectivity of synaptic inputs in visual cortical neurons: a diversity of combinations produces spike tuning. Neuron 37: 663–680.

Mountcastle VB (1957) Modality and topographic properties of single neurons of cat's somatic sensory cortex. J Neurophysiol 20(4): 408–34.

Mrsic–Flogel TD, Hofer SB, Ohki K, Reid RC, Bonhoeffer T, Hubener M (2007) Homeostatic regulation of eye–specific responses in visual cortex during ocular dominance plasticity. Neuron 54: 961–972.

Müller JR, Metha AB, Krauskopf J, Lennie P (2001) Information conveyed by onset transients in responses of striate cortical neurons. J Neurosci 21: 6978–6990.

Murphy EH, Berman N (1979) The rabbit and the cat: a comparison of some features of response properties of single cells in the primary visual cortex. J Comp Neurol 188: 401–427.

Nauhaus I, Nielsen KJ, Callaway EM (2012) Nonlinearity of two–photon Ca2+ imaging yields distorted measurements of tuning for V1 neuronal populations. J Neurophysiol 107: 923–936.

Nauhaus, I., Nielsen, K.J., Disney, A.A., Callaway, E.M. (2012) Orthogonal micro–organization of orientation and spatial frequency in primate primary visual cortex. Nat Neurosci 15, 1683–1690.

Nieder A, Wagner H (2000) Horizontal–disparity tuning of neurons in the visual forebrain of the behaving barn owl. J Neurophysiol 83: 2967–2979.

Niell CM, Stryker MP (2008) Highly selective receptive fields in mouse visual cortex. J Neurosci 28: 7520–7536.

Nikara T, Bishop PO, Pettigrew JD (1968) Analysis of retinal correspondence by studying receptive fields of rinocular single units in cat striate cortex. Exp Brain Res 6: 353–372.

Nowak LG, Sanchez–Vives MV, McCormick DA (2008) Lack of orientation and direction selectivity in a subgroup of fast–spiking inhibitory interneurons: cellular and synaptic mechanisms and comparison with other electrophysiological cell types. Cereb Cortex 18: 1058–1078.

O'Keefe LP, Levitt JB, Kiper DC, Shapley RM, Movshon JA (1998) Functional organization of owl monkey lateral geniculate nucleus and visual cortex. J Neurophysiol 80(2):594–609.

Ohki K, Chung S, Ch'ng YH, Kara P, Reid RC (2005) Functional imaging with cellular resolution reveals precise micro–architecture in visual cortex. Nature 433: 597–603.

Ohki K, Chung S, Kara P, Hübener M, Bonhoeffer T, Reid RC (2006) Highly ordered arrangement of single neurons in orientation pinwheels. Nature 442, 925–928.

Ohki K (2007) Specificity and randomness in the visual cortex. Curr Opin Neurobio 17(4): 401−407.

Ohzawa I (1998) Mechanisms of stereoscopic vision: the disparity energy model. Curr Opin Neurobio 8: 509−515.

Ohzawa I, DeAngelis GC, Freeman RD (1990) Stereoscopic depth discrimination in the visual cortex: neurons ideally suited as disparity detectors. Science 249: 1037−1041.

Ohzawa I, Freeman RD (1986a) The binocular organization of simple cells in the cat's visual cortex. J Neurophysiol 56: 221-242.

Ohzawa I, Freeman RD (1986b) The binocular organization of complex cells in the cat's visual cortex. J Neurophysiol 56: 243−259.

Ogden TE (1975) The receptor mosaic of Aotes trivirgatus: distribution of rods and cones. The J Comp Neurol 163(2):193-202.

Oswald AM, Doiron B, Rinzel J, Reyes AD (2009) Spatial profile and differential recruitment of GABA−B modulate oscillatory activity in auditory cortex. J Neurosci 29: 10321-10334.

Packer AM, Yuste R (2011) Dense, unspecific connectivity of neocortical parvalbumin−positive interneurons: a canonical microcircuit for inhibition? J Neurosci 31, 13260-13271.

Packwood J, Gordon B (1975) Stereopsis in normal domestic cat, Siamese cat, and cat raised with alternating monocular occlusion. J Neurophysiol 38: 1485-1499.

Palmer C, Cheng SY, Seidemann E (2007) Linking neuronal and behavioral performance in a reaction−time visual detection task. J Neurosci 27: 8122−8137.

Pardhan S, Rose D (1999) Binocular and monocular detection of gabor patches in binocular two−dimensional noise. Perception 28: 203-215.

Pei X, Volgushev M, Vidyasagar TR, Creutzfeldt OD (1991) Whole cell recording and conductance measurements in cat visual cortex in−vivo. Neuroreport 2: 485−488.

Pelli DG (1997) The VideoToolbox software for visual psychophysics: Transforming numbers into movies. Spatial Vis 10: 437–442.

Perry VH, Oehler R, Cowey A (1984) Retinal ganglion cells that project to the dorsal lateral geniculate nucleus in the macaque monkey. Neuroscience 12: 1101–1123.

Pettigrew JD (1986) Evolution of binocular vision. Section IV: Comparative visual physiology. p:208–222.

Pettigrew J, Konishi M (1976a) Neurons selective for orientation and binocular disparity in the visual Wulst of the barn owl (Tyto alba) Science 193: 675–678.

Pettigrew JD, Konishi M (1976b) Effect of monocular deprivation on binocular neurones in the owl's visual Wulst. Nature 264: 753–754.

Pettigrew JD, Nikara T, Bishop PO (1968) Binocular interaction on single units in cat striate cortex: simultaneous stimulation by single moving slit with receptive fields in correspondence. Exp Brain Res 6: 391–410.

Piscopo DM, El–Danaf RN, Huberman AD, Niell CM (2013) Diverse visual features encoded in mouse lateral geniculate nucleus. J Neurosci 33: 4642–4656.

Poggio GF, Fischer B (1977) Binocular interaction and depth sensitivity in striate and prestriate cortex of behaving rhesus monkey. J Neurophysiol 40: 1392–1405.

Poggio GF, Gonzalez F, Krause F (1988) Stereoscopic mechanisms in monkey visual cortex: binocular correlation and disparity selectivity. J Neurosci 8: 4531–4550.

Priebe NJ (2008) The relationship between subthreshold and suprathreshold ocular dominance in cat primary visual cortex. J Neurosci 28: 8553–8559.

Priebe NJ, Ferster D (2006) Mechanisms underlying cross–orientation suppression in cat visual cortex. Nat Neurosci 9: 552–561.

Priebe NJ, Ferster D (2008) Inhibition, spike threshold, and stimulus selectivity in primary visual cortex. Neuron 57: 482–497.

Priebe NJ, Mechler F, Carandini M, Ferster D (2004) The contribution of spike threshold to the dichotomy of cortical simple and complex cells. Nat Neurosci 7: 1113–1122.

Ranson A, Cheetham CE, Fox K, Sengpiel F (2012) Homeostatic plasticity mechanisms are required for juvenile, but not adult, ocular dominance plasticity. PNAS 109: 1311−1316.

Read JC, Cumming BG (2004) Ocular dominance predicts neither strength nor class of disparity selectivity with random−dot stimuli in primate V1. J Neurophysiol 91: 1271−1281.

Read JCA, Parker AJ, Cumming BG (2002) A simple model accounts for the response of disparity−tuned V1 neurons to anticorrelated images. Vis Neurosci 19: 735−753.

Regan D, Beverley KI (1973) Disparity detectors in human depth perception: Evidence for directional selectivity. Science 181:877−879.

Reich DS, Mechler F, Victor JD (2001) Temporal coding of contrast in primary visual cortex: when, what, and why. J Neurophysiol 85: 1039−1050.

Reid RC, Alonso JM (1995) Specificity of monosynaptic connections from thalamus to visual cortex. Nature 378: 281−284.

Ringach DL, Shapely RM, Hawken MJ (2002) Orientation selectivity in macaque V1: Diversity and laminar dependence. J Neurosci 22: 5639−5651.

Roelfsema PR, Konig P, Engel AK, Sireteanu R, Singer W (1994) Reduced synchronization in the visual cortex of cats with strabismic amblyopia. Europ J Neurosci 6: 1645−1655.

Rowe AH, Rowe MP (2008) Physiological resistance of grasshopper mice (Onychomys spp.) to Arizona bark scorpion (Centruroides exilicauda) venom. Toxicon 52(5): 597−605.

Rowe AH, Xiao Y, Rowe MP, Cummins TR, Zakon HH (2013) Voltage−gated sodium channel in grasshopper mice defends against bark scorpion toxin. Science 342: 441−6.

Ruffer DG (1968) Agonistic behavior of the northern grasshopper mouse (Onychomys leucogaster breviauritus). J Mammal 49(3): 481−7.

Runyan CA, Schummers J, Van Wart A, Kuhlman SJ (2010) Response features of parvalbumin−expressing interneurons suggest precise roles for subtypes of inhibition in visual cortex. Neuron 67: 847−857.

Sarko DK, Leitch DB, Girard I, Sikes RS, Catania KC (2011) Organization of somatosensory cortex in the Northern grasshopper mouse (Onychomys leucogaster), a predatory rodent. J Comp Neurol 519(1):64−74.

Sarnaik R, Wang B−S, Cang J (2014) Experience−dependent and independent binocular correspondence of receptive field subregions in mouse visual cortex. Cereb Cortex 24: 1658−1670.

Schall JD (2011) An alternative hypothesis for orientation columns in the visual cortex. Science E−Letters, online.

Schmidt KE, Singer W, Galuske RA (2004) Processing deficits in primary visual cortex of amblyopic cats. J Neurophysiol 91: 1661−1671.

Schmidt KF, Löwel S (2006) Optical imaging in cat area 18: Strabismus does not enhance the segregation of ocular dominance domains. Neuroimage 29: 439−445.

Schmidt KF, Löwel S (2008) Strabismus modifies intrinsic and inter−areal connections in cat area 18. Neuroscience 152: 128−137.

Scholl B, Burge J, Priebe NJ (2013a) Binocular integration and disparity selectivity in mouse primary visual cortex. J Neurophysiol 109: 3013−3024.

Scholl B, Tan AYY, Priebe NJ (2013b) Strabismus disrupts binocular synaptic integration in primary visual cortex. J Neurosci 33: 17108−17122.

Schuett S, Bonhoeffer T, Hübener M (2002) Mapping retinotopic structure in mouse visual cortex with optical imaging. J Neurosci 22: 6549−6559.

Schummers J, Mariño J, Sur M (2002) Synaptic integration by V1 neurons depends on location within the orientation map. Neuron 36: 969−978.

Sengpiel F, Blakemore C (1994) Interocular control of neuronal responsiveness in cat visual cortex. Nature 368: 847−850.

Sengpiel F, Blakemore C, Kind PC, Harrad R (1994) Interocular suppression in the visual cortex of strabismic cats. J Neurosci 14: 6855–6871.

Sengpiel F, Jirmann KU, Vorobyov V, Eysel UT (2006) Strabismic suppression is mediated by inhibitory interactions in the primary visual cortex. Cereb Cortex 16: 1750–1758.

Sharma J, Angelucci A, Sur M (2000) Induction of visual orientation modules in auditory cortex. Nature 404: 841–847.

Shatz CJ, Lindstrom S, Wiesel TN (1977) The distribution of afferents representing the right and left eyes in the cat's visual cortex. Brain Res 131: 103–116.

Shepherd G, Svoboda K (2005) Laminar and columnar organization of ascending excitatory projections to layer 2/3 pyramidal neurons in rat barrel cortex. J Neurosci 25, 5670–5679.

Shou T, Leventhal AG, Thompson KG, Zhou Y (1995) Direction biases of X and Y type retinal ganglion cells in the cat. J Neurophysiol 73: 1414-1421.

Shou TD, Leventhal AG (1989) Organized arrangement of orientation–sensitive relay cells in the cat's dorsal lateral geniculate nucleus. J Neurosci 9: 4287-4302.

Shriki O, Kohn A, Shamir M (2012) Fast coding of orientation in primary visual cortex. PLoS Comput Biol 8: e1002536.

Sillito AM, Jones HE, Gerstein GL, West DC (1994) Feature–linked synchronization of thalamic relay cell firing induced by feedback from the visual cortex. Nature 369: 479-482.

Simpson AJ, Fitter MJ (1973) What is the best index of detectability? Psychol Bull 80: 481-488.

Simpson WA, Manahilov V, Shahani U (2009) Two eyes: square root 2 better than one? Acta Psychol (Amst) 131: 93-98.

Skottun BC, De Valois RL, Grosof DH, Movshon JA, Albrecht DG, Bonds AB (1991) Classifying simple and complex cells on the basis of response modulation. Vis Res 31: 1079–1086.

Smith EL, Chino YM, Ni J, Cheng H, Crawford ML, Harwerth RS (1997) Residual binocular interactions in the striate cortex of monkeys reared with abnormal binocular vision. J Neurophysiol 78: 1353−1362.

Smith EL, Chino YM, Ridder WH, Kitagawa K, Langston A (1990) Orientation bias of neurons in the lateral geniculate nucleus of macaque monkeys. Vis Neurosci 5: 525-545.

Smith, E.L., Chino, Y.M., Ni, J., Ridder, W.H., Crawford, M.L. (1997) Binocular spatial phase tuning characteristics of neurons in the macaque striate cortex. J Neurophysiol 78, 351-365.

Sohya K, Kameyama K, Yanagawa Y, Obata K, Tsumoto T (2007) GABAergic neurons are less selective to stimulus orientation than excitatory neurons in layer II/III of visual cortex, as revealed by in vivo functional Ca2+ imaging in transgenic mice. J Neurosci 27: 2145−2149.

Sokal RR, Rohlf FJ (1995) The principles and practice of statistics in biological research. New York: Edition.

Song S, Miller KD, Abbott LF (2000) Competitive Hebbian learning through spike−timing−dependent synaptic plasticity. Nat Neurosci 3: 919−926.

Soodak RE, Shapley RM, Kaplan E (1987) Linear mechanism of orientation tuning in the retina and lateral geniculate nucleus of the cat. J Neurophysiol 58: 267-275.

Stanley GB, Jin J, Wang Y, Desbordes G, Wang Q, Black MJ, Alonso JM (2012) Visual orientation and directional selectivity through thalamic synchrony. J Neurosci 32: 9073-9088.

Stewart DL, Chow KL, Masland RH (1971) Receptive−field characteristics of lateral geniculate neurons in the rabbit. J Neurophysiol 34: 139-147.

Stosiek C, Garaschuk O, Holthoff K, Konnerth A (2003) In vivo two−photon calcium imaging of neuronal networks. Proc Natl Acad Sci USA 100: 7319-7324.

Swets JA (1986) Form of empirical ROCs in discrimination and diagnostic tasks: implications for theory and measurement of performance. Psychol Bull 99: 181-198.

Swindale NV (1998) Orientation tuning curves: empirical description and estimation of parameters. Bio Cybernetics 78: 45−56.

Tagawa Y, Kanold PO, Majdan M, Shatz CJ (2005) Multiple periods of functional ocular dominance plasticity in mouse visual cortex. Nat Neurosci 8: 380-388.

Tan AYY, Brown BD, Scholl B, Mohanty D, Priebe NJ (2011) Orientation selectivity of synaptic input to neurons in mouse and cat primary visual cortex. J Neurosci 31: 12339-12350.

Taylor WR, He S, Levick WR, Vaney DI (2000) Dendritic computation of direction selectivity by retinal ganglion cells. Science 289: 2347-2350.

Thompson KG, Zhou Y, Leventhal AG (1994) Direction−sensitive X and Y cells within the A laminae of the cat's LGNd. Vis Neurosci 11: 927-938.

Timberlake W, Washburne DL (1989) Feeding ecology and laboratory predatory behavior toward live and artificial moving prey in seven rodent species. Animal Learning Behavior 17(1): 2−11.

Trachtenberg JT, Trepel C, Stryker MP (2000) Rapid extragranular plasticity in the absence of thalamocortical plasticity in the developing primary visual cortex. Science 287: 2029−2032.

Ts'o DY, Frostig RD, Lieke EE, Grinvald A (1990) Functional organization of primate visual cortex revealed by high resolution optical imaging. Science 249: 417-420.

Tzounopoulos T, Kim Y, Oertel D, Trussell LO (2004) Cell−specific, spike timing−dependent plasticities in the dorsal cochlear nucleus. Nat Neurosci 7: 719−725.

Usrey WM, Reppas JB, Reid RC (1999) Specificity and strength of retinogeniculate connections. J Neurophysiol 82: 3527-3540.

Van Hooser SD, Heimel JAF, Chung S, Nelson SB, Toth LJ (2005) Orientation selectivity without orientation maps in visual cortex of a highly visual mammal. J Neurosci 25(1):19–28.

Van Hooser SD (2007) Similarity and diversity in visual cortex: Is there a unifying theory of cortical computation? The Neuroscientist 13(6): 639–655.

Venkataramani S, Taylor WR (2010) Orientation selectivity in rabbit retinal ganglion cells is mediated by presynaptic inhibition. J Neurosci 30: 15664–15676.

Vidyasagar TR, Heide W (1984) Geniculate orientation biases seen with moving sine wave gratings: implications for a model of simple cell afferent connectivity. Exp Brain Res 57: 176–200.

Viswanathan S, Jayakumar J, Vidyasagar TR (2011) Role of feedforward geniculate inputs in the generation of orientation selectivity in the cat's primary visual cortex. J Physiol (Lond) 589: 2349–2361.

Von Melchner L, Pallas SL, Sur M (2000) Visual behaviour mediated by retinal projections directed to the auditory pathway. Nature 404: 871–876.

Von Noorden GK, Campos EC (2002) Binocular vision and ocular motility: theory and management of strabismus, 6th Edition. St. Louis, Mo.

Vreysen S, Zhang B, Chino YM, Arckens L, Van den Bergh G (2012) Dynamics of spatial frequency tuning in mouse visual cortex. J Neurophysiol 107: 2937–2949.

Wagor E, Mangini NJ, Pearlman AL (1980) Retinotopic organization of striate and extrastriate visual cortex in the mouse. J Comp Neurol 193: 187–202.

Wallace GK (1959) Visual scanning in the desert locust Schistocerca gregaria Forskål. J Exp Bio 36: 512–525.

Wang B–S, Sarnaik R, Cang J (2010) Critical period plasticity matches binocular orientation preference in the visual cortex. Neuron 65: 246–256.

Wang L, Kloc M, Gu Y, Ge S, Maffei A (2013) Layer–specific experience–dependent rewiring of thalamocortical circuits. J Neurosci 33: 4181–4191.

Wei W, Hamby AM, Zhou K, Feller MB (2011) Development of asymmetric inhibition underlying direction selectivity in the retina. Nature 469: 402–406.

Weliky M, Bosking WH, Fitzpatrick D (1996) A systematic map of direction preference in primary visual cortex. Nature 379: 725–728.

Weng S, Sun W, He S (2005) Identification of ON–OFF direction–selective ganglion cells in the mouse retina. J Physiol (Lond) 562: 915–923.

Wikler KC, Rakic P (1990) Distribution of photoreceptor subtypes in the retina of diurnal and nocturnal primates. J Neurosci 10(10): 3390–33401.

Willigen RF van der, Frost BJ, Wagner H (1998) Stereoscopic depth perception in the owl. Neuroreport 9: 1233–1237.

Wilson NR, Runyan CA, Wang FL, Sur M (2012) Division and subtraction by distinct cortical inhibitory networks in vivo. Nature 488, 343–348.

Woodin MA, Ganguly K, Poo MM (2003) Coincident pre– and postsynaptic activity modifies GABAergic synapses by postsynaptic changes in Cl– transporter activity. Neuron 39: 807–820.

Xu X, Bosking W, Sáry G, Stefansic J, Shima D, Casagrande V (2004) Functional organization of visual cortex in the owl monkey. J Neurosci 24(28):6237–6247.

Xu X, Bosking WH, White LE, Fitzpatrick D, Casagrande VA (2005) Functional organization of visual cortex in the prosimian bush baby revealed by optical imaging of intrinsic signals. J Neurophysiol 94(4):2748–62.

Xu X, Ichida J, Shostak Y, Bonds AB, Casagrande VA (2002) Are primate lateral geniculate nucleus (LGN) cells really sensitive to orientation or direction? Vis Neurosci 19: 97–108.

Yazaki–Sugiyama Y, Kang S, Cateau H, Fukai T, Hensch TK (2009) Bidirectional plasticity in fast–spiking GABA circuits by visual experience. Nature 462: 218–221.

Yinon U, Auerbach E (1975) The ocular dominance of cortical neurons in cats developed with divergence and convergent squint. Vis Res 15: 1251–1256.

Yu J, Ferster D (2010) Membrane potential synchrony in primary visual cortex during sensory stimulation. Neuron 68: 1187−1201.

Zaltsman JB, Heimel JA, Van Hooser SD (2015) Weak orientation and direction selectivity in lateral geniculate nucleus representation central visual in the gray squirrel sciurus carolinensis. J Neurophysiol online.

Zar JH (1999) Biostatistical analysis. Pearson: Edition.

Zhao X, Chen H, Liu X, Cang J (2013) Orientation−selective Responses in the Mouse Lateral Geniculate Nucleus. J Neurosci 33(31): 12751−12763.